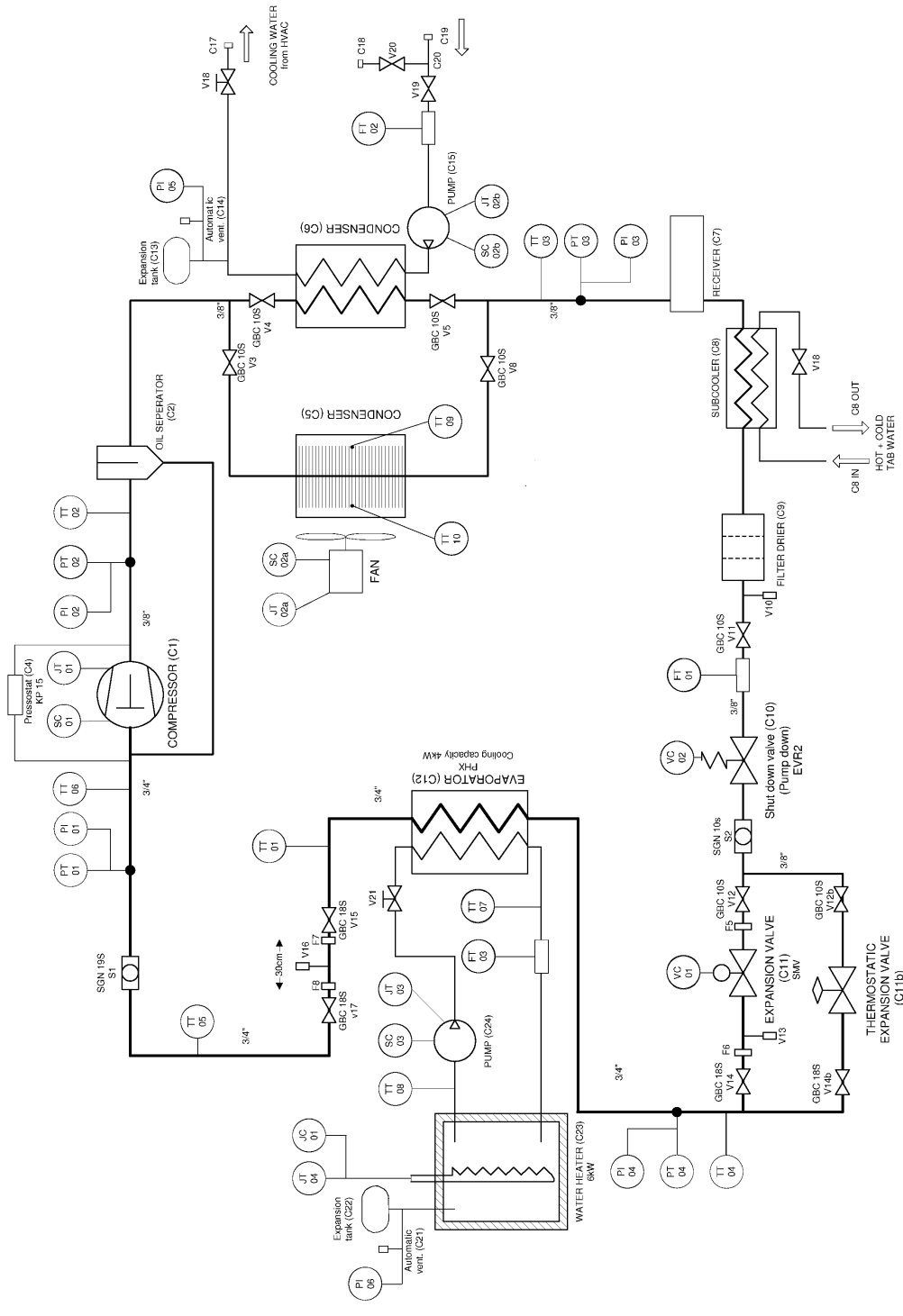


Model Based Nonlinear Control of Refrigeration Systems

MASTER THESIS, AAU
SECTION FOR AUTOMATION AND CONTROL

Group 1032a, 2008

Gustav Høgh
Rasmus Nielsen



Synopsis:

Title:

Model Based Nonlinear Control
of Refrigeration Systems

Projectperiod:

9th - 10th semester

Project group:

1032a

Members:

Gustav Høgh
Rasmus Nielsen

Supervisor:

Henrik Rasmussen
Rafael Wisniewski

Copies: 6

Pages in report: 93

Printed: June 3, 2008

Refrigeration systems are traditionally controlled using a thermostatic expansion valve. This thesis presents a new control strategy. The new strategy uses the compressor to control the superheat and an electronic expansion valve to control the cooling capacity. The refrigerant system is modelled to allow for the use of model-based feedback and feedforward. This yields better control of the superheat level. An analysis of the system efficiency is made to find the optimal superheat setpoint. Operating the system at the optimal superheat will reduce the energy needed to provide a given cooling capacity. The optimal superheat is found to be approximately 12 degrees celsius. At lower temperatures the efficiency is decreasing due to refrigerant spray. An autonomous method of detecting the optimal superheat is presented. The control problem is comprehensive investigated and a number of controllers are developed. They are all capable of stabilising and controlling the system and utilise both linear and nonlinear control theory. This thesis proves that is possible to control the refrigeration system using the new control strategy. Furthermore it is shown that it is possible to maintain the correct superheat over a wide range of working points.

Preface

This thesis is written by group 1032a during the 9th and 10th semester of the Master program in Intelligent Autonomous Systems at the section for Automation and Control at Aalborg University (AAU). The project was carried out in the period from the 1st of September 2007 to the 4th of July 2008 under the supervision of Associate Professor Henrik Rasmussen and Professor Rafal Wisniewski.

The reader of this report is presumed to have a similar technical background as the project group, including knowledge of the courses given during the 9th semester, which are on the subject of Modeling and Control.

A few of the chapters in this thesis features a resume of the chapter. The resumes are typographically marked by been placed within grey boxes. The resume will provide the reader with an overview of the succeeding content.

References to other publications is indicated with square brackets e.g. "[name, date]". An complete list of references can be found in the bibliography.

Gustav Høgh

Rasmus Nielsen

Measurements:

P_e	Evaporator pressure	PT04
P_c	Condenser pressure	PT03
$T_{w,i}$	Water inlet temperature	TT07
$T_{w,o}$	Water outlet temperature	TT08
T_e	Evaporation temperature	TT04
$T_{e,o}$	Evaporator outlet temperature	TT01
\dot{m}_r	Refrigerant flow	FT01
\dot{Q}_{fan}	Condenser fan power	JT02a
\dot{Q}_{com}	Compressor power	JT01

Control signals:

u_{exv}	Electronic expansion valve	VC01
u_{com}	Compressor	SC01
u_{fan}	Condenser fan	SC02a
u_{heat}	Water heater	JC01

Other stuff:

T_w	Water temperature
T_{sh}	Superheat, $T_{e,o} - T_e$
ω_{com}	Compressor speed
\dot{Q}_{load}	Heat load
\dot{Q}_{cool}	Cooling capacity
\dot{Q}_{net}	$\dot{Q}_{load} - \dot{Q}_{cool}$

General notation:

V	Volume
\dot{V}	Volume flow
A	Area
v	Velocity
ρ	Density
W	Work (non thermic)
Q	Thermic energy
\dot{Q}	Thermic energy flow (work)

Special functions:

$P_{dew}(\cdot)$	Dew point pressure, given a temperature
$T_{bub}(\cdot)$	Bubble temperature, given a pressure
$SAT_b^a(\cdot)$	Saturate at upper limit a or lower limit b

Terms

Isentropic describes a process during which the entropy remains constant.

Adiabatic A process is adiabatic when it occurs without exchanging heat with its surroundings.

Capacity or cooling capacity is the rate with which the system is capable of removing heat (energy) from the cooled medium.

COP is an acronym for Coefficient Of Performance. It is the relation between the cooling capacity and the work added by the compressor.

Enthalpy is the internal energy per kilogram of substance e.g. refrigerant.

Refrigerant is the substance used to transfer the heat. Its should be able to evaporate at the desired cooling temperature and condensate above the ambient temperature, both at manageable pressures.

R134a is the specific refrigerant used in this project. DuPont [2004]

Cooled medium is the medium from which the heat is removed. This is often air, but in this case it is a 30% ethylene glycol / water solution.

Superheat is the temperature a vapor is above its evaporation temperature.

Subcool is the temperature a liquid is below its condensation temperature.

Vapor is a state where the refrigerant is on vapor (gas) phase.

Liquid is a state where the refrigerant is on liquid (fluid) phase.

Two-phase is a state where the refrigerant is locally on both vapor and gas phase.

Saturated is a state where the refrigerant is between either the vapor or the liquid state and the two-phase state.

Expansion valve is the valve responsible for creating the pressure drop from the high pressure part to the low pressure part

EXV is an acronym for Electronic eXpansion Valve.

TXV is an acronym for Thermostatic eXpansion Valve.

HVAC is an acronym for Heating, Ventilation and Air Conditioning systems.

Contents

1	Introduction	11
1.1	The Vapour-Compression Cycle	11
1.2	The Test Rig	13
1.3	Classic Control Strategy	14
1.4	Minimising Energy Consumption	15
1.5	Thesis	18
2	Efficiency Analysis	19
2.1	Evaporator Overflow	19
2.2	Optimal Superheat	20
2.3	Summary	21
3	Modelling	23
3.1	Evaporator	26
3.2	Electronic Expansion Valve	33
3.3	Compressor	35
3.4	Condenser	41
3.5	Water Tank	41
3.6	Superheat Gain Analysis	44
4	Controller Design	49
4.1	Controller Strategy	51
4.2	Temperature Controller (TC)	52
4.3	Superheat Controller (SHC)	58
4.4	Condenser Pressure Controller (CPC)	66
4.5	Controller Conclusion	67
5	Nonlinear Control	69
5.1	Reference Signal	71
5.2	Feedback Linearization	72
5.3	Backstepping	77
6	Supervisor	83
6.1	Superheat Setpoint	84
6.2	Summary	90

CONTENTS

7 Conclusion	91
Bibliography	93
A The Test Rig	95
B Expansion Valve	99
B.1 Presentation	99
B.2 Analysis	100
B.3 Conclusion	100
C COP Experiment	105
C.1 Purpose	105
C.2 Method	105
C.3 Calculating COP	106
C.4 Results	106
D Derivation of f_{te}	109
E Working Point Consideration	111
F R134a	115

Chapter 1

Introduction

This chapter contains a basic introduction to refrigeration, the processes and equipment involved. First the vapour-compression cycle is described followed by a short description of the test rig available at AAU. The classic control strategy used with refrigeration systems is then presented, to give an overview of the control problem. An analysis of how to minimise the energy consumption of the refrigeration system is then completed. This analysis is the basis for the thesis and suggest controlling the refrigeration system using a new control strategy.

1.1 The Vapour-Compression Cycle

The following section will cover the basic theory of a two-phase refrigeration system.

The purpose of a refrigeration system is to provide cooling of a given location. The cooling process involves moving heat from one location to another. This is done by exploiting the chemical properties of the refrigerant during phase transition. In a vapour-compression system the phase transition between liquid and gas is utilised. This transition occur at different temperatures at different absolute pressure levels. E.g. at high pressure levels the phase transition from liquid to gas or from gas to liquid occur at a higher temperature than at lower pressure levels. The transition from liquid to gas, called vaporisation, requires energy. The refrigerant moves from one state (liquid) to another state (gas) which have a higher heat energy content. The energy content per mass is called enthalpy and is measured in [J/kg]. The transition from gas to liquid, called condensation, dissipates energy. E.g. at a constant pressure level the enthalpy of matter has a lower enthalpy in liquid state than in gas phase. Figure 1.1 is an illustration of a refrigeration system.

In order to utilise the phase change properties the system must operate at two different pressure levels. The upper part of the figure operates at a higher pressure level than the lower part. In the low pressure part of the system, the phase transition from liquid to gas happens at temperature T_e . If the ambient temperature on the low pressure side is above T_e the refrigerant will evaporate and remove energy from the higher temperature environment, thus having a cooling effect. In the high pressure part of the system the phase transition happens at T_c which is higher than T_e . If the ambient temperature on the high pressure side is lower than T_c energy will dissipate from the refrigerant, thus heating the lower temperature environment.

1.1. THE VAPOUR-COMPRESSSION CYCLE

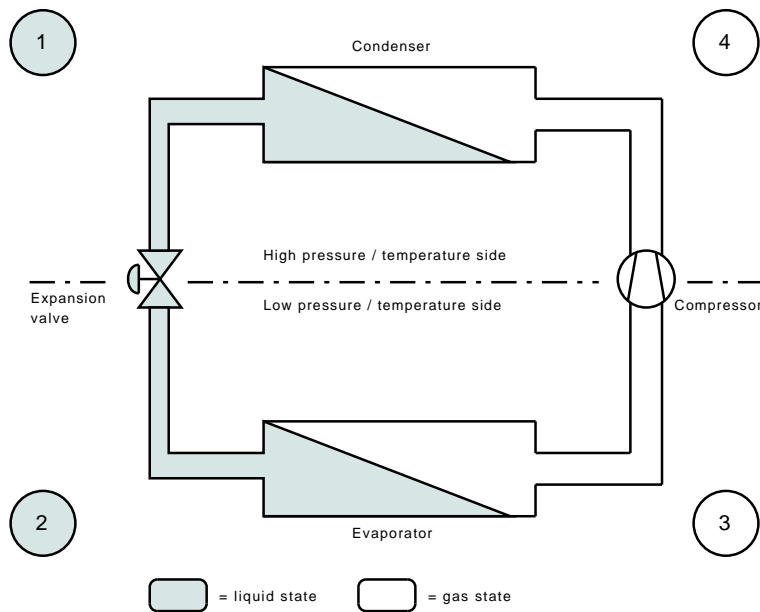


Figure 1.1: Illustration of the vapour-compression cycle.

The unit of heat content, enthalpy, was shortly mentioned. Enthalpy is defined as

$$H = U + pV \quad (1.1)$$

where:

- H is the enthalpy [J/kg]
- U is the internal energy [J/kg]
- p is the pressure [pa]
- V is the volume [m^3]

One way to describe the vapour-compression cycle is using a $\log(p)$ - H diagram. Figure 1.2 shows a $\log(p)$ - H diagram of the refrigerant used in the test refrigeration system. A detailed version can be found in appendix F on page 115.

The marked points in figure 1.1 correspond to the points in figure 1.2.

- **[1 - > 2]** At (1) the refrigerant is in a liquid state at high pressure but with low enthalpy. The liquid flow through the expansion valve causes a pressure drop. The $\log(p)$ - H diagram shows that the enthalpy remains constant across the valve.
- **[2 - > 3]** At (2) the refrigerant is in a liquid-gas mixed state at low pressure and low enthalpy. This can be seen on the $\log(p)$ - H diagram as the state enters the two-phase area. It is called two-phase because refrigerant exist in two different phases. Since the pressure is low, the evaporation temperature T_e is low. Heat energy is absorbed from the ambient environment, thus the enthalpy of the refrigerant increases. At some point the refrigerant state goes into the gas area, this happens when all the liquid has evaporated. It is important to notice that T_e is constant as long as there is still refrigerant on liquid state.

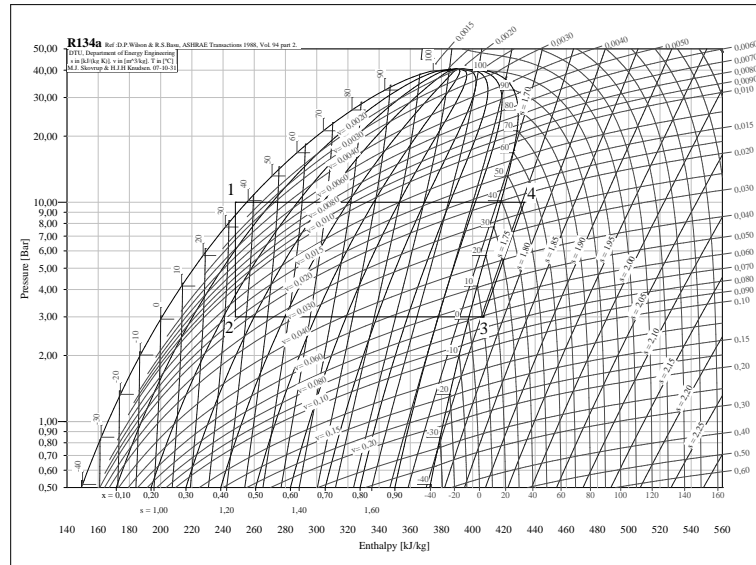


Figure 1.2: Log(p)-H diagram of refrigerant R134a.

- [3 – > 4] At (3) all the liquid refrigerant has evaporated and the gas has been superheated. Superheat is a measure of how much the gas has been heated above T_e . The compressor increases the pressure of the gas. Since the compressor can not compress the gas without adding work, the enthalpy increases.
- [4 – > 1] At (4) the refrigerant is at high pressure and high enthalpy. The high pressure results in a high temperature T_c . The condenser dissipate the energy of the gas to the cooler ambient environment. The enthalpy decreases and the refrigerant changes to liquid state. The liquid may be subcooled. Subcooling is a measure of how much the liquid is cooled below T_c .

1.2 The Test Rig

The refrigeration laboratory at Aalborg University consist of a state of the art refrigeration system. The refrigeration system is constructed with sponsorship from a number of companies, including Danfoss A/S, Danfoss Drives A/S, Siemens A/S, Grundfos A/S and Findan A/S. More information about the refrigeration system can be found on the refrigeration laboratory homepage: <http://control.aau.dk/koelelab>. A diagram of the system can be found on the back of the front page or in appendix A. The diagram shows all the major components such as the compressor, evaporator, condenser and expansions valves etc. The diagram also shows a number of transducers and control signals marked with an encircled four letter ID. All the transducers and control signal are interfaced with a Matlab Simulink model using National Instruments sampling boards. See appendix A for a short description of the key components.

1.3 Classic Control Strategy

The following section describes the classic control strategy used in refrigeration systems as shown in figure 1.3. The condenser pressure is controlled using a pressure controller

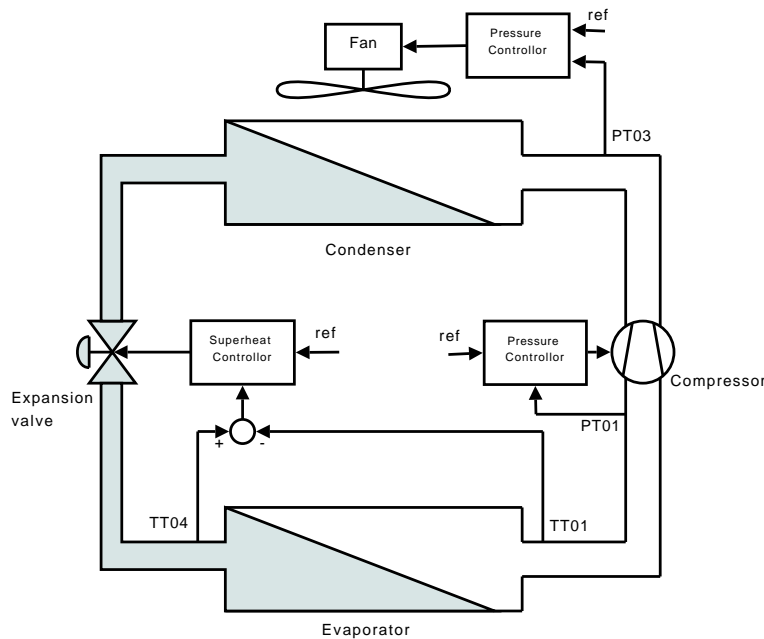


Figure 1.3: Classic control strategy.

regulating the speed of the fan. Increasing the speed of the fan increases the cooling effect on the refrigerant. With sufficient cooling the refrigerant enters liquid state and due to the increase in density the pressure drops. The cooling capacity is depended on the difference between the evaporation temperature and the temperature of the cooled medium. The evaporation temperature is a function of the evaporator pressure. Given an estimated required cooling capacity the evaporator pressure must be selected. The evaporator pressure is controlled by the speed of the compressor. The superheat is a function of the refrigerant level in the evaporator. The amount of refrigerant in the evaporator is controlled by the expansion valve. Normally refrigeration systems are fitted with a thermostatic expansion valve, which by a measure of superheat regulates the refrigerant flow.

The key advantage of this control strategy is it's simplicity. There is however one problem. The control strategy is know to suffer from 'hunting' effects, which are caused by two controllers affecting the same state. A change in evaporator pressure affect the cooling capacity which affect the superheat. The pressure controller therefore acts as a disturbance to the refrigerant flow controller. This problem can be reduced by decoupling the two controller [Petersen & Lund, 2004].

1.4 Minimising Energy Consumption

The goal of this project is to minimise the energy required to deliver a given cooling capacity. The energy optimisation methods proposed in this section also indicates the existence of a new approach to controlling refrigeration systems, which does not suffer from hunting effects as seen in the classic control strategy. This new approach will be described in details later in this thesis. A simple refrigeration system may have the layout as illustrated in figure 1.4. There are two main uses of energy in the vapour-compression cycle, the primary is the compression of the refrigerant (\dot{W}_{com}), while the secondary is the forced draft through either evaporator ($\dot{W}_{e,f}$), condenser ($\dot{W}_{c,f}$) or both. The optimal

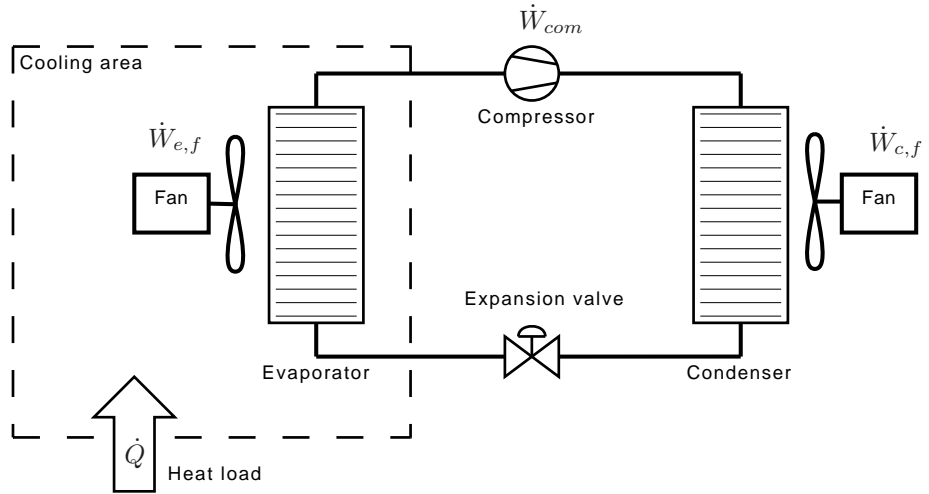


Figure 1.4: Typical refrigeration system layout.

control algorithm will minimise the overall energy usage while upholding the required cooling capacity

$$\min_{P_c, P_e, \dot{Q}_{cool}} (\dot{W}_{com} + \dot{W}_{c,f} + \dot{W}_{e,f}) \quad (1.2)$$

subject to: $\dot{Q}_{cool} = \dot{Q}_{ref}$

1.4.1 Condenser Fan Optimisation

The fan energy consumption depends on the rotational speed. In order to minimise the energy usage by the fan, the rotational speed must be as low as possible. However reducing the speed of the fan increases the condenser pressure and thus the energy usage by the compressor. The optimisation problem

$$\min_{P_c, \dot{Q}_{cool}} (\dot{W}_{com} + \dot{W}_{c,f}) \quad (1.3)$$

with subject to ambient air temperature is treated in the Ph.D. Thesis [Larsen, 2005]. Since this part of the energy optimisation is not the focus of this project, a constant condenser pressure of 10 bar is used.

1.4.2 Evaporator Fan Optimisation

As with the condenser fan optimisation there is a trade off between fan speed and evaporator pressure. In the available system the refrigerant is evaporated by heat from water circulated by a pump. The same consideration applies to the pump as the fan. In this project the energy consumption of the pump is assumed constant.

1.4.3 Compressor Optimisation

The optimisation problem using a fixed condenser pressure and fixed water flow is reduced to

$$\min_{P_e, \dot{Q}_{cool}} (\dot{W}_{com}) \quad (1.4)$$

subject to: $\dot{Q}_{cool} = \dot{Q}_{ref}$

The only free parameter is the evaporator pressure. The value of \dot{W}_{com} can be found using energy considerations [Guntoft & Lauritsen, 2003, p. 100].

$$\dot{W}_c = \dot{W}_{gas} + \dot{W}_{loss} \quad (1.5)$$

$$= \dot{m}_{com} \cdot (h_{com,o} - h_{com,i}) + \dot{W}_{loss} \quad (1.6)$$

where:

\dot{W}_{gas} is the work from the compressor [W]

\dot{W}_{loss} is the power loss [W]

\dot{m}_{com} is the refrigerant flow through the compressor [kg/s]

$h_{com,i}$ is the enthalpy of the refrigerant before the compressor [J/kg]

$h_{com,o}$ is the enthalpy of the refrigerant after the compressor [J/kg]

The value of \dot{W}_{loss} is assumed constant. If the dew point enthalpy (or $h_{com,i}$ and h_o with zero superheat) is assumed constant for all evaporator pressures (between 2 and 3 bar), the value of \dot{m}_r is constant and determined by the required cooling capacity (see equation (1.7)), then the only free parameter in equation (1.6) is $h_{com,o}$.

Figure 1.5 shows two vapour-compression cycles. The cooling capacity and condenser pressure is the same, but the evaporator pressure is 2 or 2.5 bar respectively. It is clear from the figure that the vapour-compression cycle using the highest evaporator pressure have the lowest enthalpy at the compressor outlet side. It is therefore clear that minimising the compressor power usage is archived by maximising the evaporator pressure. It should be noted that \dot{W}_{loss} is not constant. Data from the compressor datasheet, shows that the efficiency of the compressor increases when the pressure difference over it is decreased. This further supports that the evaporator pressure should be as high as possible to minimise the compressor power usage.

The optimisation problem of equation (1.4) is subject to a required cooling capacity. The cooling capacity is given by

$$\dot{Q} = \dot{m}_r \cdot (h_o - h_i) \quad (1.7)$$

$$= \alpha \cdot A_e \cdot (T_w - T_e) \quad (1.8)$$

where:

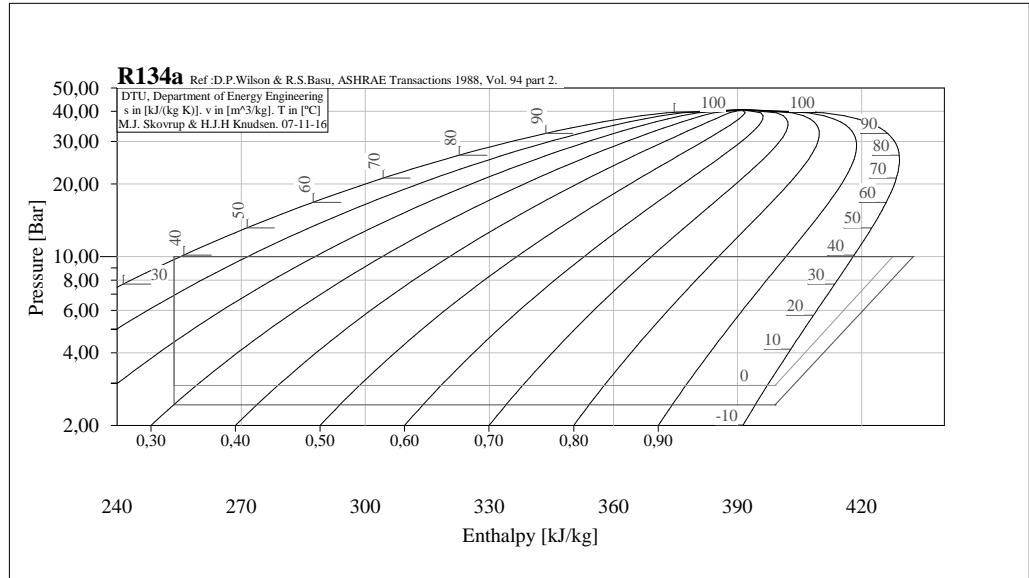


Figure 1.5: Two vapour-compression cycles. The condenser pressure and cooling capacity are constant. The evaporator pressure is 2 or 2.5 bar respectively.

- \dot{m}_r is the refrigerant flow through the evaporator [kg/s]
- h_o is the enthalpy of the refrigerant running into the evaporator [J/kg]
- h_i is the enthalpy of the refrigerant running from the evaporator [J/kg]
- α is the thermal resistance between the water and the refrigerant [J/Km^3]
- A_e is the surface area of the evaporator [m^2]
- T_w is the average water temperature in the evaporator [$°C$]
- T_e is the evaporation temperature [$°C$]

The water temperature and the thermal resistance is assumed constant. It is clear that if the surface area is increased, the evaporation temperature can be increased without changing the cooling capacity. The evaporation temperature is a function of the pressure. Increasing the pressure increases the evaporation temperature. The active surface of the evaporator, i.e., the part of the evaporator that is filled with refrigerant, can be increased if the superheat is decreased. The optimisation problem is therefore a problem of minimising the superheat.

$$\min_{P_e, \dot{Q}_{cool}} (\dot{W}_{com}) \rightarrow \min_{P_e, \dot{Q}_{cool}} (T_{sh}) \quad (1.9)$$

subject to: $\dot{Q}_{cool} = \dot{Q}_{ref}$

where:

- T_{sh} is the superheat temperature [$°C$]

While the evaporator should be filled for maximum cooling capacity, any evaporation of refrigerant outside the evaporator, i.e., not used to cool the desired medium, is a waste. Therefore the optimal efficiency will be to trade some filling for reduced risk of waste due to model uncertainty, unmodelled behaviour and unknown disturbances. Figure 1.6 illustrates how the heat transfer is distributed with the same cooling capacity, but at different pressures and degrees of superheat.

Figure 1.6A is a case of high superheat, the heat transfer is concentrated in the two-phase area. Increasing the pressure would distribute the heat transfer more evenly and reduce the required work. Figure 1.6B is a case of optimal pressure, the entire evaporator area is utilised. Figure 1.6C is a case of an overfilled evaporator, the pressure is high, reducing the compressor work, but with two-phase refrigerant outside the evaporator the cooling efficiency is reduced.

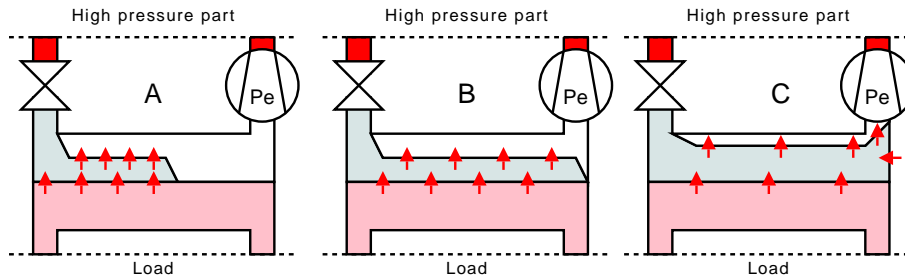


Figure 1.6: Constant capacity at, A: Low pressure, B: Optimal pressure, C: High pressure. The arrows illustrate heat transfer.

1.5 Thesis

The considerations described in the 'Compressor Optimisation' are apparently not covered in the literature. The primary differences are outlined below.

The usual approach is to select an evaporation pressure/temperature below the required temperature of the cooled goods depending on the expected load. I.e. the cooling capacity is controlled using a compressor. The superheat is controlled using a TXV which keeps the evaporator filled to obtain a preset superheat.

Our suggestion is to continuously determine the required cooling capacity more directly. The capacity will be realised by controlling an EXV, which will provide the required refrigerant flow. Optimisation is performed by keeping the evaporation pressure 'as high as possible' i.e. controlling the compressor to obtain the optimal superheat.

This new approach is expected to have the following characteristics:

- Full control of the temperature error / cooling capacity relationship.
- Possible autonomous tracking of required capacity.
- Optimal evaporation temperature at any capacity only limited by the systems actuators.
- Decoupling inherent from principle, expanded by model-based control.

This project seeks to show that the following hypotheses are valid:

- The novel control approach described above is feasible.
- Furthermore it provides superior efficiency.
- Fast startup (ON-OFF).

Chapter 2

Efficiency Analysis

The previous chapter outlined a method of minimising the energy consumption of the system by minimising the superheat. This chapter will describe how the superheat is measured on the test rig using the available temperature sensors. Measurement of the superheat with the system running at different working points will then be presented. These measurement are used to analyse the system and find the optimal superheat level. Finally the cooling COP-value is evaluated at different superheat levels.

2.1 Evaporator Overflow

The rig has been fitted with three temperature sensors on the pipe going from the evaporator to the compressor. The three sensors all measure the temperature $T_{e,o}$ but at different distances along the pipe. They have been named 'TT A', 'TT B' and 'TT C', see figure 2.1. An experiment is performed in order to analyse the superheat measured

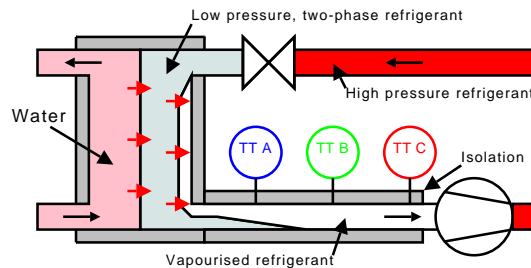


Figure 2.1: Illustration of the system with temperature sensor placement. The red arrows indicate energy transfer.

with the available sensors. During the experiment both the flow of refrigerant and the water temperature are kept constant. A ramp signal is applied to the compressor. The upper left part of figure 2.2 shows the superheat calculated using the three different temperature sensors, while the lower shows the compressor speed. The right part of the figure is a zoom of the superheat. It can be seen that the superheat generally decreases when the compressor speed is decreased. This is as expected since a lower superheat

2.2. OPTIMAL SUPERHEAT

should yield a lower energy consumption by the compressor (lower speed). The calculated superheat levels are not the same for all sensors over the entire measurement. The

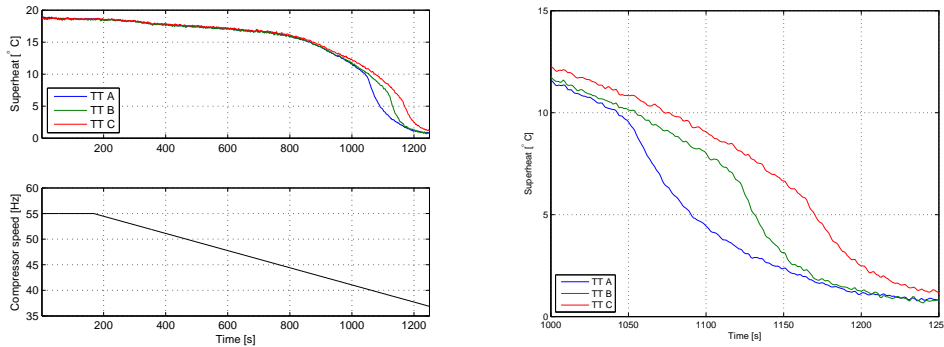


Figure 2.2: Measured superheat with constant flow and decreasing compressor speed. To the right is a zoom of the superheat.

three superheats are almost equal until approximately time 1050. After this time the superheat based on measurement from 'TT A' drops, later the superheat based on measurements from TT B drops as well and finally the superheat from 'TT C' follows. The temperature sensor 'TT A' is closest to the evaporator and the sudden drop in superheat can perhaps be explained by liquid refrigerant spraying onto the part of the pipe where the sensor is attached, causing a rapid cooling of the sensor probe. The superheat is further decreased and the spray hits sensor 'TT B' causing the drop in its superheat. Finally the spray hits the last sensor, 'TT C'. The concept of refrigerant spray impose a lower bound on the superheat level to reach optimal energy efficiency. The next section will describe this in details.

2.2 Optimal Superheat

To find the optimal superheat and to support the concept of refrigerant spray an experiment is made to evaluate the COP-value at different levels of superheat. The COP-value is a measure of the ratio between compressor power usage and the achieved cooling capacity. Decreasing the superheat is normally considered to increase the COP. However the previous graph indicate that refrigerant spray hits the sensors. Since these sensors are located outside the evaporator, the spray refrigerant is lost, causing a lowered COP-value. If this is the case, optimal superheat will be around 10 to 12 degrees. Experimental data is obtained to support this hypothesis. See appendix C on page 105 for a description of the experiment and detailed results. Figure 2.3 shows the results of the experiment. The upper part of the figure shows the COP-value plotted as a function of superheat measured using 'TT C'. It is clear that the maximum COP is obtained at approximately 12 degrees superheat. The superheat measurement and superheat control is done using sensor 'TT C' because the superheat measurement from sensor 'TT A' is useless when the refrigerant spray starts to hit the sensor. This has a small effect on the measured superheat levels because the superheat measured with sensor 'TT A' and 'TT C' differs a small amount even when the spray does not hit any of the sensors. The lower part of the plot shows the average difference between the temperature measured by sensors

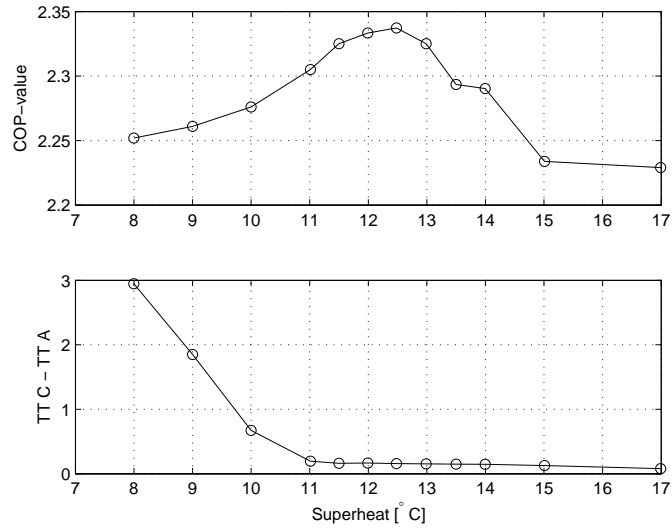


Figure 2.3: The COP-value and the differences on $T_{e,o}$ at different levels of superheat.

'TT A' and 'TT C'. A positive value in the graph means that sensor 'TT C' measures a higher mean temperature than 'TT A', which would indicate that the spray has hit sensor 'TT A'. Comparing the upper and lower graph it is clear that the maximum COP is obtained approximately 2 degrees before the difference is significantly increased by the refrigerant spray. It can also be concluded that refrigerant spray has a negative effect on the COP-value.

2.3 Summary

The COP-value at different superheat levels is evaluated. The optimal superheat level is found to be approximately 12 degrees. At superheat temperatures below 12 degrees the COP-value begins to decrease. This is likely caused by refrigerant spray exiting the evaporator and thereby not providing any useful cooling. In the later controller design the superheat reference should therefore be approximately 12 degrees.

2.3. SUMMARY

Chapter 3

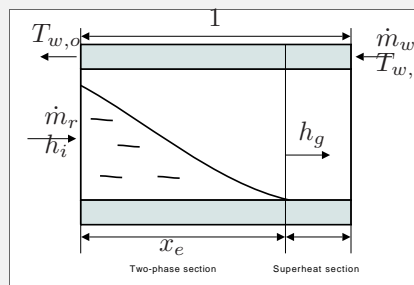
Modelling

In this chapter the key parts of the test rig will be modelled. These include the evaporator, expansion valve and compressor. The condenser and water heater are outside the main scope of this thesis and are therefore not thoroughly modelled.

Resume:

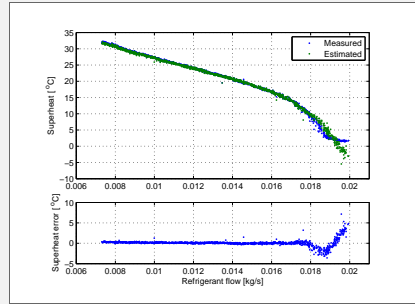
Evaporator

The evaporator model is based on the moving-boundary formulation, where the idea is to have a single state describing how far along the evaporator the refrigerant is on two-phase from. This value is normed with the evaporators length and called the relative filling or x_e .

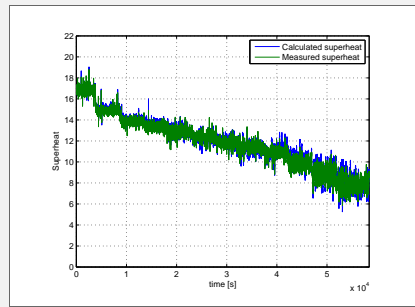


The relative filling is described by a dynamic expression with a number of parameters, many of which are working point (or time) dependent. The relative filling cannot be measured directly, but the model includes a static expression for the measurable superheat, which depends on the filling.

Two of the constant parameters were estimated by bringing the system to a state with known filling, i.e. flooded evaporator or no superheat. From there, the superheat was slowly increased by reducing the refrigerant flow while the other system parameters were kept constant. The refrigerant flow was reduced very slowly to allow for an assumption of steady state.

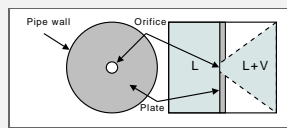


The last constant parameter, the time constant, was estimated by fitting simulations to measurements during various steps.



Electronic Expansion Valve

The electronic expansion valve is considered an orifice plate with variable orifice area.



The upstream / downstream balance of pressure and velocity of a flow passing an obstacle like an orifice plate, is described by the Bernoulli Equation.

$$P_c + \frac{1}{2} \cdot \rho_c \cdot v_p^2 = P_e + \frac{1}{2} \cdot \rho_e \cdot v_o^2$$

Using various assumptions, lumping of parameters and conversion of units, the refrigerant flow through the evaporator can be expressed by

$$\dot{m} = K \cdot u_{exv}^2 \cdot \sqrt{\Delta P}$$

Requiring only one parameter to be estimated from experiments.

Compressor

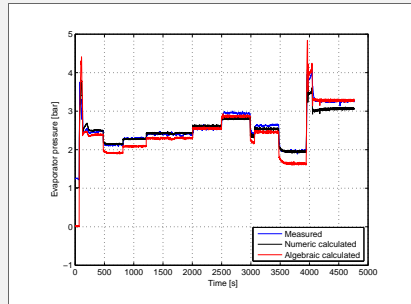
For the ideal reciprocating compressor, the volume flow would be the displacement times the rotational frequency. For non ideal compressors the delivery rate λ is the relationship between the ideal and the actual volume flow. The compressor datasheet includes data which can be used for calculating the delivery rate at different condenser and evaporator pressures. Knowing the refrigerant density, the mass flow through the compressor can be found.

$$\dot{m}_{com} = \rho_{(P_{e,o}, T_{e,o})} \cdot \lambda_{(P_{e,o}, P_{c,i})} \cdot V_{com} \cdot \omega_{com}$$

However the expansion valve is used for control of the refrigerant flow. In steady state the flow through the expansion valve and through the compressor are assumed equal. Hence given the refrigerant flow, the compressor speed to evaporator pressure relation can be found by numerically searching for the pressure resulting in the best match between the actual refrigerant flow and the estimated compressor flow. [Rasmussen, 2008] has provided a very simple algebraic expression

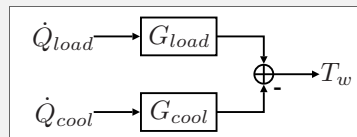
$$P_{e,o} = \frac{\dot{m}_{com}}{\alpha \cdot \omega_{com}}$$

which also approximates the compressor speed / evaporator pressure relation.



Water Tank

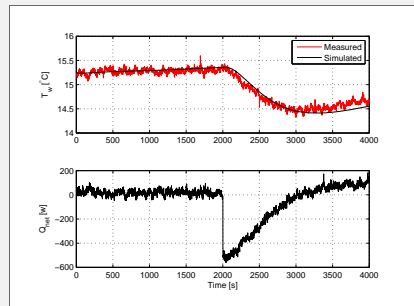
The water tank stores the water to be pumped through the evaporator and features a water heater to from a load. The water temperature is a function of both the cooling and the heating. The response to both inputs also depends on where the temperature is measured.



$$G_{load}(s) = c_l \cdot \frac{e^{-\tau_{d,l} \cdot s}}{s + \tau_l \cdot s^2}$$

$$G_{cool}(s) = c_c \cdot \frac{e^{-\tau_{d,c} \cdot s}}{s + \tau_c \cdot s^2}$$

The model parameters have been estimated for both inputs and to both temperature measurement points. For simplicity the model is reduced to a system having only the difference between \dot{Q}_{load} and \dot{Q}_{cool} , \dot{Q}_{net} as input. The averaged system parameters are used as parameters for the simplified system. The model is useful as a description of the water tank dynamics, it is not reliable for water temperature estimation as even small errors integrate to significant size over time. The figure below shows the measured and estimated water temperature during a drop in the cooling capacity.



Superheat Gain Analysis

The developed nonlinear models are used to analyse the gain from the compressor to the superheat. i.e. how much the superheat change when the compressor speed is changed.

$$gain = \frac{\partial T_{sh}}{\partial \omega_{com}}$$

The gain is found to be between 0.36 and 2.78 for all valid working points. Limiting the work points to those obtained during normal operation reduces the range to gains between 0.92 and 2.61.

3.1 Evaporator

The modelling of the two-phase evaporator is based on a first principle approach where mass and energy of the refrigerant, evaporator and water is conserved. To simplify the model a number of assumptions are made: [He et al., July 1998]

- One dimensional fluid flow.
- Negligible pressure drop along the evaporator.
- Negligible heat conduction along the flow direction of the evaporator.
- Invariant mean void fraction in the two-phase section.

The model is based on a formulation presented by [Grald & MacArthur, 1992] describing a moving-boundary between the two-phase section and the superheat section in the evaporator. An illustration of the evaporator with the moving-boundary can be seen in figure 3.1. Conservation of mass and energy in the two-phase section of the evaporator

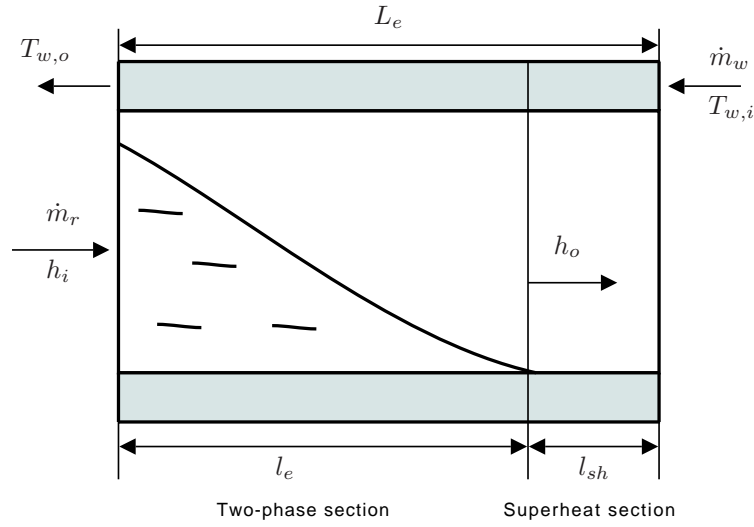


Figure 3.1: Illustration of the evaporator with moving-boundary.

yield the following equation, describing the time derivative of l_e .

$$\rho_{le} h_{lg} A_e (1 - \bar{\gamma}_e) \frac{dl_e}{dt} = \dot{m}_r (h_o - h_i) - \dot{Q} \quad (3.1)$$

where:

- ρ_{le} is the refrigerant density [kg/m^3]
- h_{lg} is the specific evaporation energy [J/kg]
- A_e is the cross section area of the evaporator [m^2]
- $\bar{\gamma}_e$ is the mean void fraction (vapour to liquid ratio) [-]
- \dot{m}_r is the mass flow of refrigerant [kg/s]
- h_i is the enthalpy of the inflow refrigerant [J/kg]
- h_o is the enthalpy of the outflow refrigerant [J/kg]
- \dot{Q} is the heat transfer to the refrigerant [J/s]

The first term on the right side is the power flow out of the evaporator, caused by the difference in the enthalpy of the inflow and outflow of refrigerant mass. The second term is the heat transfer from the ambient water to the cooler refrigerant. The two terms gives the net energy change rate of the two-phase section. If the system is in steady state the heat power is equal to the power used to evaporate the refrigerant inflow mass. If the heat power is increased, more refrigerant than the inflow mass is evaporated, thus l_e decreases. The heat exchange in the superheat section is assumed negligible compared to that of the two-phase section. The last term in equation (3.1) can be expressed as

$$\dot{Q} = C_w \dot{m}_w (T_{w,i} - T_{w,o}) \quad (3.2)$$

where:

- C_w is the specific heat capacity of the water/antifreeze solution [J/Kkg]
- \dot{m}_w is the mass flow of water [kg/s]
- $T_{w,i}$ is the water inflow temperature [$^{\circ}C$]
- $T_{w,o}$ is the water outflow temperature [$^{\circ}C$]

3.1. EVAPORATOR

The value of $T_{w,o}$ can be derived as follows. Consider a cross section of the evapo-

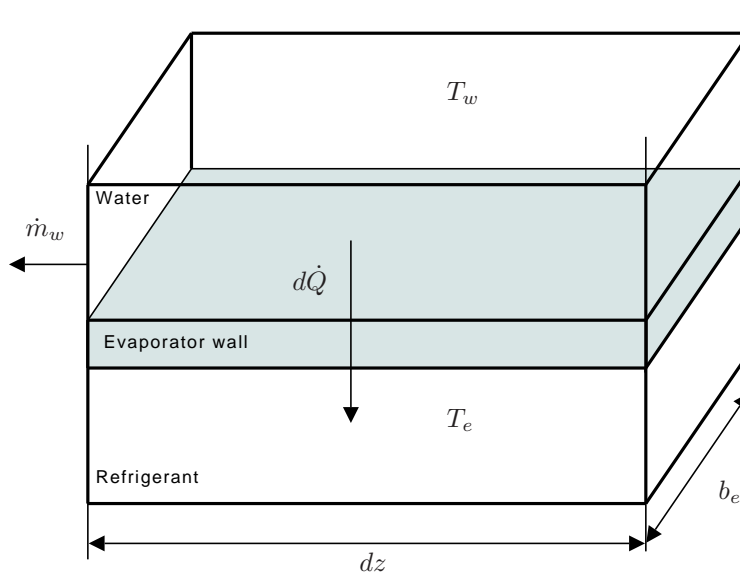


Figure 3.2: Cross section of the evaporator.

rator (dz), which is illustrated in figure 3.2. The heat transfer rate from the water to the refrigerant over this cross section is

$$d\dot{Q} = \alpha_{w,r} b_e (T_w(z) - T_e(z)) dz \quad (3.3)$$

where:

- $\alpha_{w,r}$ is the thermal resistance between the water and the refrigerant [J/Km^2]
- b_e is the width of the evaporator plates [m]
- $T_w(z)$ is the temperature of the water [$^{\circ}C$]
- $T_e(z)$ is the evaporation temperature [$^{\circ}C$]

Considering energy conservation, the heat transfer from the water to the refrigerant must cause a decrease in the water temperature.

$$d\dot{Q} = -\dot{m}_w C_w dT_w(z) \quad (3.4)$$

Combining equations (3.3) and (3.4) yields

$$-\dot{m}_w C_w dT_w(z) = \alpha_{w,r} b_e (T_w(z) - T_e(z)) dz \quad (3.5)$$

$$\frac{dT_w(z)}{dz} = -\frac{\alpha_{w,r} b_e}{\dot{m}_w C_w} (T_w(z) - T_e(z)) \quad (3.6)$$

The value of $T_e(z)$ is equal to the evaporation temperature of the refrigerant and assumed constant over the entire two-phase section. The resulting first order differential equation is on the same form as Newton's cooling law and solving it with initial condition $T_w(0) = T_{w,i}$ yields

$$T_w(z) = (T_{w,i} - T_e) e^{-\frac{\alpha_{w,r} b_e}{\dot{m}_w C_w} z} + T_e \quad (3.7)$$

The changes in the outlet water temperature caused by the superheat section is assumed negligible compared to that of the two-phase section. The outlet temperature can then be found using equation (3.7) and assuming ($z = l_e$).

$$T_{w,out} = (T_{w,i} - T_e)e^{-\frac{\alpha_{w,r}b_e}{\dot{m}_w c_w}l_e} + T_e \quad (3.8)$$

Rewriting equation (3.8) with $L_w = \frac{\alpha_{w,r}b_e}{\dot{m}_w c_w}$ yields

$$T_{w,o} = (T_{w,i} - T_e)e^{-L_w l_e} + T_e \quad (3.9)$$

Inserting this equation into equation (3.2) yields

$$\begin{aligned} \dot{Q} &= C_w \dot{m}_w (T_{w,i} - ((T_{w,i} - T_e)e^{-L_w l_e} + T_e)) \\ &= C_w \dot{m}_w (T_{w,i} - T_e)(1 - e^{-L_w l_e}) \end{aligned} \quad (3.10)$$

There are unknown parameters in ($L_w l_e$), however it is reasonable to assume that ($L_w l_e \ll 1$). Remembering that $e^{-x} \approx 1 - x$ for $x \ll 1$ and inserting the expression for L_w equation (3.10) can be rewritten as

$$\begin{aligned} \dot{Q} &= C_w \dot{m}_w (T_{w,i} - T_e) L_w l_e \\ &= (T_{w,i} - T_e) \alpha_{w,r} b_e l_e \end{aligned} \quad (3.11)$$

The equation shows that the heat transfer is a function of the temperature difference between the water and the refrigerant and does not model any temperature drop in the water through the evaporator. The accuracy of the assumption ($L_w l_e \ll 1$) therefore depends on a small temperature drop of the water temperature. Inserting equation (3.11) into equation (3.1) yields

$$\rho_{l_e} h_{l_g} A_e (1 - \bar{\gamma}_e) \frac{dl_e}{dt} = \dot{m}_r (h_o - h_i) - (T_{w,i} - T_e) \alpha_{w,r} b_e l_e \quad (3.12)$$

The superheat temperature can be expressed as [He et al., July 1998]

$$T_{sh} = (T_{w,i} - T_e) \left(1 - e^{-\frac{\sigma(L_e - l_e)}{C_r \dot{m}_r}} \right) \quad (3.13)$$

where:

L_e is the length of the evaporator [m]

C_r is the specific heat capacity of the refrigerant [J/Kkg]

σ is the thermal resistance between the water and the refrigerant gas [J/Km^2]

To make the model more genetic many of the unknown parameters can be lumped together. It is also possible to define a new parameter which describe the filling level of the evaporator. This is done in equations (3.14) - (3.16).

$$x_e = \frac{l_e}{L_e} \quad (3.14)$$

$$c_1 = \rho_{l_e} h_{l_g} A_e (1 - \bar{\gamma}_e) L_e \quad (3.15)$$

$$c_2 = \alpha_{w,r} b_e L_e \quad (3.16)$$

Using these parameters the system can be written as

$$c_1 \frac{dx_e}{dt} = \dot{m}_r (h_o - h_i) - c_2 (T_{w,i} - T_e) x_e \quad (3.17)$$

3.1. EVAPORATOR

and

$$T_{sh} = (T_{w,i} - T_e) \left(1 - e^{-\frac{\sigma(1-x_e)}{c_r \dot{m}_r}} \right) \quad (3.18)$$

There are now three unknown constant to be fitted. The superheat depends on x_e which depends on \dot{m}_r . In steady state ($dx_e/dt = 0$) the value of x_e can be expressed as

$$\begin{aligned} 0 &= \dot{m}_r(h_o - h_i) - c_2(T_{w,i} - T_e)x_e \\ x_e &= \frac{\dot{m}_r(h_o - h_i)}{c_2(T_{w,i} - T_e)} \end{aligned} \quad (3.19)$$

The constant c_2 is unknown. It can be estimated if knowledge about the value of x_e exists. If the refrigeration system is in a state, where the superheat is zero the length of l_{sh} must also be zero and x_e must be unity. A measurement of the superheat as a function of \dot{m}_r should provide enough data to estimate the two unknown constants. However since equation (3.19) is only valid in steady state ($x_e = k_1, \dot{m}_r = k_2$) the measurement must be made with a very slow changing \dot{m}_r to ensure steady state like behaviour. The left part of figure 3.3 shows a measurement of the superheat as a function of \dot{m}_r . The

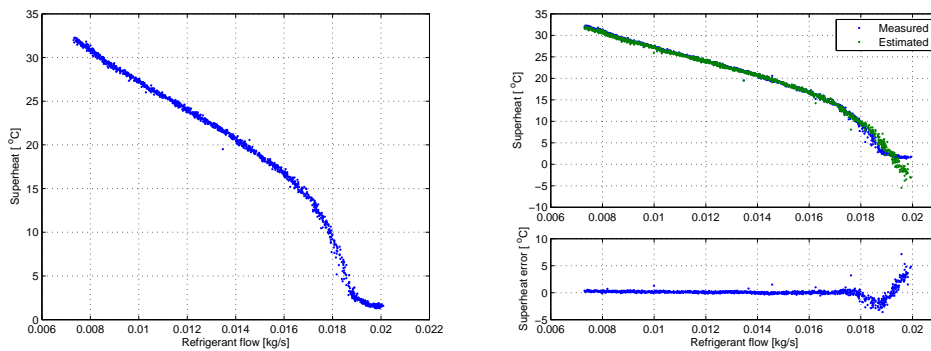


Figure 3.3: Estimated and measured superheat as a function of \dot{m}_r .

measurement is made by manually finding a \dot{m}_r -value, that results in zero superheat and then slowly decreasing the \dot{m}_r -value. A $d\dot{m}_r/dt$ value of 0.00001 was used. During the measurement it is important to keep all other states constant. The measurement is with constant $T_{w,i}$, condenser pressure and compressor speed. Using this measurement the constants can be fitted to the data. The right part of figure 3.3 shows the estimated superheat using the fitted constants $\sigma = 220$ and $c_2 = 250$ and the measured superheat. The lower right graph is the error between the measured and estimated superheat. As it can be seen the estimation is not perfect and other data sets shows that the constant values are different when using different data sets. One of the main sources of error is the estimate of x_e . Figure 3.4 shows a measurement where \dot{m}_r is slowly decreased from a superheat equal to zero. It is important to note that the superheat does not start to drop before \dot{m}_r has been decreased from approximately 0.033 to 0.029 kg/s. The model does not take this effect into account. The phenomenon is likely caused by the refrigerant spray described in chapter 2.

The only unknown constant to be fitted is c_1 . The value of c_1 has to do with the dynamics of the system and can therefore not be evaluated in steady state like behaviour. Equation

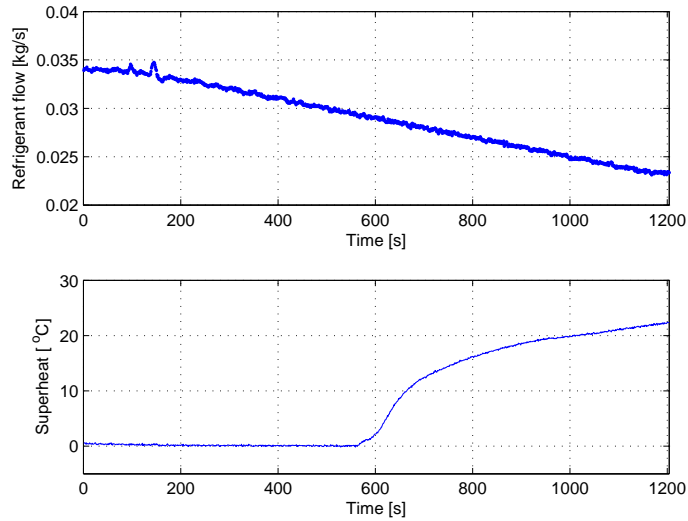


Figure 3.4: Measured superheat and refrigerant flow.

(3.18) can be used to calculate the filling given a measurement of the superheat. Figure 3.5 show the filling calculated by using superheat measurement and the filling calculated using the dynamic system described in equation (3.17) using a c_1 value of 100000. The figure shows that the dynamic system have approximately the same dynamics as expected from equation (3.18). Figure 3.6 shows the resulting superheat compared with the measured superheat.

3.1.1 Summary

The evaporator is modelled using a first principle approach and the moving-boundary formulation presented by [Grald & MacArthur, 1992]. Multiple assumptions are made to simplify the model. These include: One dimensional fluid flow, negligible pressure drop along the evaporator, negligible heat conduction along the flow direction of the evaporator and invariant mean void fraction in the two-phase section. The parameters in the resulting model are then lumped together and fitted to experimental data. Additional data is used to validate the model. An algebraic expression of the superheat is also presented.

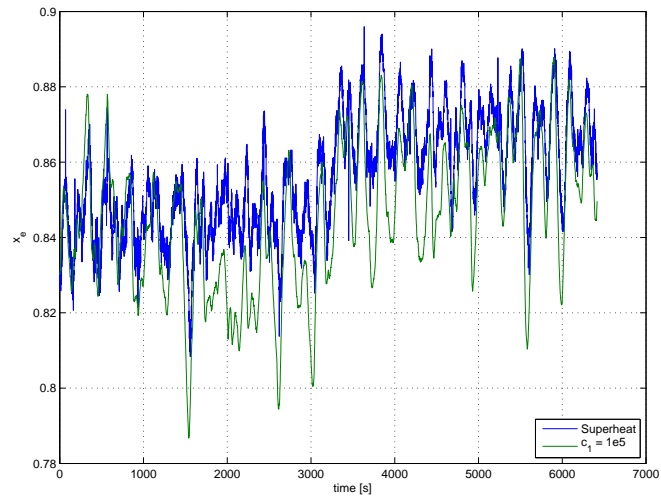


Figure 3.5: Fitting of c_1 .

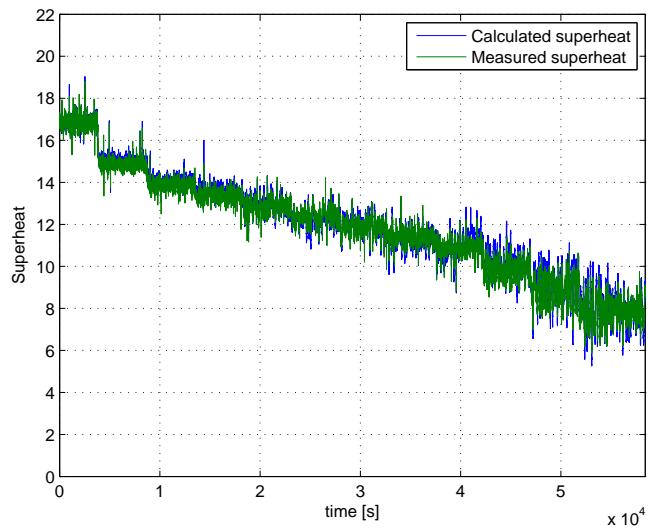


Figure 3.6: Calculated and measured superheat.

3.2 Electronic Expansion Valve

The expansion valve is used to control the refrigerant flow. It acts like a variable orifice plate on the flow of refrigerant from the condenser to the evaporator, see figure 3.7. Due to the fact that the mass flow is the same in both ends of a pipe, the velocity will increase to compensate for the reduced cross section area. With constant energy the increased velocity means reduced pressure, which is expressed by the Bernoulli Equation (3.20). [Auld & Srinivas, 1995-2007]

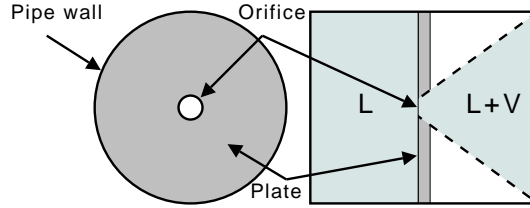


Figure 3.7: The expansion valve illustrated as an orifice. The refrigerant is liquid upstream and two-phase downstream.

$$P_c + \frac{1}{2} \cdot \rho_c \cdot v_p^2 = P_e + \frac{1}{2} \cdot \rho_e \cdot v_o^2 \quad (3.20)$$

where:

- P_c is the condenser pressure [bar]
- P_e is the evaporator pressure [bar]
- ρ_c is the upstream refrigerant density [kg/m³]
- ρ_e is the downstream refrigerant density [kg/m³]
- v_p is the refrigerant velocity in the pipe [m/s]
- v_o is the refrigerant velocity in through the orifice [m/s]

Assuming known cross section areas equation (3.20) can be written in terms of volume flow. The volume flow is defined in equation (3.21)

$$\dot{V} = v \cdot A \quad (3.21)$$

where:

- \dot{V} is the refrigerant volume flow [m³/m]
- v is the refrigerant velocity [m/s]
- A is the cross section areas [m²]

The volume flow is assumed constant at this point ($\dot{V} = \dot{V}_o = \dot{V}_p$), so is the density ($\rho = \rho_e = \rho_c$) although the refrigerant is subject to a partly phase change. Inserting equation (3.21) into (3.20) yields equation (3.22).

$$P_c + \frac{1}{2} \cdot \rho \cdot \left(\frac{\dot{V}}{A_p} \right)^2 = P_e + \frac{1}{2} \cdot \rho \cdot \left(\frac{\dot{V}}{A_o} \right)^2 \quad (3.22)$$

where:

- A_p is the cross section area of the pipe [m²]
- A_o is the cross section area of the orifice [m²]

3.2. ELECTRONIC EXPANSION VALVE

It is now possible to find the pressure drop across the orifice. The pressure drop is calculated in equation (3.23).

$$\Delta P = P_c - P_e = \frac{1}{2} \cdot \rho \cdot \left(\frac{\dot{V}^2}{A_o^2} - \frac{\dot{V}^2}{A_p^2} \right) \quad (3.23)$$

Solving equation (3.23) for the volume flow.

$$\dot{V} = \sqrt{\frac{1}{1 - \frac{A_o^2}{A_p^2}}} \cdot A_o \cdot \sqrt{\frac{2 \cdot \Delta P}{\rho}} \quad (3.24)$$

The massflow can then be found by multiplying equation (3.24) with the refrigerant density.

$$\dot{m} = C \cdot A_o \cdot \sqrt{2 \cdot \rho \cdot \Delta P} \quad (3.25)$$

$$C = \sqrt{\frac{1}{1 - \frac{A_o^2}{A_p^2}}} \quad (3.26)$$

Simulations have shown that, for $A_o < 0.4 \cdot A_p$, $C \cdot A_o$ is quite linear with A_o , see figure

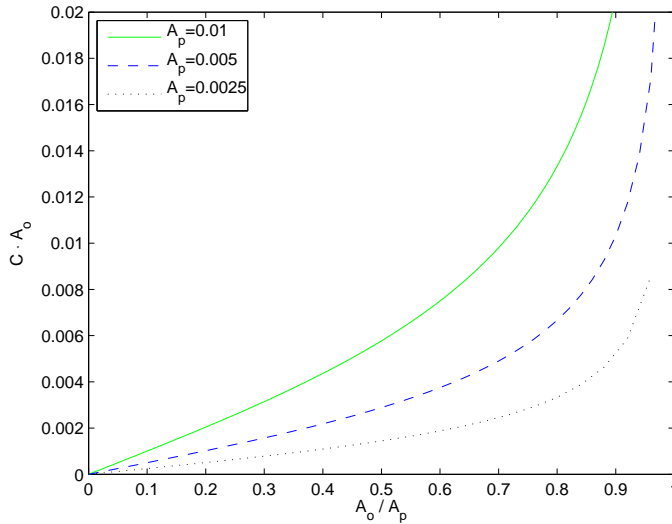


Figure 3.8: For $A_o < 0.4 \cdot A_p$, C is approximately constant.

3.8. Assuming $A_o < 0.4 \cdot A_p$, C can be approximated by a constant.

$$\dot{m} = C \cdot A_o \cdot \sqrt{2 \cdot \rho \cdot \Delta P} \quad (3.27)$$

The work of [Petersen & Lund, 2004, p. 60] suggests a squared relationship between the control signal u_{exv} and the flow \dot{m}_r . Hence the orifice area, A_o , in equation (3.27) is substituted by u_{exv}^2 . The constant C is renamed K as it has to include other factors which has to be estimated. The resulting equation can be seen in equation (3.28).

$$\dot{m}_r = K \cdot u_{exv}^2 \cdot \sqrt{\Delta P} \quad (3.28)$$

3.2.1 Verification

The value of K is estimated through experiments and should be constant for the model to be valid. The plant should be excited with different expansion valve control signals (u_{exv}) and different pressure drops across the expansion valve.

Appendix B describes the experiments performed and estimates the value of K to 0.0152. The appendix also describes the issue of occasional inconsistency between measured and calculated flow. Figure 3.9 is a plot of some of the results.

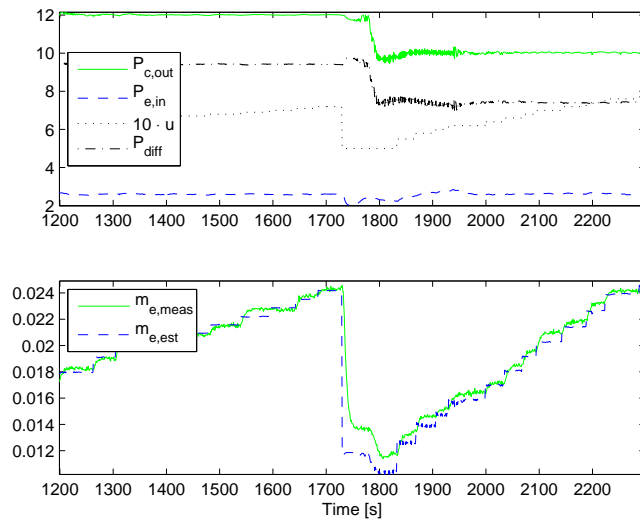


Figure 3.9: Steps on expansion valve, measured and estimated flow.

3.2.2 Summary

The flow through the expansion valve primarily depends on the pressure drop and the control signal. The relationship has been modeled using the Bernoulli Equation and different assumptions about the behaviour of the refrigerant and the valve. All the unknown parameters have been collected in a single constant, whose value has been estimated by experiments. The same experiments revealed sudden changes in the control signal / refrigerant flow relationship, often triggered by operation of the solenoid valve.

3.3 Compressor

In this section concerns the development of a model of the compressor. The model describes the mass flow of refrigerant through the compressor. After the model of the compressor is verified, it is used to calculate the evaporator pressure. The following is largely based on [Guntoft & Laurtisen, 2003]. The ideal volume flow of a reciprocating compressor is the piston displacement times the rotational speed

$$\hat{V}_{com} = V_{com} \cdot \omega_{com} \quad (3.29)$$

3.3. COMPRESSOR

where:

- ω_{com} is the compressor rotational speed [s^{-1}]
- V_{com} is the compressor piston displacement [l]

However this does not hold and the rate of delivery is introduced to express the relationship between the actual and the ideal volume flow.

$$\lambda = \frac{\dot{V}_{com}}{\hat{V}_{com}} \quad (3.30)$$

where:

- λ is the rate of delivery [-].

It is possible to calculate the value of λ based on performance data of the compressor. The following is based on [Guntoft & Laurtisen, 2003, p. 100]. The compressor performance data describes a cooling capacity at known condenser and evaporator temperatures. Assuming zero subcool the enthalpy of the refrigerant flow into the evaporator equals the enthalpy at the bubbling point at the condenser pressure. The enthalpy of the refrigerant flow out of the evaporator is known given the evaporator pressure and a measure of the superheat. The cooling capacity per kilogram of refrigerant is given as

$$\Delta h = h_o - h_i \quad (3.31)$$

The performance data of compressor specifies a cooling capacity \dot{Q}_0 . The required refrigerant flow to provide the cooling capacity can be calculated by

$$\dot{m}_r = \frac{\dot{Q}_0}{\Delta h} \quad (3.32)$$

If the temperature and pressure of the refrigerant into the compressor is known it is possible to calculate the density of the refrigerant. The density can be used to calculate the volume flow.

$$\dot{V}_{com} = \frac{\dot{m}}{\rho} \quad (3.33)$$

By inserting equation (3.33) and (3.29) into (3.30) it is possible to calculate the rate of delivery based on the performance data of the compressor. The performance data of the compressor is given for a number of different evaporator and condenser temperatures. Figure 3.10 shows the calculated rate of delivery based on the available performance data. The mass flow can now be calculated by multiplying equation (3.29) with the density and the rate of delivery

$$\dot{m}_{com} = \rho \cdot \lambda \cdot V_{com} \cdot \omega_{com} \quad (3.34)$$

The rotational speed is controlled by a frequency drive, whose frequency is determined by equation (3.35). According to its datasheet, the compressor takes 2900 RPM at 50 Hz input, yielding equation (3.36).

$$f_{com} = 35s^{-1} + 2.5s^{-1} \cdot u_{com} \quad (3.35)$$

$$\omega_{com} = f_{com} \cdot 0.967 \quad (3.36)$$

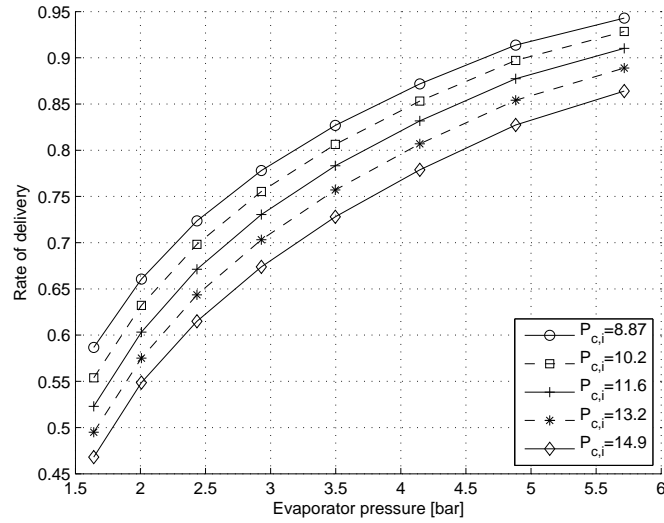


Figure 3.10: The rate of delivery at different evaporator and condenser pressures.

3.3.1 Verification

In order to verify the mass flow model an experiment was performed on the system, where the compressor speed and refrigerant inflow was changed in steps. Figure 3.11 shows the steps in compressor speed and refrigerant flow and how this resulted in changes in the superheat. It is clear that it takes some time after a change before the system reach steady state. Figure 3.12 shows the measured refrigerant inflow and the calculated refrigerant flow through the compressor. The refrigerant inflow and refrigerant flow through the compressor should be equal when the superheat is constant. As it can be seen from the figure, the inflow refrigerant is almost the same as the flow through the compressor, however they deviate somewhat, especially after 4000 seconds. The refrigerant flow through the compressor can now be calculated, but more important the evaporator pressure can also be calculated using equation (3.34) if \dot{m}_{com} is known. It has been shown that $\dot{m}_{com} = \dot{m}_r$ is a good assumption in steady state. Rewriting equation (3.34) using this assumption and a more strict notation yields

$$\dot{m}_{com} = \rho_{(P_{e,o}, T_{e,o})} \cdot \lambda_{(P_{e,o}, P_{c,i})} \cdot V_{com} \cdot \omega_{com} \quad (3.37)$$

It should now be possible find the evaporator pressure as a function of refrigerant flow (\dot{m}_r) and the compressor speed (ω_{com}). This can later be used to derive the model gain $dPe/d\dot{m}$ and $dPe/d\omega_{com}$ which is needed to control the system. There is however one problem, the refrigerant density ρ is an 'unknown' function of pressure and temperature i.e. available through a 'blackbox' function or as a lookup table. The value of λ is a function of evaporator and condenser pressure and available as a interpolation of a lookup table. It is therefore not possible to algebraic solve equation (3.37). It is however possible to numerical find the evaporator pressure in a least square sense.

$$\min_{P_{e,o}} \left| \dot{m}_{com} - (\rho_{(P_{e,o}, T_{e,o})} \cdot \lambda_{(P_{e,o}, P_{c,i})} \cdot V_{com} \cdot \omega_{com}) \right| \quad (3.38)$$

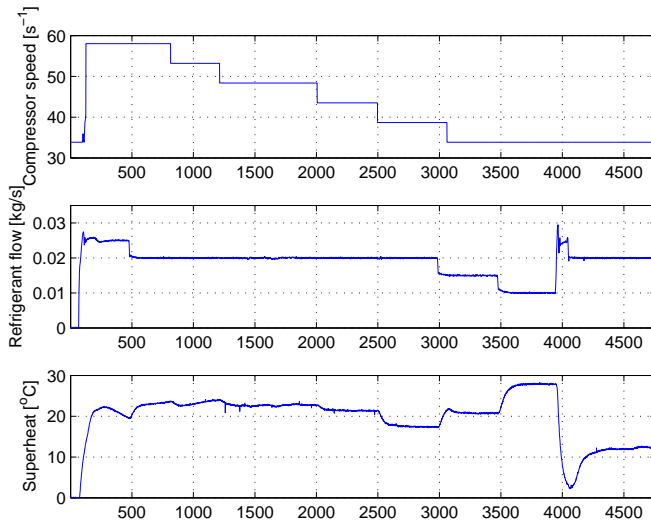


Figure 3.11: Measured compressor speed, refrigerant flow and superheat

Figure 3.13 shows the calculated pressure and the measured pressure of the data set shown in figure 3.11. It can be seen from the figure that the calculated pressure overall fits the measured pressure.

Later in this thesis an algebraic expression is needed to simplify calculations. A good approximation is possible using equation (3.39) [Rasmussen, 2008].

$$P_{e,o} = \frac{\dot{m}_{com}}{\alpha \cdot \omega_{com}} \quad (3.39)$$

where:

α is a system constant [kg/bar]

Figure 3.14 shows the pressure calculated using equation (3.39) with a α -value of $1.8 \cdot 10^{-4}$. The figure also shows the measured pressure and the pressure calculated using equation (3.37) (same as in figure 3.13). It can be seen from the figure that the pressure calculated numerically is closer to the measured pressure than the algebraically calculated pressure. This is expected since the algebraic equation is much simpler.

3.3.2 Summary

The refrigerant flow through the compressor has been modelled. The flow primarily depends on the control signal to the compressor, the refrigerant density and the rate of delivery. The rate of delivery is a measure of how efficient the compressor can pump the refrigerant. E.g. at high pressure differences over the compressor, the rate of delivery is low and the flow is reduced. Both a numerical and an algebraic expression for the mass flow is presented. The numerical expression is more accurate than the algebraic expression, but is harder to utilise in the control design.

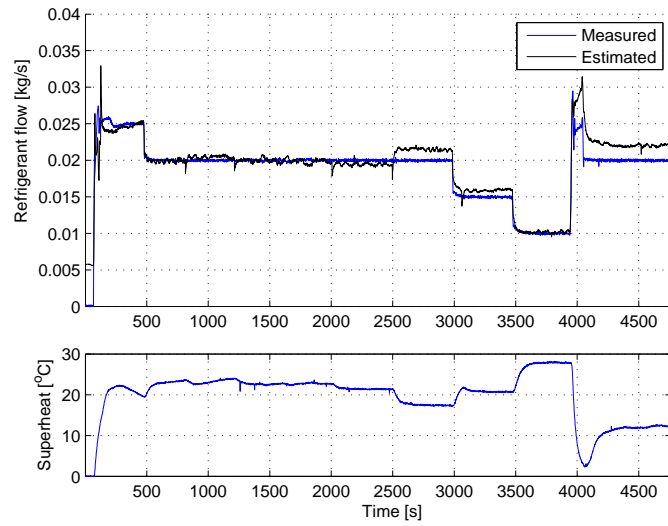


Figure 3.12: Estimated and measured refrigerant flow.

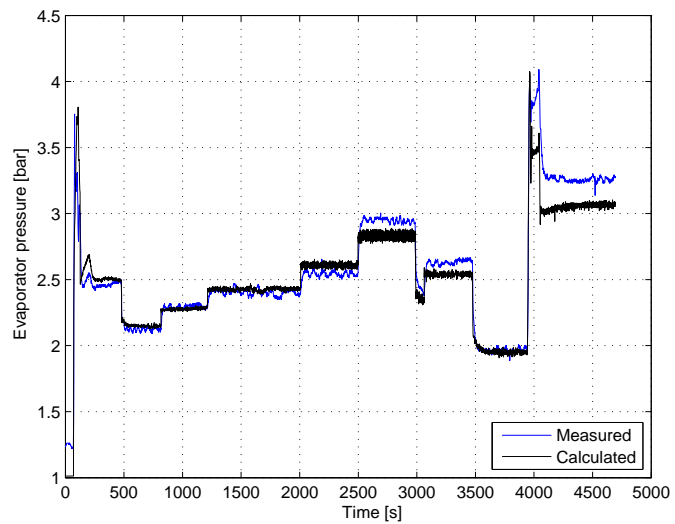


Figure 3.13: Measured and calculated evaporator pressure.

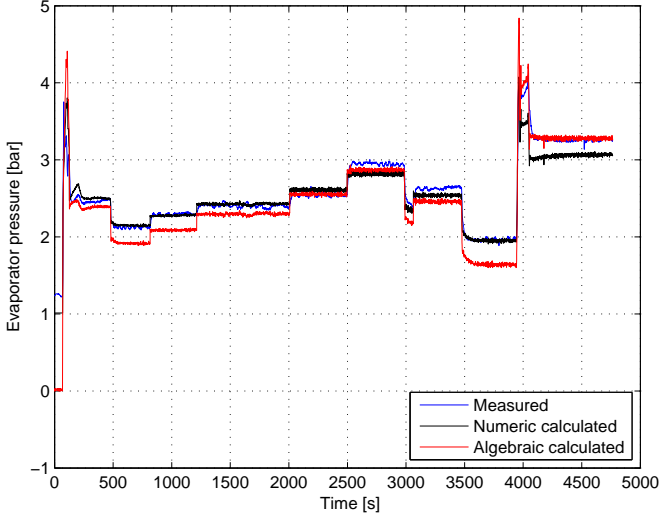


Figure 3.14: Measured and calculated evaporator pressures.

3.4 Condenser

A makeshift PI regulator of the condenser fan has been implemented to keep the condenser pressure constant. As the condenser is outside the main scope of this project, it will not be modelled.

3.5 Water Tank

This section concerns the development of a model of the water temperature. The water temperature is a function of the heat energy added by the load and the heat energy removed by the cooling process. Figure 3.15 and equations (3.40) and (3.41) illustrates an assumption about the relationship between load, cooling, time and water temperature. Besides gains and time constants it contains time delays to reflect the transportation of the water and integration to reflect the accumulation of energy.

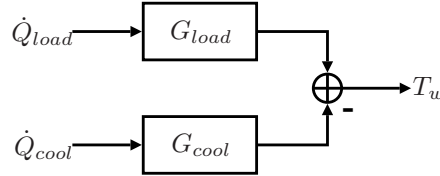


Figure 3.15: Water tank model with separate inputs.

$$G_{load}(s) = c_l \cdot \frac{e^{-\tau_d, l \cdot s}}{s + \tau_l \cdot s^2} \quad (3.40)$$

$$G_{cool}(s) = c_c \cdot \frac{e^{-\tau_d, c \cdot s}}{s + \tau_c \cdot s^2} \quad (3.41)$$

where:

c are the power to temperature gains (inverse heat capacity) [kg/J]

τ_d are the time delays [s]

τ are the time constants [s]

\dot{Q}_{load} is the rate of energy added to the water [W]

\dot{Q}_{cool} is the rate of energy removed from the water [W]

If the responses to \dot{Q}_{load} and \dot{Q}_{cool} can be assumed equal the model can be simplified by considering the resulting energy rate, see figure 3.16 and equation (3.42).



Figure 3.16: Water tank model with combined input.

$$G_{tank}(s) = c \cdot \frac{e^{-\tau_d \cdot s}}{s + \tau \cdot s^2} \quad (3.42)$$

$$\dot{Q}_{net} = \dot{Q}_{load} - \dot{Q}_{cool} \quad (3.43)$$

3.5. WATER TANK

where:

\dot{Q}_{net} is the resulting energy rate [W]

Table 3.1 lists the parameters from equation (3.42) fitted to different measurements. The first two columns are steps in the cooling capacity with no load. The first is the response at the temperature sensor just after the evaporator while the second is the response just before the evaporator, i.e. through the water tank. The next two are two different measurements with no cooling and multiple or a single step in the load respectively. The last column is the average parameter values. The figures 3.17 and 3.18 shows plots of

Parameter	cool-TT07	cool-TT08	heat-TT07	heat-TT07	Average
c	$3.9 \cdot 10^{-6}$	$3.95 \cdot 10^{-6}$	$3.15 \cdot 10^{-6}$	$3.45 \cdot 10^{-6}$	$3.6 \cdot 10^{-6}$
τ_d	0	60	30	70	40
τ	0	20	355	215	148

Table 3.1: Model parameters.

the water temperature during the measurements associated with column two and four of table 3.1 respectively. Both plots features the measured temperature, the temperature estimated from the fitted parameters and the temperature estimated from the average parameters. Notice how the average parameters results in increasing errors. This is due to small errors being integrated up. Fortunately the water tank model is not used for water temperature estimation, but its dynamics are used for controller parameter tuning. Figure 3.19 is a similar plot of a measurement with both cooling and heating. The estimated temperature uses the average parameters, but the gain from u_{heat} to \dot{Q}_{load} was changed from 600 to 610 to give the correct balance in \dot{Q}_{net} .

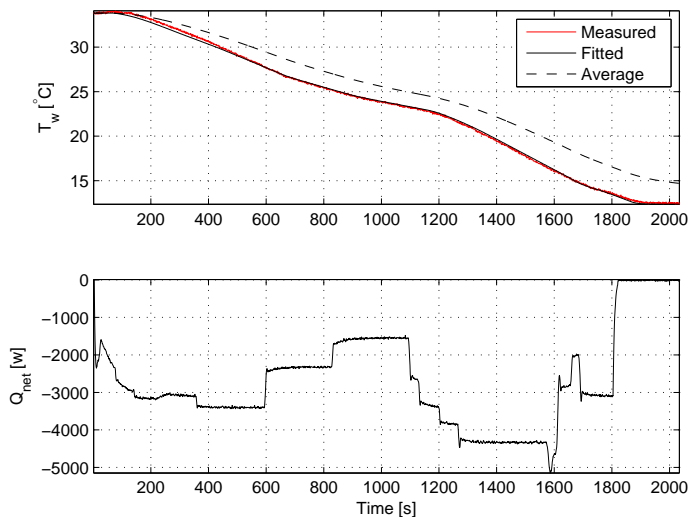


Figure 3.17: Water temperature (TT08) during varying cooling capacity.

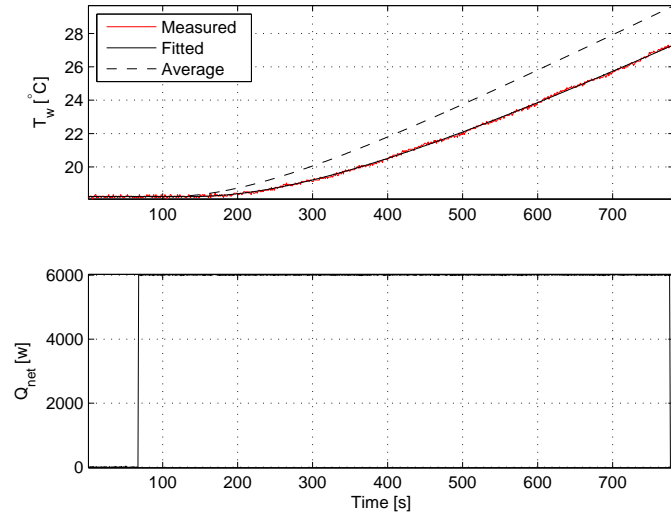


Figure 3.18: Water temperature (TT07) during steady heating.

3.5.1 Water Tank Summary

The water tank contains the cooled medium, the water. The temperature can be manipulated by both the load from the water heater and the cooling in the evaporator. The response to these inputs depends on both which input is actuated and where the temperature is measured. For simplicity the developed model only has one input: the difference between the two actual inputs. The model parameters are found by averaging parameters fitted to the different possible system responses. Due to the integrating nature of the water temperature and the error introduced by the simplification, this model is not reliable for temperature estimation, but describes the water temperature dynamics well.

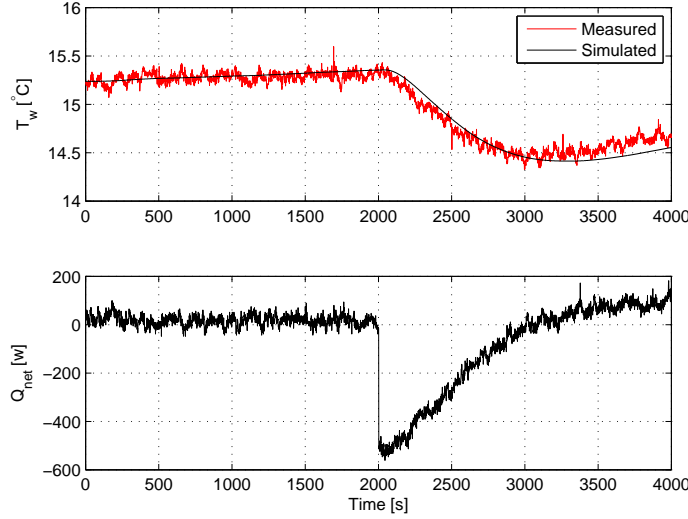


Figure 3.19: Water temperature (TT08) during 'normal' operation.

3.6 Superheat Gain Analysis

This section utilise the developed models of the system to derive the gain from the compressor speed to the superheat. The gain is then evaluated in normal working conditions. The gain is defined as

$$gain = \frac{\partial T_{sh}}{\partial \omega_{com}} \quad (3.44)$$

From the superheat equation (3.13) the gain can be derived as

$$\frac{\partial T_{sh}}{\partial \omega_{com}} = \frac{\partial T_{sh}}{\partial T_e} \cdot \frac{\partial T_e}{\partial P_{e,o}} \cdot \frac{\partial P_{e,o}}{\partial \omega_{com}} + \frac{\partial T_{sh}}{\partial x_e} \cdot \frac{\partial x_e}{\partial T_e} \cdot \frac{\partial T_e}{\partial P_{e,o}} \cdot \frac{\partial P_{e,o}}{\partial \omega_{com}} \quad (3.45)$$

$$\frac{\partial T_{sh}}{\partial \omega_{com}} = \frac{\partial T_e}{\partial P_{e,o}} \cdot \frac{\partial P_{e,o}}{\partial \omega_{com}} \left(\frac{\partial T_{sh}}{\partial T_e} + \frac{\partial T_{sh}}{\partial x_e} \cdot \frac{\partial x_e}{\partial T_e} \right) \quad (3.46)$$

The first part describes how the change in evaporator pressure and evaporation temperature affects the superheat. The last part describes how the change in pressure and evaporation temperature affects the superheat through changes in the filling of the evaporator. The refrigerant mass flow can be estimated using equation (3.47).

$$\dot{m}_r = \alpha \cdot \omega_{com} \cdot P_{e,o} \quad (3.47)$$

yielding

$$\frac{\partial P_{e,o}}{\partial \omega_{com}} = -\frac{\dot{m}_r}{\alpha \cdot \omega_{com}^2} \quad (3.48)$$

The evaporation temperature at a given pressure can be found using [Skovrup, 2001] as $T_e = T_{bub}(P_{e,o})$. The exact function is unknown, but as figure 3.20 shows, the second order function in equation (3.49) is a good approximation.

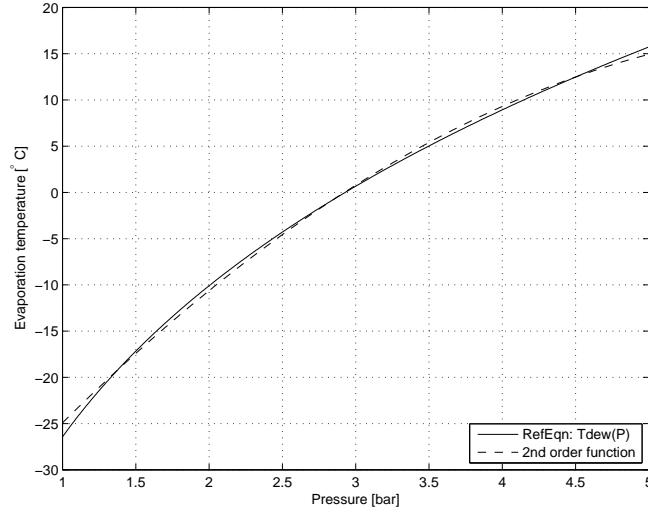


Figure 3.20: Output from RefEqn's T_{bub} function and fitted function.

$$T_e = T_{bub}(P_{e,o}) \approx -1.44P_{e,o}^2 + 18.62P_{e,o} - 42.11 \quad (3.49)$$

which yields

$$\frac{\partial T_e}{\partial P_{e,o}} = -2.88P_{e,o} + 18.62 \quad (3.50)$$

Calculating the partial derivative $\partial T_{sh}/\partial T_r$ from equation (3.13) yields

$$\frac{\partial T_{sh}}{\partial T_e} = \left(e^{\frac{\sigma x_e}{c_r m_r}} - e^{\frac{\sigma}{c_r m_r}} \right) e^{\frac{-\sigma x_e}{c_r m_r}} \quad (3.51)$$

Again using the superheat equation, (3.13), the partial derivative $\partial T_{sh}/\partial x_e$ yields

$$\frac{\partial T_{sh}}{\partial x_e} = \frac{-\sigma(T_e - T_w)e^{\frac{\sigma}{c_r m_r} - \frac{\sigma x_e}{c_r m_r}}}{c_r m_r} \quad (3.52)$$

Finally the partial derivative $\partial x_e/\partial T_e$ must be calculated. Since we are not interested in the time continuous description of x_e but only the steady state gain, it is possible to use equation (3.19). The partial derivative yields

$$\frac{\partial x_e}{\partial T_e} = \frac{m_r(H_g - H_i)}{c_2(T_e - T_w)^2} \quad (3.53)$$

Using equation (3.48) and (3.50)-(3.53) it is now possible to calculate the gain $\partial T_{sh}/\partial \omega_{com}$ in any system state.

In the later superheat controller design process it is beneficial to have information about the gain in the reachable states of the system. E.g. if the gain is almost constant it might be possible to design a simple controller. In the following the constraints of the system states are calculated given information about the external environment. It is assumed that

3.6. SUPERHEAT GAIN ANALYSIS

- Inlet water temperature is known ($T_{w,i}$).
- Ambient temperature is known (T_a).
- Minimum temperature difference between inlet water temperature and evaporation temperature is known (ΔT).
- Negligible heat transfer in the superheat section.

Furthermore the test rig absolute maximum and minimum values are maintained i.e.

- Maximum condenser pressure: 15 bar
- Minimum evaporator pressure: 1.6 bar
- Maximum evaporator pressure: 4.9 bar
- Minimum compressor speed: 35 Hz
- Maximum compressor speed: 60 Hz

It is now possible to find the extreme evaporator pressure levels

$$P_{e,o,min} = 1.6 \quad (3.54)$$

$$P_{e,o,max} = P_{bub}(T_{w,i} - \Delta T) \quad (3.55)$$

The maximum pressure level corresponds to the evaporation temperature given by the water inlet temperature and the ΔT temperature. The extreme values of the compressor speed are known. It is therefore possible to calculate the resulting refrigerant flow bounded by the extreme values of the evaporator pressure and compressor speeds using equation (3.47).

Since the energy transfer in the superheat section is assumed neglectable the enthalpy of the refrigerant out of evaporator is found by assuming zero superheat. It can then be calculated as a function of the evaporator pressure. The enthalpy of the refrigerant into the evaporator is lower bounded by assuming that the refrigerant is on liquid phase and subcooled down to the ambient temperature. The upper bounded value is the saturation enthalpy at maximum condenser pressure.

The idea is to numerically loop through all the combinations of evaporator pressure, compressor speed and inflow enthalpy. For each set of values the refrigerant flow is calculated using equation (3.47). The filling of the evaporator is then calculated using equation (3.19). If the filling is less than unity, the gain $\partial T_{sh} / \partial \omega_{com}$ for the set of values is calculated using the previously described method. If the filling is more than unity the set of values is not valid.

Figure 3.21 shows an example of the calculation using the following values $T_{w,i} = 15$, $T_a = 30$ and $\Delta T = 10$ degrees. The upper left part of figure 3.21 shows the refrigerant flow with minimum inflow refrigerant enthalpy. The lower left shows the corresponding gain. The right part of the graph shows the same but with the maximal inflow refrigerant enthalpy. The maximum gain is 2.78 and the minimum is 0.36

Figure 3.22 shows a similar figure, however the filling level is not used as the constraint. In this figure only states resulting in a superheat between 10 and 15 degrees are plotted as it can be seen the valid states are quite limited. The maximum gain is 2.61 and the minimum is 0.92

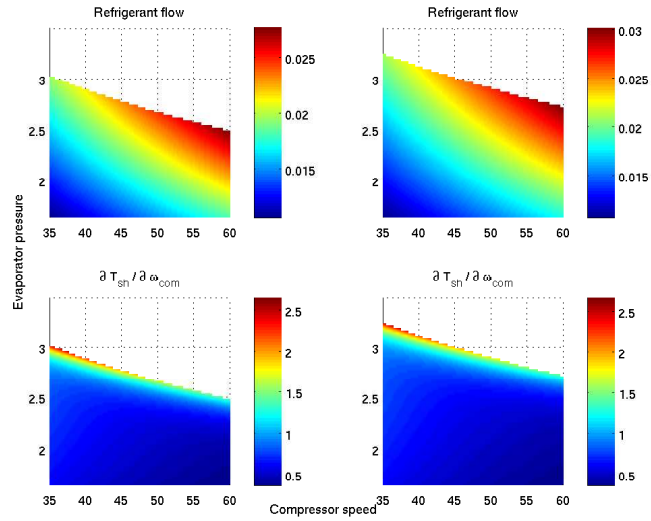


Figure 3.21: Refrigerant flow and gain $\partial T_{sh} / \partial \omega_{com}$. Only working points with $x_e < 1$ are shown.

3.6.1 Summary

The developed system models are used to calculate the compressor to superheat gain. The gain is found to be between 0.36 and 2.78 for all valid working points. Limiting the working point to those found during normal operation i.e. with superheat levels higher than 10 and lower than 15 degrees the gain is between 0.92 and 2.61. This information can be used when designing the controllers.

3.6. SUPERHEAT GAIN ANALYSIS

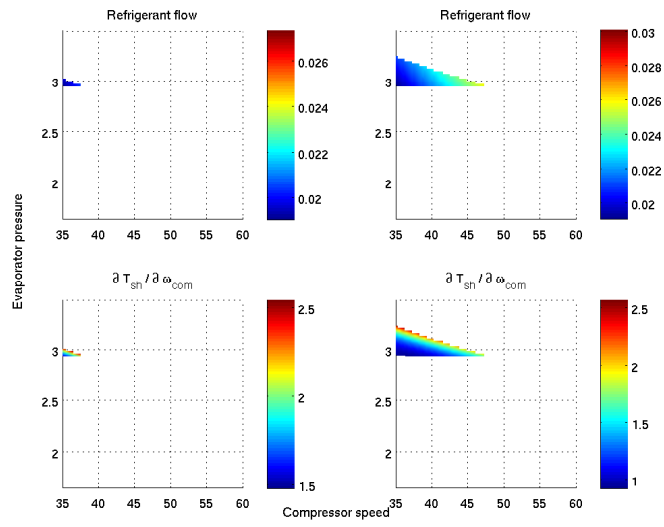


Figure 3.22: Refrigerant flow and gain $\partial T_{sh} / \partial \omega_{com}$. Only working points with $10 < T_{sh} < 15$ are shown.

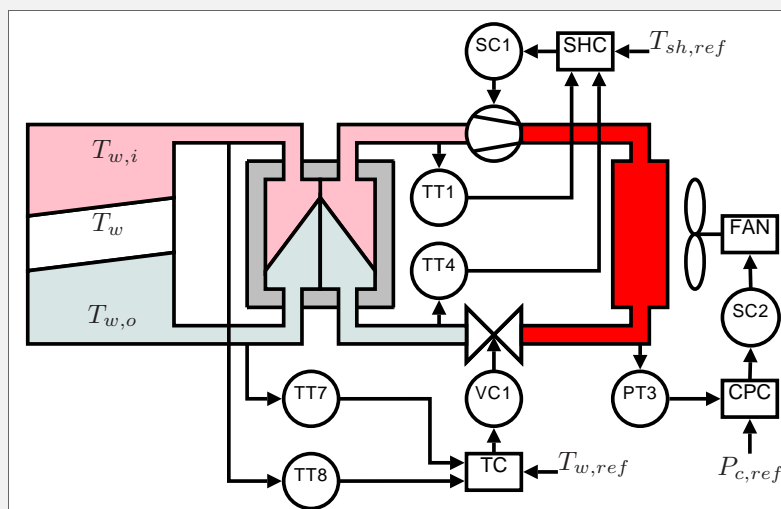
Chapter 4

Controller Design

This chapter covers the design of the controllers, which will implement the control paradigm described in the thesis (section 1.5 on page 18). The first section features a brief overview of the three primary control tasks and the difference between the new and classic control strategy. The control strategy is broken down into three controllers which are described in the following three sections. Experiments are used to validate the controller designs and tune the controller constants. The final section wraps up the chapter with an overall description of the controller performance.

Resume:

A new control strategy is suggest, where the superheat is controlled using the compressor and the cooling capacity is controlled using the electronic expansion value. The next figure illustrates the controller strategy.



It consists of a feedback loop and a model-based feedforward loop. The feedforward is used to calculate the evaporation temperature needed to reach the reference superheat level. The evaporator model is

$$c_1 \frac{dx_e}{dt} = \dot{m}_e(h_o - h_i) - c_2(T_w - T_e)x_e$$

In steady state it is possible to calculate the evaporator filling as

$$x_e = \frac{\dot{m}_r(h_o - h_i)}{c_2(T_w - T_e)}$$

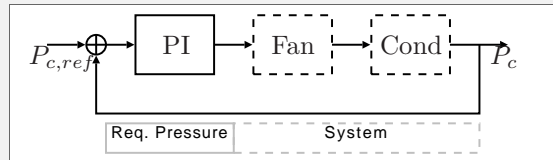
This expression can then be inserted into

$$T_{sh} = (T_w - T_e) \left(1 - e^{-\frac{\sigma(1-x_e)}{C_r \dot{m}_e}} \right)$$

Solving for T_e yields the evaporation temperature which is need to obtain a given superheat level. This function is denoted $f_{te}()$. The remaining part of the feedforward calculates the evaporator pressure given by the evaporation temperature. The compressor speed needed to reach the pressure is the last part of the feedforward. A standard PI controller is used as feedback.

Condenser Pressure controller

The condenser pressure is controlled by the condenser fan. A higher condenser fan speed will provide better cooling of the refrigerant and the pressure will drop. The next figure illustrate the implemented PI controller.



4.1 Controller Strategy

The thesis suggested a new approach to controlling the refrigeration system. Figure 4.1 illustrates the overall control of the refrigeration rig for both the classic and the new method. The classic approach uses a thermostatic expansion valve to control the superheat and the compressor to control the cooling capacity. The new approach controls the superheat using the compressor and the capacity using an electronic expansion valve.

The controllers includes more inputs to improve performance and properly utilise the models. The three new controllers are:

TC The temperature controller calculates the required cooling capacity from the error between the desired temperature ($T_{w,ref}$) and the estimated temperature of the cooled goods (T_w). The value of T_w might be estimated as $T_{w,i}$, $T_{w,o}$ or a combination depending on the application. The cooling capacity depends on the rate of evaporation, hence TC controls the flow of refrigerant through the expansion valve to the evaporator.

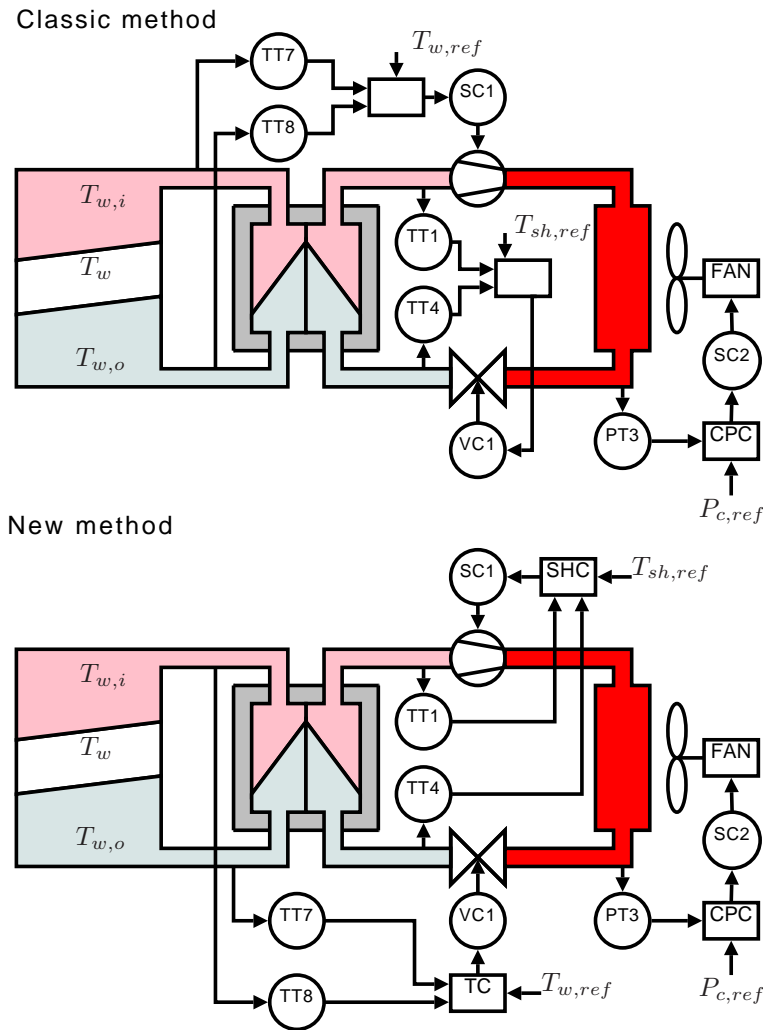


Figure 4.1: Overview of the classic and new controller strategy.

SHC The superheat controller regulates the compressor speed to keep the superheat at the reference level ($T_{sh,ref}$). In the design process feedforward is included from the flow controller to the superheat controller to archive better performance and disturbance rejection.

CPC The condenser pressure controller keeps the condenser pressure constant by regulating the condenser fan.

4.2 Temperature Controller (TC)

This section concerns the water temperature controller. The water temperature controller determines how much cooling capacity is needed to reach and hold the desired water temperature ($T_{w,ref}$), this is the topic of the first subsection. Some applications may benefit from determining the the required cooling capacity from other sources e.g.

an operator set constant or some supervisor. The second subsection describes the conversion from required cooling capacity to required refrigerant flow. Hereafter a subsection deals with realising the required flow through control of the electronic expansion valve (EXV). The expansion valve controller features both model-based feedforward and classic feedback. The expansion valve controller constitutes an inner cascaded loop. Figure 4.2 shows an overview of the temperature controller.

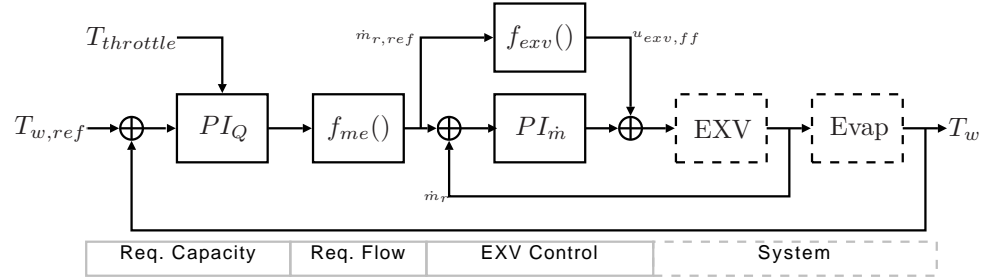


Figure 4.2: Temperature controller overview.

4.2.1 Required Cooling Capacity

The water temperature (T_w) is to be controlled by regulating the cooling capacity (\dot{Q}_{cool}) while the load (\dot{Q}_{load}) is an unknown, 'steady' disturbance. The drift introduced by the load and the fact that \dot{Q}_{cool} is constrained by the limits of the setup (approximately the range between 1000 and 7000 Watt) makes it a nonlinear system. The regulator is based on feedback of the measured water temperature, as seen in figure 4.2. The regulator parameters are tuned to the simplified water tank model developed in section 3.5 on page 41, see equation (4.1). As the actual load is unknown to the temperature controller, the value of \dot{Q}_{net} is found using a working point (\dot{Q}_{wp}) which approximates the load.

$$G_{tank}(s) = c \cdot \frac{e^{-\tau_d \cdot s}}{s + \tau \cdot s^2} \quad (4.1)$$

$$\dot{Q}_{net}(t) = \dot{Q}_{wp}(t) - \dot{Q}_{cool}(t) \quad (4.2)$$

where:

- \dot{Q}_{net} is the resulting energy rate [W]
- \dot{Q}_{wp} is the working point [W]
- c is the power to temperature gain ($3.6 \cdot 10^{-6}$) []
- τ_d is the time delay (40) [s]
- τ is the time constant (148) [s]

Figure 4.3 is a root locus plot of equation (4.1) with unit feedback and varying proportional gain. The time delay is approximated by a third order Pade Approximation. Using `sisotool` this approximated, linearised system is found to be stable up to a proportional gain of 7000. The phase margin is 45 degrees at 1550, where the gain margin is 13 dB.

The working point has to track the load for the resulting energy rate assumption (\dot{Q}_{net}) to be valid. The leftmost plot in figure 4.4 on the following page shows a simulation

4.2. TEMPERATURE CONTROLLER (TC)

of the linearised system with a proportional gain of 1500 and \dot{Q}_{cool} saturated to 7000 W. The initial temperature ($T_{w,0}$) is 20 °C and the temperature reference ($T_{w,ref}$) is 14 °C. The working point (\dot{Q}_{wp}) is fixed at 3500 W, the load starts at 3500 W but steps to 3000 W at 5000 s. This clearly introduces a temperature offset, as expected when using a P controller with limited gain. If one has a good guess of the load, the temperature offset is likely to be acceptable.

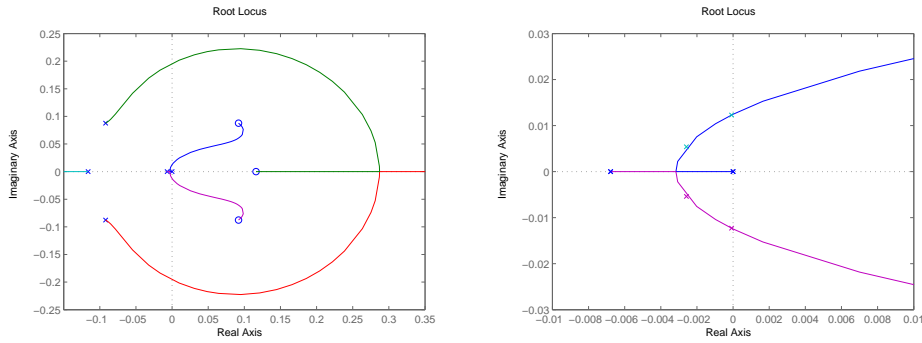


Figure 4.3: Root locus, proportional gain, $K = 1500$ and 7000 marked. The figure to the right is a zoomed version of the figure on the left.

On the other hand it is possible to let \dot{Q}_{wp} automatically track \dot{Q}_{load} . One solution is to integrate the temperature error to get a working point with no temperature offset, i.e. the true working point. The integral effect can be achieved by using a PI controller, see equation (4.3).

$$K_p + K_i \cdot \frac{1}{s} \Rightarrow K_p \cdot \frac{\frac{K_i}{K_p} + s}{s} \quad (4.3)$$

Again using `sisotool` the system was tuned to 45 degrees P.M., giving a 21 dB G.M. and requiring a proportional gain of 550 and an integral gain of 0.49. The rightmost plot in figure 4.4 shows a simulation identical to the previous, but with integral action and $K_p = 500$, $K_i = 0.5$ (P.M.:42, G.M.:22). The initial value of the integrator corresponds to the initial load. The new root locus can be seen in figure 4.5.

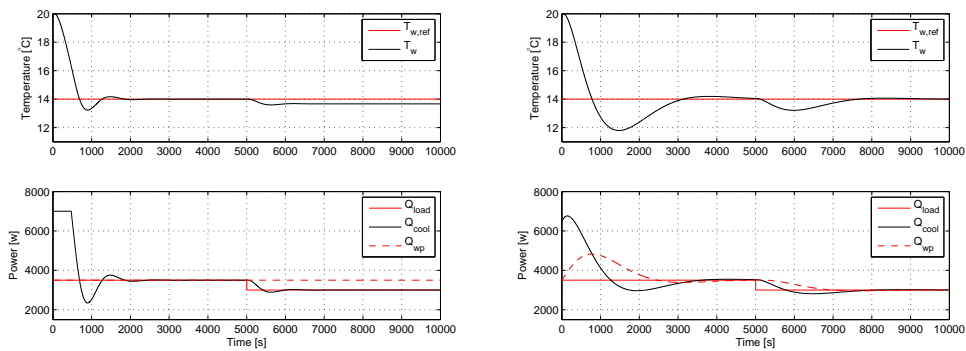


Figure 4.4: Simulations, P / PI regulator, i.e. fixed / tracked working point.

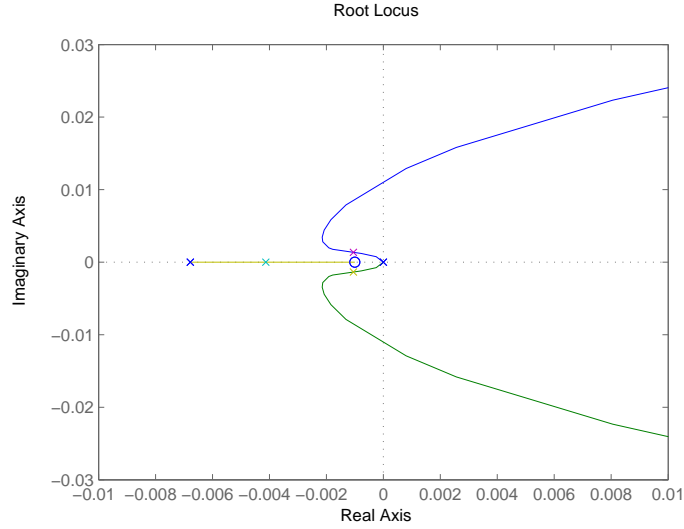


Figure 4.5: Root locus, with extra pole in origo, $K_i = K_p/1000$, $K_p = 500$ marked.

$$T_{w,err} = T_w - T_{w,ref} \quad (4.4)$$

$$\dot{Q}_{wp} = \dot{Q}_{wp,guess} + 0.5 \cdot \int (T_{w,err} + T_{throttle}) \quad (4.5)$$

$$\dot{Q}_{ref} = 500 \cdot T_{w,err} + \dot{Q}_{wp} \quad (4.6)$$

where:

$\dot{Q}_{wp,guess}$ is an initial guess on the cooling capacity [W]
 $T_{throttle}$ is used to prevent the evaporator from flooding []

Equation (4.6) is the developed expression for the required cooling capacity. Contrary to when the superheat (through the refrigerant flow) is regulated by a TXV, this new scheme has no inherent protection against flooding the compressor if the calculated required capacity is beyond the compressors capabilities. In the previous two simulations the cooling capacity was saturated to 7000 W, however the actual limit varies with the operating conditions.

The superheat controller easily detects compressor saturation. This is exploited in a 'throttle' feedback signal from the superheat controller to the capacity calculation. Details are given later in this chapter.

4.2.2 Required Refrigerant Flow

When the required cooling capacity is found it has to be converted to a refrigerant flow so it can be realised by control of the expansion valve.

The relationship between the cooling capacity and the refrigerant flow depends on the different working points of the entire system. Recall figure 1.2 on page 13, repeated in figure 4.6. The gain in enthalpy from [2] to [3] is a measure of how much energy is

4.2. TEMPERATURE CONTROLLER (TC)

absorbed per kg refrigerant, hence it can be used to calculate the refrigerant flow required to absorb energy at a given rate.

The enthalpy gain depends on the two pressures (P_c and P_e), the subcooling and the superheat. With a 8 – 10 bar condenser pressure and a 2 – 3 bar evaporator pressure the enthalpy is approximately increased by 145 ± 9 kJ/kg plus a contribution from the subcool and superheat. For simplicity the capacity to flow factor is held constant at 155 kJ/kg, noting that the integral action in the capacity calculation will compensate the error. The expression can be seen in equation (4.7).

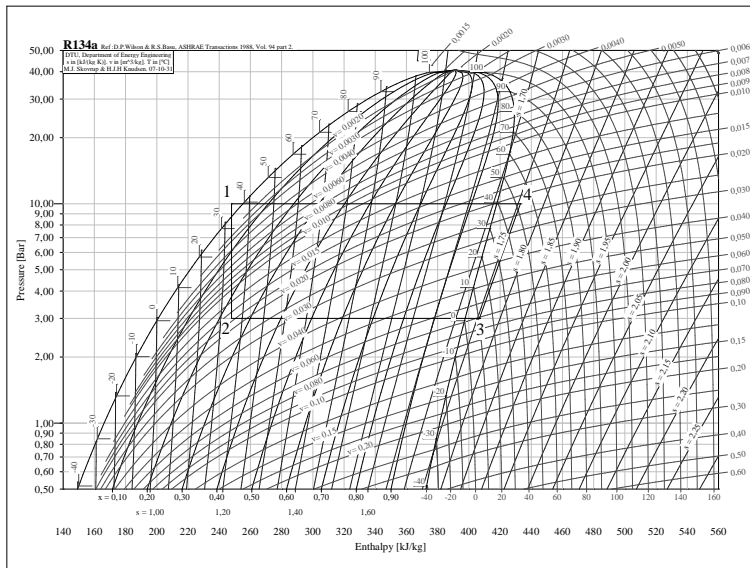


Figure 4.6: Log(p)-H diagram of refrigerant R134a.

$$\dot{m}_{r,ref} = \frac{\dot{Q}_{ref}}{h_o - h_i} = \frac{\dot{Q}_{ref}}{155 \text{ kJ/kg}} \quad (4.7)$$

4.2.3 Expansion Valve Control

The final stage in the temperature controller is responsible of finding the expansion valve control signal resulting in the refrigerant flow calculated from the required cooling capacity. By isolating the control signal in the expansion valve model, found in section 3.2 on page 33, it is possible to do open loop control of the expansion valve, see equation (4.8). Unlike most real refrigeration systems the test rig also measures the actual flow, making an additional feedback loop an option, see equation (4.10).

The combined control signal is saturated to lie in the range 0 – 10 V, as seen in equation (4.11).

$$u_{exv,ff} = \sqrt{\frac{\dot{m}_{r,ref}}{K_{exv} \cdot \sqrt{\Delta P}}} \quad (4.8)$$

$$\dot{m}_{r,err} = \dot{m}_{r,ref} - \dot{m}_{r,meas} \quad (4.9)$$

$$u_{exv,fb} = K_{P,\dot{m}} \cdot \dot{m}_{r,err} + \int (K_{I,\dot{m}} \cdot \dot{m}_{r,err}) \quad (4.10)$$

$$u_{exv} = SAT_0^{10}(u_{exv,ff} + u_{exv,fb}) \quad (4.11)$$

where:

- $u_{exv,ff}$ is the model-based component of EXV control signal [-]
- $u_{exv,fb}$ is the feedback component of EXV control signal [-]
- $K_{P,\dot{m}}$ is the proportional gain for the flow feedback [-]
- $K_{I,\dot{m}}$ is the integral gain for the flow feedback [-]
- ΔP is the pressure difference $P_c - P_e$ [bar]
- K_{exv} is the EXV constant fitted in section 3.2 [-]

The values of $K_{P,\dot{m}}$ and $K_{I,\dot{m}}$ have been hand-tuned to 200 and 10 respectively.

4.2.4 TC Test

The leftmost plot in figure 4.7 shows a measurement of the water temperature controlled with the automatic working point tracking (PI control, equation (4.6)). Similar to the simulations, \dot{Q}_{load} steps from the initial 3500 W to 3000 W at 5000 s. It is evident that the simulated water temperature response, reprinted in the rightmost plot, is close to the measured. The main differences are contributed to the throttling during startup. Where the simulated working point increases while the water temperature is too high, the implemented working point is lowered slightly because the compressor is saturating. The simulated and measured responses to the step in \dot{Q}_{load} are almost identical. The left

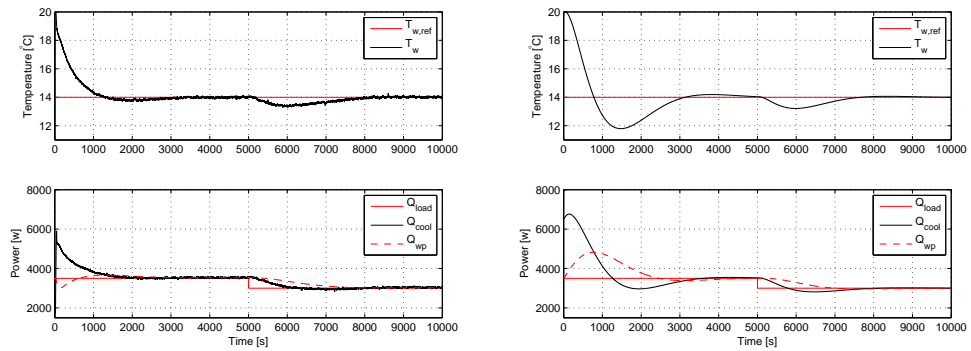


Figure 4.7: Temperature control with \dot{Q}_{wp} tracking, measurement / simulation.

plot of figure 4.8 shows the flow reference and measurement during the step in \dot{Q}_{load} . As seen, the inner loop (EXV controller) tracks the calculated flow reference well. The right plot of figure 4.8 shows the response to a step in the flow reference. From the figures it is clear that the expansion value control is capable of controlling the refrigerant flow.

4.3. SUPERHEAT CONTROLLER (SHC)

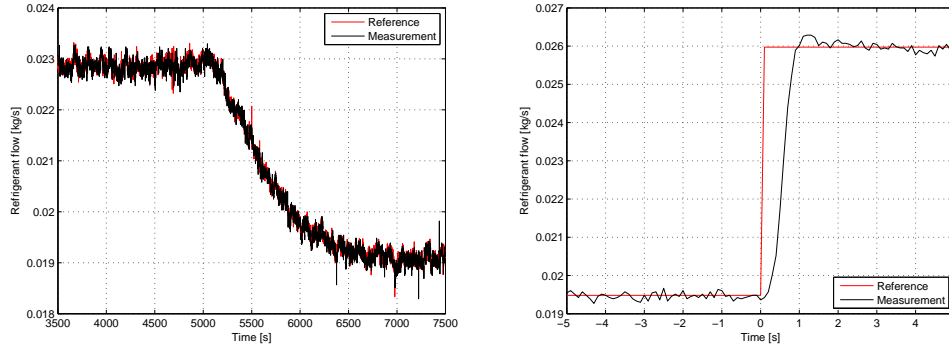


Figure 4.8: Control of the refrigerant, tracking and step response.

4.2.5 TC Summary

The water temperature is controlled by regulating the cooling capacity. The required cooling capacity is calculated by a PI regulator which was tuned to the water tank model. The cooling capacity is obtained by regulating the refrigerant flow, whose reference is calculated proportional to the required cooling capacity. The actual flow is actuated by the EXV, which is controlled by an inner loop consisting of both model-based feedforward and PI feedback. Tests have shown consistency between simulations of the regulated water temperature and actual measurements on the regulated system.

4.3 Superheat Controller (SHC)

The topic of this section is regulation of the superheat. The goals for the superheat controller are as follows:

- Keep T_{sh} near reference.
- Fast convergence after startup and steps in capacity.

The evaporator model and the superheat equation from equation (3.17) and (3.18) on page 29 is for convenience repeated here:

$$\frac{dx_e}{dt} = \frac{\dot{m}_r(h_o - h_i)}{c_1} - \frac{c_2}{c_1}(T_{w,i} - T_e)x_e \quad (4.12)$$

$$T_{sh} = (T_{w,i} - T_r) \left(1 - e^{-\frac{\sigma(1-x_e)}{C_r \dot{m}_r}} \right) \quad (4.13)$$

Assuming a constant (or uncontrollable) water inlet temperature ($T_{w,i}$) and the almost constant values of h_o and h_i and finally that the value of \dot{m}_r is given by the temperature controller, the only method of controlling the filling of the evaporator is by controlling the evaporation temperature. The superheat is a function of both the evaporator filling and the evaporation temperature, hence the superheat must be controlled through the evaporation temperature. The evaporation temperature is a function of the evaporator pressure, which can be controlled by the compressor speed. To ensure optimal efficiency the superheat should be kept as close to the optimal value as possible during normal operation. Efficiency during low capacity operation (start-stop-start-stop) depends on

the controllers ability to quickly bring the superheat to the desired operating point.

An important characteristic of the overall control strategy is that the regulation of the cooling capacity can be considered a disturbance to the required compressor speed.

The disturbance can be suppressed by predicting its influence and feeding it forward, parallel to the feedback-controller. Figure 4.9 illustrates the overall layout of the superheat controller. The use of model-based control (feedforward) reduces the feedback-controller to correcting the model mismatch, hence its performance requirements can be relaxed. This makes it acceptable to have fixed parameters during the entire working area, despite the gain variation documented in section 3.6 on page 44.

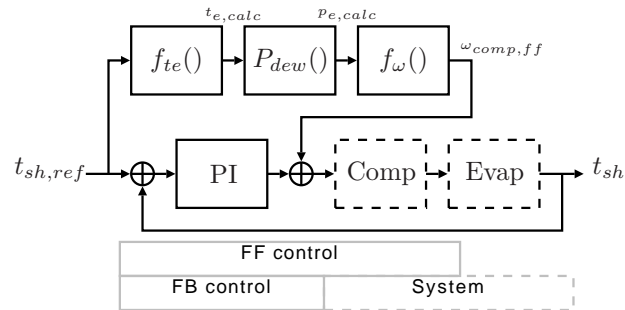


Figure 4.9: Superheat controller overview.

The feedforward and feedback will be described in the following sections.

4.3.1 SHC Feedforward

The purpose of the feedforward is to calculate the compressor speed needed to keep the superheat at a reference level. From equation (4.12) and (4.13) it is possible to solve for the evaporation temperature (T_e), deriving a function (f_{te}). This function calculates the steady state evaporation temperature needed to reach the correct superheat. The inputs to the function are the superheat reference, the water temperature and the refrigerant flow. The calculated evaporation temperature translates to an evaporation pressure which, by rearranging equation (3.39), yields an estimated required compressor speed, see equation (4.16).

$$T_{e,calc} = f_{te}(T_{sh,ref}, T_w, \dot{m}_r) \quad (4.14)$$

$$P_{e,calc} = P_{dew}(T_{e,calc}) \quad (4.15)$$

$$\omega_{com,ff} = \frac{\dot{m}_r}{\alpha \cdot P_{e,calc}} \quad (4.16)$$

where:

- $T_{e,calc}$ is the estimated required evaporation temperature [$^{\circ}C$]
- $P_{e,calc}$ is the estimated required evaporation pressure [bar]
- α is a compressor constant found in section 3.3 [kg/bar]
- $P_{dew}()$ is an interpolated lookup for T_e to P_e conversion [bar]
- $\omega_{com,ff}$ is the model-based component of the compressor speed [Hz]

The compressor speed calculated from equation (4.16) responds to changes in both refrigerant flow and water temperature, before they influence the superheat. The function $f_{te}()$ is derived and validated in appendix D.

4.3.2 SHC Feedback

Although the feedforward responds instantaneous to changes in capacity and water temperature, it results in varying offsets from the superheat reference given varying working points. This is caused by the model not being perfect. A P or PI controller should be able to eliminate or reduce these offsets. The PI feedback law is described in equation (4.18).

$$T_{sh,err} = T_{sh} - T_{sh,ref} \quad (4.17)$$

$$\omega_{com,fb} = K_{P,sh} \cdot T_{sh,err} + \int (K_{I,sh} \cdot T_{sh,err}) \quad (4.18)$$

where:

$K_{P,sh}$ is the proportional gain for the superheat feedback [-]

$K_{I,sh}$ is the integral gain for the superheat feedback [-]

4.3.3 Stability analysis

The system is controlled by changing the compressor speed and thereby the evaporation temperature. I.e. the system is controlled by changing the model parameter T_e . This complicates stability analysis. However it is possible to analyse the system behaviour by simulations to confirm that it is stable. The combined control signal from the feedforward and feedback is saturated at the compressor lower and upper speed.

$$\omega_{com} = SAT_{35}^{60}(\omega_{com,ff} + \omega_{com,fb}) \quad (4.19)$$

Experiments have shown that the evaporation temperature does not change instantly when the compressor speed is changed. The change in temperature can be approximated using a first order system with a settling time of approximately 70 seconds. With a sample frequency of 1 Hz this yields

$$T_e(k) = 0.9311 \cdot T_e(k-1) + 0.0687 \cdot u(k) \quad (4.20)$$

where:

u is the steady state value of T_e [$^{\circ}C$]

As described earlier the system is controlled using the compressor to change the evaporator pressure and consequently the evaporation temperature. A new nonlinear system can now be formulated:

$$\frac{dx_e}{dt} = \frac{\dot{m}_r(h_o - h_i)}{c_1} - \frac{c_2}{c_1}(T_{w,i} - T_e)x_e \quad (4.21)$$

$$T_e(k) = 0.9311 \cdot T_e(k-1) + 0.0687 \cdot u(k) \quad (4.22)$$

The value of u is used as the input signal. In the simulation the input signal must be calculated from the control signal ω_{com} .

$$P_{e,o} = \dot{m}_r / (\alpha \cdot \omega_{com}) \quad (4.23)$$

$$u = T_{bub}(P_{e,o}) \quad (4.24)$$

Equations (4.23) - (4.24) describes the implementation of the controller simulation. When simulating the close loop system the value of T_{sh} is calculated using the superheat equation. Phase plots (or trajectories) can be used to examine stability. Simulated trajectories of the closed loop system using a $K_{P,sh}$ value of 2 can be seen in figure 4.10. The simulations are done with four different values of the water temperature (5, 10, 15 and 20 °C) and matching refrigerant flow. The same superheat reference (12 °C) is used for all the simulations. The simulations are started with a wide range of initial evaporator filling levels and evaporation temperature levels. All the trajectories converge to a single working point with a superheat of approximately 12 degrees. Figure 4.11 on the next

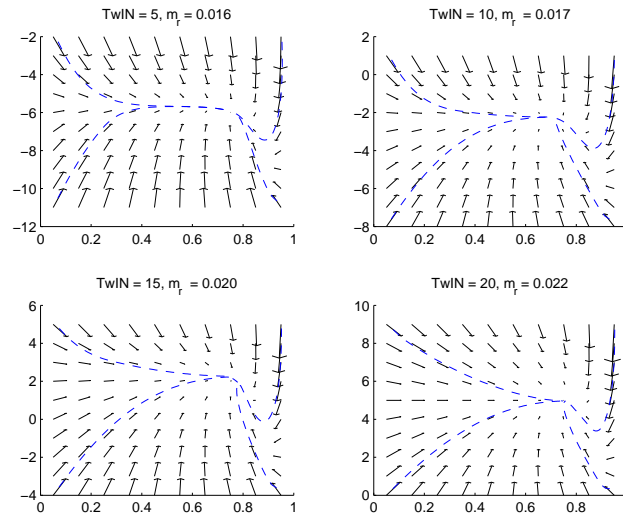


Figure 4.10: Phase plot of the system using a P controller. A number of trajectories are shown with dashed lines.

page shows the same simulations, this time using a PI controller with $K_{P,sh} = 2$ and $K_{I,sh} = 0.015$. All the trajectories converge to a single working point with a superheat of approximately 12 degrees. It should therefore be possible to control the system using both a P and PI controller. Later in this chapter it will be clear that the PI controller is the best. But first measures are taken to prevent the evaporator from being completely filled with refrigerant. The next section describes a method of limiting the refrigerant flow.

4.3.4 Throttle

In some cases the combination of high cooling capacity determined by the temperature controller and low water temperature calls for a compressor speed in excess of the maximal bound. In these cases the superheat controller must ask the flow controller to throttle

4.3. SUPERHEAT CONTROLLER (SHC)

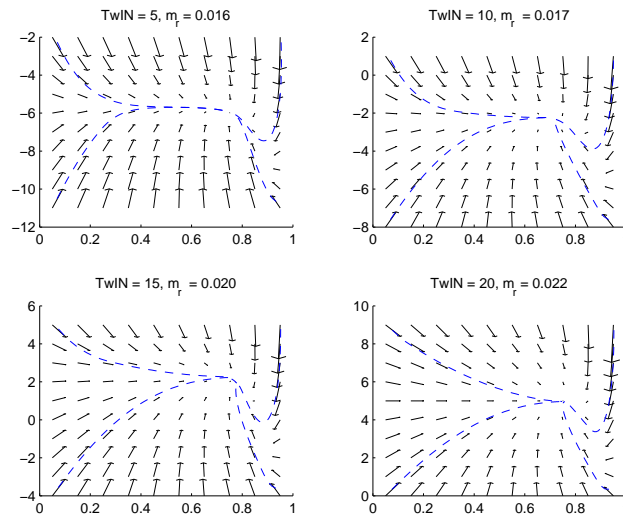


Figure 4.11: Phase plot of the system using a PI controller. A number of trajectories are shown with dashed lines.

the cooling capacity. This problem is similar to the anti-windup problem: When the compressor saturates, the integrator in the flow controller must be prevented from winding up cooling capacity. Figure 4.12 shows an overview of the throttle implementation between the temperature controller and the superheat controller. Figure 4.13 shows an experiment where the throttle is utilised. The water temperature and superheat references are constant at 14 and 12 degrees respectively. The upper plot shows an increasing heat load and the calculated capacity tracking the load up to approximately 5000 s. At that time, the middle plot shows that the compressor saturates. This throttles the capacity calculation, preventing it from tracking the heat load. The effect of the throttling is that the unsaturated compressor control signal stays near the saturation threshold, i.e. the resulting capacity approximately matches the maximal achievable cooling capacity under the given conditions. As the heat load is no longer matched by the cooling capacity, the water temperature increases, which is seen in the lower plot.

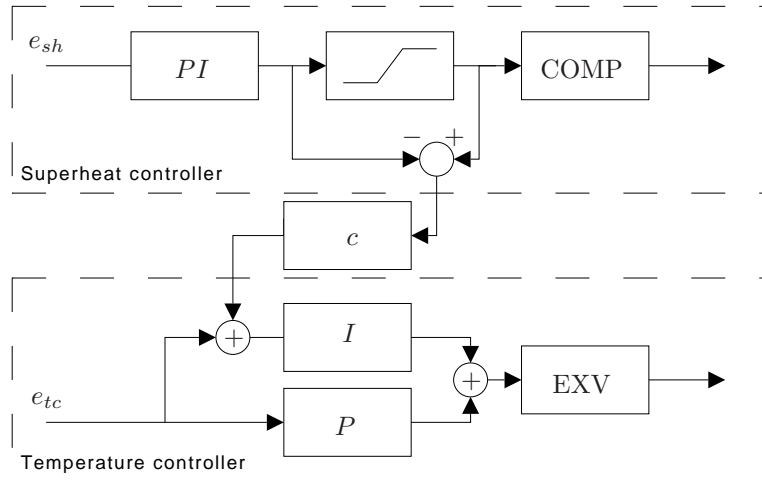


Figure 4.12: Illustration of the implemented throttle.

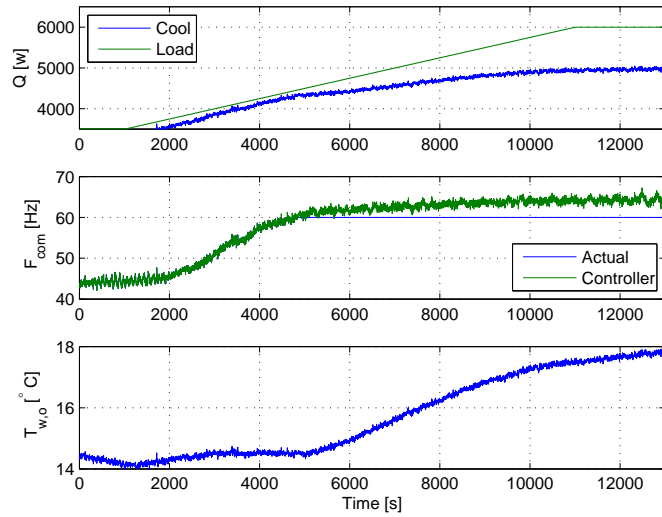


Figure 4.13: Experiment utilising throttle.

4.3.5 SHC Test

The superheat controller performance is tested by introducing a disturbance in the refrigerant flow. The refrigerant flow changes are generated by introducing several steps between 3000 and 4000 watt in the required cooling capacity. The resulting superheat is measured to see how the closed loop system holds the superheat reference. The step in cooling capacity is done by changing the reference on the refrigerant flow (i.e. the capacity is changed almost instantaneously). The water outlet temperature is maintained constant by controlling the power used to heat the water. Figure 4.14 shows how respectively the P controller and PI controller, both with feedforward, performs. From the

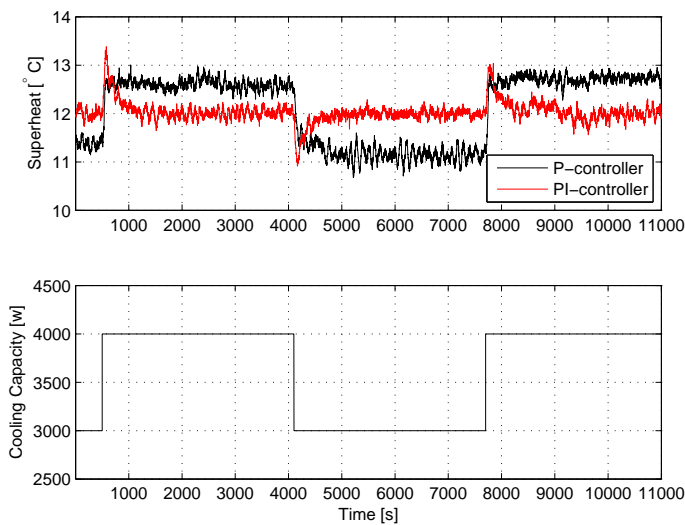


Figure 4.14: Performance of the P and PI superheat controllers.

figure it is clear that both controllers are able to keep the superheat at approximately the reference value. However it is clear that the P controller has a small amount of steady state error, which is removed using the PI controller. Figure 4.15 shows a measurement of the feedforward control signal and the control signal including feedback. As it can be seen the feedforward signal is not perfect, but overall it matches the 'correct' compressor speed. It should be noted that the system in some working points is affected by an unmodelled property. Appendix E describes this property and finds that there appears to be a relationship between this property and the vapourised refrigerant volume flow [m^3/s] through the evaporator: At a given volume flow the required compressor speed changes approximately 2 Hz.

In cases where the load is very low, the compressor will saturate at the lower bound, 35 Hz. This might prevent the superheat controller from maintaining a reasonable low superheat. In these cases it might be beneficial to set a lower limit for normal operation and switch the cooling process on and off to achieve cooling below that limit. Whether and when this is beneficial depends on the superheat controllers performance when recovering from a halted system. In the test shown in figure 4.16 the heat load is 2000 W, but the system is limited to a minimum cooling capacity of 3000 W. To match the

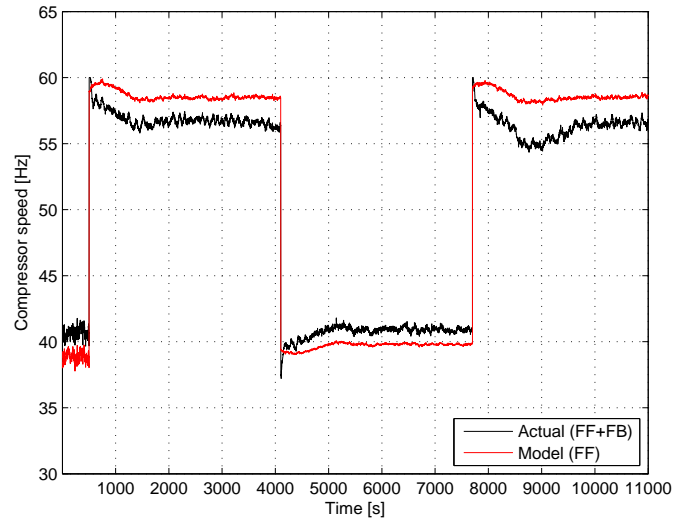


Figure 4.15: Combined control signal to the compressor and the model-based component.

load, the system utilises the solenoid valve to completely shut off the refrigerant flow when $T_{w,o}$ reaches $T_{w,ref} - 1$ and reopens the valve when the water reaches $T_{w,ref} + 1$. When the refrigerant flow is stopped the compressor continues at 35 Hz until P_e is low enough for the pressostat to shut it off. During the off periods all controller integrators are reset. The upper plot of figure 4.16 is the superheat. The middle plot is the water temperature which zigzags in the range $T_{w,ref} \pm 1$. The lower plot is the refrigerant flow which toggles on and off when $T_{w,o}$ reaches the respective thresholds.

From figure 4.16 the controller is deemed reasonably fast at recovery from halt, but it will require a number of comparable high superheat / switched system measurements to determine when which strategy is more efficient.

4.3.6 SHC Summary

The superheat is controlled by regulation the compressor speed. The superheat controller utilises model-based feedforward and a PI controller as feedback. The feedforward calculates the steady state compressor speed needed to obtain the reference superheat. Due to the quality of the feedforward signal a low gain PI controller can be used. Phase plots are used to evaluate the stability of the system. Simulations and experimental data shows that the controller performs as expected.

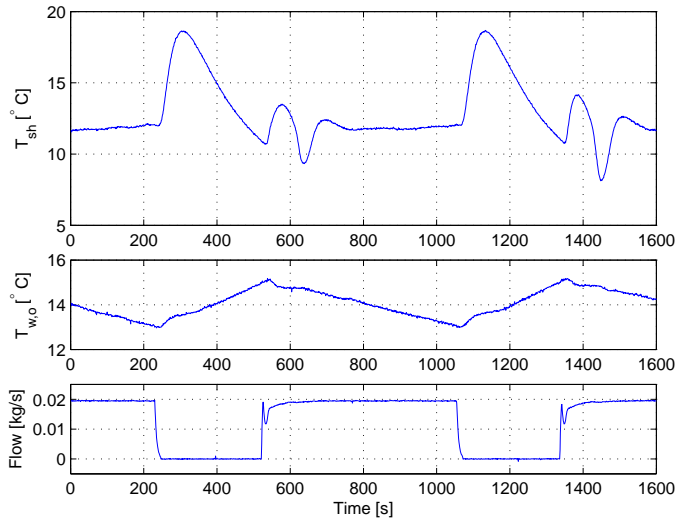


Figure 4.16: The system is periodically halted to match a low load.

4.4 Condenser Pressure Controller (CPC)

The condenser pressure is regulated with a plain PI regulator, see figure 4.17. Equation (4.26) describe a standard PI controller.

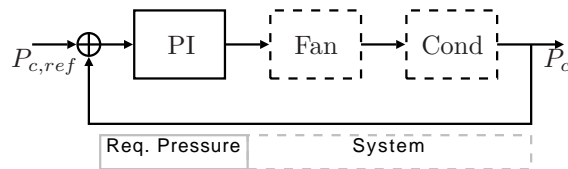


Figure 4.17: Condenser pressure controller overview.

$$P_{c,err} = P_c - P_{c,ref} \quad (4.25)$$

$$u_{fan} = K_{P,P_c} \cdot P_{c,err} + \int (K_{I,P_c} \cdot P_{c,err}) \quad (4.26)$$

where:

K_{P,P_c} is the proportional gain for the condenser pressure regulator [-]

K_{I,P_c} is the integral gain for the condenser pressure regulator [-]

Figure 4.18 shows the measured condenser pressure. The controller are using the following constants: $K_{P,P_c} = 2$ and $K_{I,P_c} = 0.1$. The pressure reference is 10 bar. The system is started at $t = 0$, and pressure slowly builds in the condenser. At approximately 140 s the control signal is large enough to start the rotation of the fan. After the fan is in motion the controller keeps the condenser pressure close to the reference.

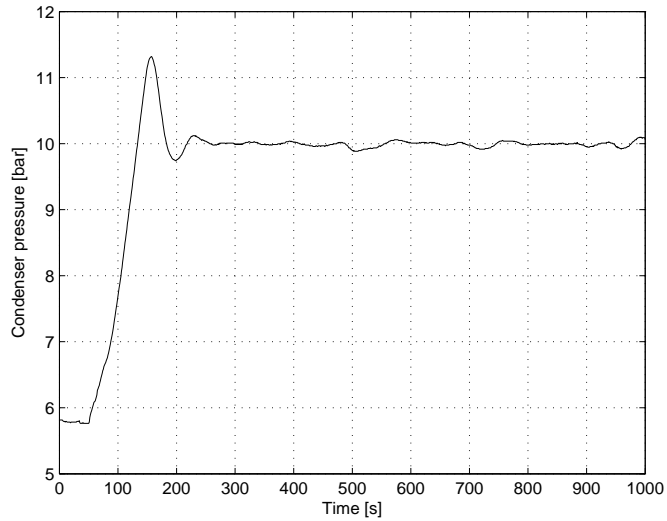


Figure 4.18: Condenser pressure measured during startup.

4.5 Controller Conclusion

As evident by the different plots during this chapter, the proposed control paradigm works. The flow controller determines a cooling capacity from the temperature error and lets the corresponding flow of refrigerant through the evaporator. From startup excess capacity is utilised to bring the water to the desired temperature. As the water temperature settles the capacity converges to match the load.

The superheat controller regulates the compressor speed to maintain the desired amount of superheat. For good disturbances suppression the controller is based on feedforward control, derived from the models developed in chapter 3 on page 23. The superheat controller also features feedback to compensate model errors. Furthermore the superheat controller is allowed to throttle the refrigerant flow if the compressor saturates, this prevents flooding the evaporator or even the compressor.

So far, all the tuning parameters have been coarsely hand-tuned during experiments, which suggests that this performance can be easily transferred to similar systems, given the feedforward model fits, or even tuned for improved performance.

4.5. CONTROLLER CONCLUSION

Chapter 5

Nonlinear Control

Section 4.3 on page 58 describes the design of a superheat controller using methods similar to those used in linear control design. This chapter describe two controller designs using nonlinear control theory. These methods include feedback linearization and backstepping. The two controllers both uses the evaporator filling as the reference. It is possible to use a fixed evaporator filling as the reference or calculate a reference filling that will result in a given superheat at the working point. Using a fixed reference is the simplest, but the superheat level will change when the working point is changed.

Resume:

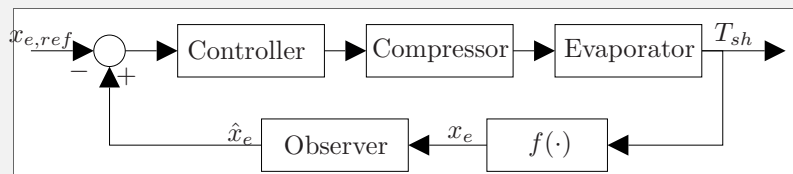
Two different nonlinear controllers are developed in this chapter. They are respectively based on feedback linearization and backstepping. Both controllers regulates the evaporator filling x_e . The filling can not be measured directly, but it is possible to isolate the filling in the superheat equation. The resulting equation is

$$x_e = \frac{1}{\sigma} \log \left(-\frac{T_{sh}}{T_{w,i} - T_e} + 1 \right) (C_r \cdot \dot{m}_r) + 1$$

The controllers make use of both the evaporator filling and the time derivative of the evaporator filling. Any noise in the measurement of the superheat or the refrigerant flow will deteriorate the quality of the calculated signals. To reduce the problem, an observer is used for estimating the evaporator filling. The observer is made using the following model

$$\hat{x}_e(k+1) = A(\cdot) \cdot \hat{x}_e(k) + B(\cdot) \cdot u(k) + q[x_e(k) - \hat{x}_e(k)]$$

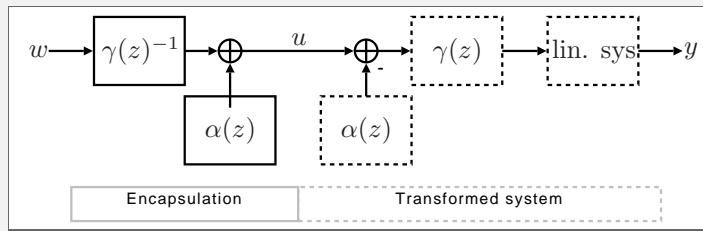
The next figure illustrates the control strategy used for both controllers.



The principle of feedback linearization is that a nonlinear system is made to appear linear by modifying the system inputs. Once the system appears linear it is possible to use linear control theory. In order for the system to be feedback linearizable the nonlinearities must appear together with the input [Khalil, 2002, p. 505-509]. The general form of a feedback linearizable system is

$$\begin{aligned}\dot{z} &= Az + B \cdot \gamma(z) \cdot (u - \alpha(z)) \\ u &= \alpha(z) + \gamma^{-1}(z) \cdot w\end{aligned}$$

The system will appear linear using the control signal w . The next figure illustrate process of feedback linearization.



The nonlinear evaporator model does not fit this form directly and a transformation is utilised. Once the system is feedback linearized a P-controller is used to control the evaporator filling. Simulation and experiments are used to validate the control law.

The principle of backstepping is to use Lyapounov functions to express feedback laws that will stabilise the system. It is possible to 'backstep' through the system model until a controllable system parameter is included in the stabilizing control law. The generic model for a second order system is

$$\begin{aligned}\dot{x}_1 &= f(x_1) + g(x_1)x_2 \\ \dot{x}_2 &= -x_2 + u\end{aligned}$$

The nonlinear evaporator model does not fit this form directly, but it is possible to transform the system to make it fit. Introducing two new states ε_1 and ε_2 , where ε_1 is the evaporator filling and ε_2 'contains' the 'non-stable' parts of the system, it is possible to formulate a Lyapounov candidate function

$$2V = k(\varepsilon_1 - \bar{\varepsilon}_1)^2 + \varepsilon_2^2$$

Using the candidate function it is shown that

$$\dot{V} = -k(\varepsilon_1 - \bar{\varepsilon}_1)^2 - k_2\varepsilon_2^2$$

if the following control law is used

$$u = -\frac{(k + k_2)(x_1 - \bar{x}_1) + \dot{x}_1(1 + k_2 + cT_{w,i} + cx_2)}{cx_1} + \tau T_e$$

For positive values of k and k_2 the resulting system is stable. Simulations and experiments are used to validate the control law.

5.1 Reference Signal

The evaporator filling reference can be calculated by isolating the evaporator filling in e.g. equation (3.18), this yields equation (5.1).

$$x_{e,ref} = \frac{1}{\sigma} \log \left(-\frac{T_{sh,ref}}{T_{w,i} - T_e} + 1 \right) (C_r \cdot \dot{m}_r) + 1 \quad (5.1)$$

The calculated filling reference will be affected by noise in the measured states and the controller will then try to track the noise. The reference filling should be kept 'constant' when the system is running in steady state mode. This can be done by low pass filtering the filling reference. This way the reference can change when the working point is changed, but remain unaffected by noise and small variations around the working point.

The evaporator filling can not be measured directly, but can be estimated using an equation similar to equation (5.1) where $T_{sh,ref}$ is substituted with the measured superheat level. The estimate will be affected by the high gain caused by the nonlinear logarithm function when $T_{sh}/(T_{w,i} - T_e)$ approaches unity. Figure 5.1 shows the nonlinear behaviour of the evaporator filling with $\sigma = 220$, $C_r = 1100$, $\dot{m}_r = 0.02$. The noise in the

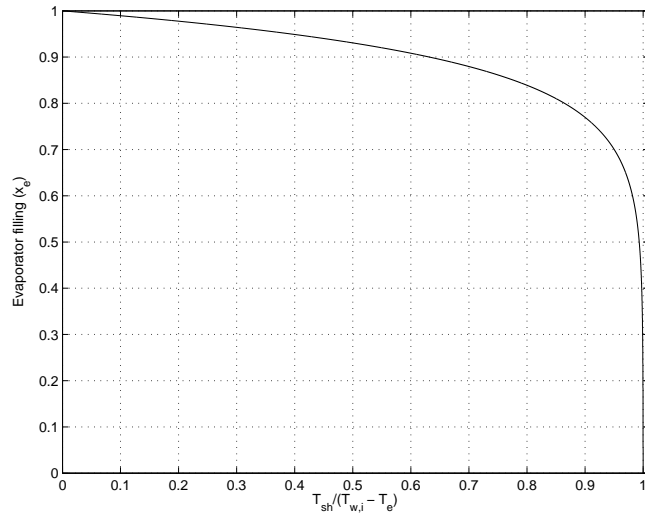


Figure 5.1: Evaporator filling as a function of $T_{sh}/(T_{w,i} - T_e)$.

measured temperatures and refrigerant flow yields a noisy calculation of the evaporator filling. To ensure a good estimate to the evaporator filling an observer is made using the model of the evaporator and the calculated evaporator filling. The following observer model is used in this chapter.

$$\hat{x}_e(k+1) = A(\cdot) \cdot \hat{x}_e(k) + B(\cdot) \cdot u(k) + q[x_e(k) - \hat{x}_e(k)] \quad (5.2)$$

If the value of q is zero then \hat{x}_e would be given purely by the model which may drift away from the true evaporator filling. A q value of 0.1 is used to 'feedback' the error between the estimated evaporator filling and the measured evaporator filling. Figure

5.2 is an illustration of the nonlinear system and controller. The rest of the system, i.e. the refrigerant flow and condenser pressure, is controlled with the already developed controllers.

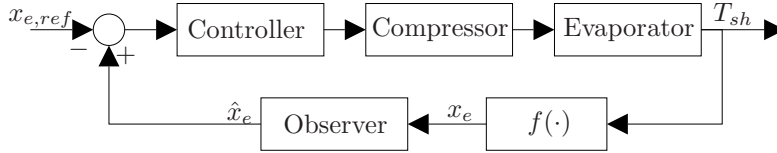


Figure 5.2: Illustration of the nonlinear controlled system.

5.2 Feedback Linearization

In feedback linearization a nonlinear system is encapsulated to make it appear as a linear system. The feedback linearization in this section is based on [Khalil, 2002, p. 505-509]. The key principle in feedback linearization is to cancel the nonlinear behaviour by modifying the system input. To make this possible the nonlinearities have to appear together with the input, hence the system model may have to be transformed.

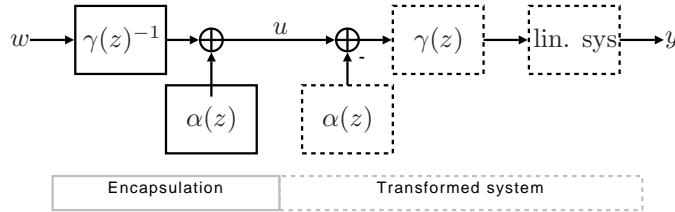


Figure 5.3: Feedback linearization.

Figure 5.3 illustrates the feedback linearization principle. The system is transformed to a form where the nonlinearities consists of two contributions which are respectively added or multiplied with the input, u , before it reaches the linear part of the system. The 'inverse' nonlinear contributions are applied to the outer input, w , hence the states of the linear part of the system will relate linear to w .

Khalil's condition for a system to be feedback linearizable is that it can be written on the form seen in equation (5.3), where (A, B) is controllable, $\gamma(x)$ and $\alpha(x)$ are defined in a domain containing origin and $\gamma(x)$ is nonsingular in that domain. Input on the form of equation (5.4) cancels the nonlinearities, [Khalil, 2002, p. 506].

$$\dot{z} = Az + B \cdot \gamma(z) \cdot (u - \alpha(z)) \quad (5.3)$$

$$u = \alpha(z) + \gamma^{-1}(z) \cdot w \quad (5.4)$$

5.2.1 Coordinate transformation

The relative filling (x_e) model is nonlinear and includes parameters which depends on the operating point. The regulated variable is the evaporation temperature, T_e , which

is considered a linear system with the steady state evaporation temperature, $T_{e,ss}$, as input.

The system is first rewritten to a more compact form by collecting the constants and parameters in \dot{x}_e . The parameter \dot{T}_e is also included in the system.

$$\dot{x}_e = \frac{\dot{m}_r}{c_1} \cdot (h_o - h_i) - \frac{c_2}{c_1} \cdot (T_w - T_e) \cdot x_e \quad (5.5)$$

$$= k_1 - k_2 \cdot (T_w - T_e) \cdot x_e \quad (5.6)$$

$$= k_1 - k_3 \cdot x_e + k_2 \cdot T_e \cdot x_e \quad (5.7)$$

$$\dot{T}_e = a \cdot (T_{e,ss} - T_e) \quad (5.8)$$

$$= -a \cdot T_e + a \cdot T_{e,ss} \quad (5.9)$$

$$k_1 = \frac{\dot{m}_r}{c_1} \cdot (h_o - h_i) \quad (5.10)$$

$$k_2 = \frac{c_2}{c_1} \quad (5.11)$$

$$k_3 = k_2 \cdot T_w \quad (5.12)$$

The value of $T_{e,ss}$ is the steady state evaporation temperature, as derived in the static models. It is utilised as the input to the above system, hence it is renamed u .

$$u = T_{e,ss} \quad (5.13)$$

The following coordinate transformation is shown to bring the input and the nonlinearities in the same expression.

$$z_1 = \dot{x}_e \quad (5.14)$$

$$z_2 = x_{e,ref} - x_e \quad (5.15)$$

Below are the state equations for the transformed system, expressed in the original coordinates.

$$\dot{z}_1 = \ddot{x}_e \quad (5.16)$$

$$= -k_3 \cdot \dot{x}_e + k_2 \cdot T_e \cdot \dot{x}_e + k_2 \cdot \dot{T}_e \cdot x_e \quad (5.17)$$

$$\dot{z}_2 = -\dot{x}_e \quad (5.18)$$

Using the inverse coordinate transformations, the above state equations can be expressed in the transformed coordinate system. The required transformations are shown in equations (5.19) - (5.24).

$$x_e = x_{e,ref} - z_2 \quad (5.19)$$

$$\dot{x}_e = z_1 \quad (5.20)$$

$$T_e = \frac{\dot{x}_e + k_3 \cdot x_e - k_1}{k_2 \cdot x_e} \quad (5.21)$$

$$= \frac{z_1 + k_3 \cdot (x_{e,ref} - z_2) - k_1}{k_2 \cdot (x_{e,ref} - z_2)} \quad (5.22)$$

$$\dot{T}_e = -a \cdot T_e + a \cdot u \quad (5.23)$$

$$= -a \cdot \frac{z_1 + k_3 \cdot (x_{e,ref} - z_2) - k_1}{k_2 \cdot (x_{e,ref} - z_2)} + a \cdot u \quad (5.24)$$

Equations (5.26) and (5.27) describes the fully transformed system.

$$\begin{aligned} \dot{z}_1 &= -k_3 \cdot z_1 + k_2 \cdot \frac{\dot{x}_e + k_3 \cdot x_e - k_1}{k_2 \cdot x_e} \cdot z_1 \\ &+ k_2 \cdot \left(-a \cdot \frac{z_1 + k_3 \cdot (x_{e,ref} - z_2) - k_1}{k_2 \cdot (x_{e,ref} - z_2)} + a \cdot u \right) \cdot (x_{e,ref} - z_2) \end{aligned} \quad (5.25)$$

$$\begin{aligned} &= a \cdot z_1 - a \cdot k_3 \cdot z_2 \\ &+ \frac{(z_1 - k_1) \cdot z_1}{x_{e,ref} - z_2} + a \cdot (k_3 \cdot x_{e,ref} - k_1) \\ &+ a \cdot k_2 \cdot (x_{e,ref} - z_2) \cdot u \end{aligned} \quad (5.26)$$

$$\dot{z}_2 = -z_1 \quad (5.27)$$

On a more compact form, the system may be expressed as equation (5.28) or (5.29). The first two terms of equation (5.26) are linear and could be included in A , however care should be taken as k_3 changes with the water temperature. For simplicity both terms are included in $f(z)$.

$$\dot{z} = Az + B \cdot (f(z) + g(z) \cdot u) \quad (5.28)$$

$$\begin{bmatrix} \dot{z}_1 \\ \dot{z}_2 \end{bmatrix} = \begin{bmatrix} 0 & 0 \\ -1 & 0 \end{bmatrix} \cdot \begin{bmatrix} z_1 \\ z_2 \end{bmatrix} + \begin{bmatrix} 1 \\ 0 \end{bmatrix} \cdot (f(x) + g(x) \cdot u) \quad (5.29)$$

$$\begin{aligned} f(z) &= a \cdot z_1 - a \cdot k_3 \cdot z_2 \\ &+ \frac{(z_1 - k_1) \cdot z_1}{x_{e,ref} - z_2} + a \cdot (k_3 \cdot x_{e,ref} - k_1) \end{aligned} \quad (5.30)$$

$$g(z) = a \cdot k_2 \cdot (x_{e,ref} - z_2) \quad (5.31)$$

Notice that equation (5.28) can be rewritten to the form of equation (5.3), by using the substitutions seen in (5.32) and (5.32). This suggests that the system can be feedback linearized.

$$\gamma(z) = g(z) \quad (5.32)$$

$$\alpha(z) = \frac{-f(z)}{g(z)} \quad (5.33)$$

5.2.2 Feedback Law

Given the transformed system in equation (5.28), the nonlinearities collected in $f(x)$ and $g(x)$ can be cancelled by using an input on the form of equation (5.34). The system will then seem linear, when seen from the outer input, w .

$$u = \frac{1}{g(x)} \cdot (w - f(x)) \quad (5.34)$$

$$\dot{z} = Az + B \cdot w \quad (5.35)$$

As the system transformation moves the original reference to origo, the states can be used for feedback, i.e. $w = -K \cdot z$. This results in the system seen in equation (5.37). The values of K can be selected to make the transformed origo, i.e. the original reference, asymptotically stable.

$$\begin{bmatrix} \dot{z}_1 \\ \dot{z}_2 \end{bmatrix} = \begin{bmatrix} 0 & 0 \\ -1 & 0 \end{bmatrix} \cdot \begin{bmatrix} z_1 \\ z_2 \end{bmatrix} - \begin{bmatrix} 1 \\ 0 \end{bmatrix} \cdot [K_1 \quad K_2] \cdot \begin{bmatrix} z_1 \\ z_2 \end{bmatrix} \quad (5.36)$$

$$\begin{bmatrix} \dot{z}_1 \\ \dot{z}_2 \end{bmatrix} = \begin{bmatrix} -K_1 & -K_2 \\ -1 & 0 \end{bmatrix} \cdot \begin{bmatrix} z_1 \\ z_2 \end{bmatrix} \quad (5.37)$$

When the required control signal u , i.e. the required steady state evaporation temperature ($T_{e,ss}$), is calculated, the required compressor speed can be estimated from equation (5.38).

$$\omega_{com} = \frac{\dot{m}_r}{\alpha \cdot P_{e,ss}} \quad (5.38)$$

$$P_{e,ss} = P_{dew}(T_{e,ss}) \quad (5.39)$$

5.2.3 Simulation

The feedback linearized has been simulated using $K = [0.01 \quad -0.05]$. Figure 5.4 shows x_e during startup from a low filling. Figure 5.5 shows the associated superheat and compressor speed. The reference for x_e is 0.85, $T_w = 16$ and $\dot{m}_r = 0.025$. As seen in

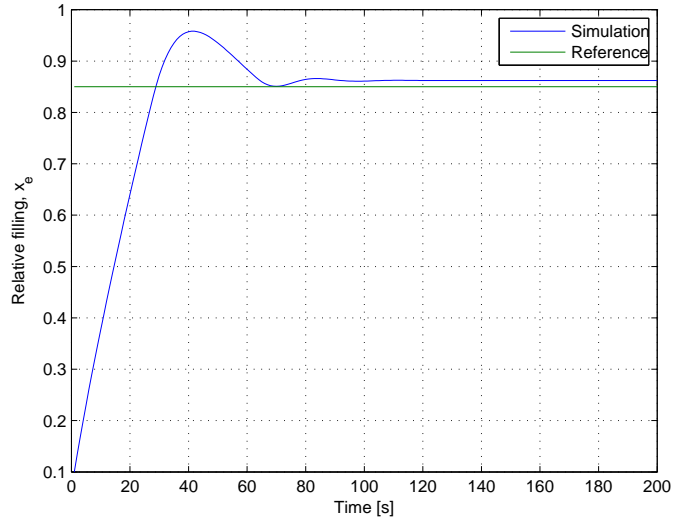


Figure 5.4: Simulated x_e , $x_{e,ref} = 0.85$.

figure 5.4, the selected gains in K results in a certain steady state error on x_e . The error can be reduced by selecting higher gains, but costs more compressor speed settling time and saturation during startup. This is subject to later tuning. The compressor behaviour with the selected K values is seen in figure 5.5.

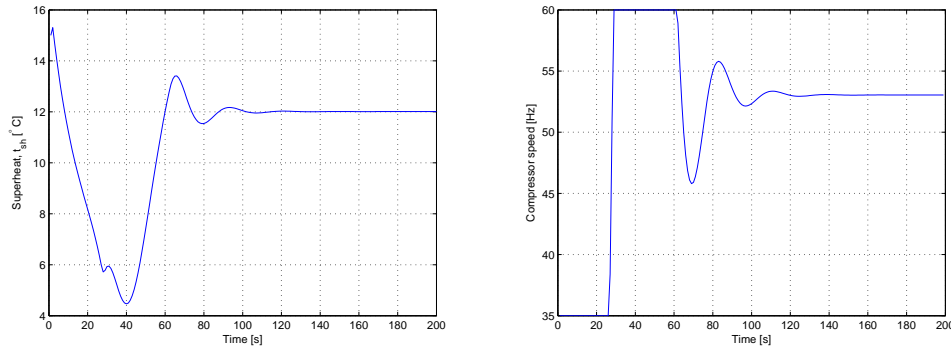
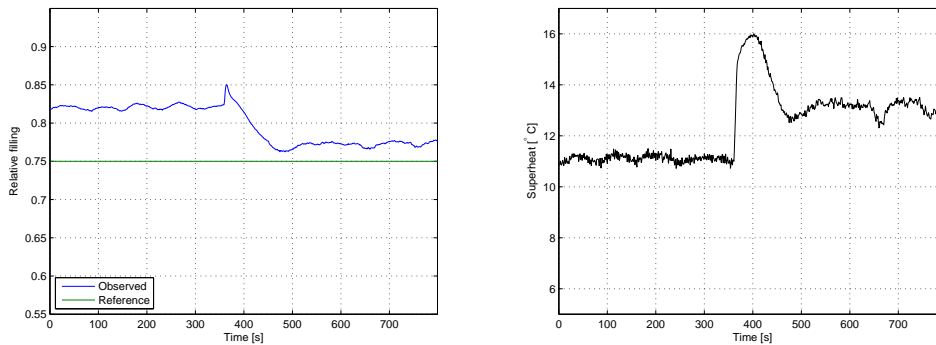


Figure 5.5: Simulated superheat and compressor speed.

5.2.4 Test

Figure 5.6 is from a test of feedback linearized control of the relative filling. The left plot is the estimated value of x_e , the reference is 0.75 and $K = [0.15 \ -0.016]$. Due to inconsistent results \dot{x}_e was found by differentiating a filtered version of the estimated x_e , rather than by equation (5.5). The right plot shows the corresponding superheat. Figure 5.7 shows the compressor speed and cooling capacity from the same test.

Figure 5.6: Measured x_e and T_{sh} .

5.2.5 Feedback Linearization Summary

The nonlinear evaporator model has been combined with the linear evaporation temperature model. The system has been transformed to make the input, the steady state evaporation temperature, appear together with the nonlinear elements. The nonlinearities are cancelled by input modification, the structure of a feedback law for the outer input has been found and the calculated, modified input can be converted to a compressor control signal. According to the simulation, the relative filling, x_e , does seem linearized, reducing the rest of the controller design (tuning of the gains) to the linear approach. Tests using feedback linearized control of x_e reveals difficulties in finding satisfactory values for K , i.e. values resulting in acceptable offsets and stability. The difficulties may be due to the

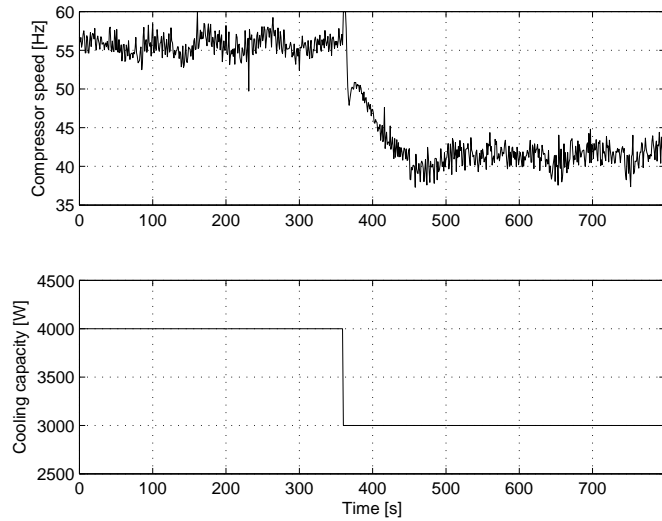


Figure 5.7: Compressor speed and cooling capacity.

controllers sensitivity to the feedback from the states, who are estimated from filtered measurements (x_e) and the numerically calculated derivative (\dot{x}_e). A possible expansion is input/output linearization, which will utilise the same coordinate transformation, but continues to linearize the output (T_{sh}).

5.3 Backstepping

This section describes a superheat controller developed using the nonlinear control theory of backstepping. Based on [Rasmussen, 2008], [Khalil, 2002] and [Åström & Wittenmark, 1995].

5.3.1 Design of backstepping controller

The refrigeration system can be described by equations (5.40) - (5.41).

$$c_1 \frac{dx_e}{dt} = \dot{m}_r (h_g - h_{in}) - c_2 T_{w.in} x_e + c_2 T_e x_e \quad (5.40)$$

$$\dot{T}_e = -\tau T_e + u \quad (5.41)$$

The genetic model for backstepping of second order is as shown in equations (5.42)-(5.43).

$$\dot{x}_1 = f(x_1) + g(x_1)x_2 \quad (5.42)$$

$$\dot{x}_2 = -x_2 + u \quad (5.43)$$

5.3. BACKSTEPPING

The system described in equations (5.40) - (5.41) can be transformed to fit the genetic model using equations (5.44) - (5.48)

$$x_1 = x_e \quad (5.44)$$

$$x_2 = T_e \quad (5.45)$$

$$f(x_1) = \frac{\dot{m}_r(h_g - h_{in})}{c_1} - cT_{w.in}x_1 \quad (5.46)$$

$$g(x_1) = cx_1 \quad (5.47)$$

$$c = \frac{c_2}{c_1} \quad (5.48)$$

Introducing $\varepsilon_1 = x_1$ yields

$$\dot{\varepsilon}_1 = -(\varepsilon_1 - \bar{\varepsilon}_1) + (\varepsilon_1 - \bar{\varepsilon}_1) + f(\varepsilon_1) + g(\varepsilon_1)x_2 \quad (5.49)$$

If x_2 could be chosen freely as a control variable and $g(\varepsilon_1) \neq 0$ for all working points, it would be possible to stabilise the system directly. However x_2 is described by the system equations and the system must therefore be stabilised through the control signal u . This is known as backstepping. Introducing ε_2 as the 'non-stable' part of $\dot{\varepsilon}_1$.

$$\varepsilon_2 = (\varepsilon_1 - \bar{\varepsilon}_1) + f(\varepsilon_1) + g(\varepsilon_1)x_2 \quad (5.50)$$

The differential equations of ε_1 and ε_2 can be now be calculated.

$$\dot{\varepsilon}_1 = -(\varepsilon_1 - \bar{\varepsilon}_1) + \varepsilon_2 \quad (5.51)$$

$$\dot{\varepsilon}_2 = \dot{\varepsilon}_1 + \frac{df}{dx_1}\dot{x}_1 + \frac{dg}{dx_1}\dot{x}_1x_2 + g(\varepsilon_1)(-\tau T_e + u) \quad (5.52)$$

The control signal u is now present in the system description. The task is now to derive a control signal that will stabilise the system. Nonlinear system stability can be analysed using Lyapunov theory. Considering the Lyapunov candidate function

$$2V = k(\varepsilon_1 - \bar{\varepsilon}_1)^2 + \varepsilon_2^2 \quad (5.53)$$

The Lyapunov candidate function yields equation (5.54).

$$\dot{V} = k(\varepsilon_1 - \bar{\varepsilon}_1) \cdot [\varepsilon_2 - (\varepsilon_1 - \bar{\varepsilon}_1)] + \varepsilon_2 \cdot \left[\frac{df}{dx_1}\dot{x}_1 + \dot{\varepsilon}_1 + \frac{dg}{dx_1}\dot{x}_1x_2 + g(\varepsilon_1)(-\tau T_e + u) \right] \quad (5.54)$$

Defining equation (5.55) as

$$k(\varepsilon_1 - \bar{\varepsilon}_1) + k_2\varepsilon_2 + \frac{df}{dx_1}\dot{x}_1 + \dot{\varepsilon}_1 + \frac{dg}{dx_1}\dot{x}_1x_2 + g(\varepsilon_1)(-\tau T_e + u) = 0 \quad (5.55)$$

By inserting equation (5.55) into equation (5.54) the Lyapunov function yields equation (5.56) and the system is stable.

$$\dot{V} = -k(\varepsilon_1 - \bar{\varepsilon}_1)^2 - k_2\varepsilon_2^2 \quad (5.56)$$

Isolation the control signal u in equation (5.55) yields

$$u = -\frac{k(\varepsilon_1 - \bar{\varepsilon}_1) + k_2\varepsilon_2 + \frac{df}{dx_1}\dot{x}_1 + \dot{\varepsilon}_1 + \frac{dg}{dx_1}\dot{x}_1x_2}{g(\varepsilon_1)} + \tau T_e \quad (5.57)$$

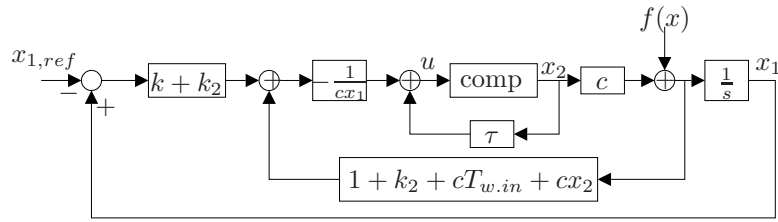


Figure 5.8: Diagram of the backstepping controller.

Rearranging equation (5.57) and inserting the previously defined values yields equation (5.58).

$$u = -\frac{(k + k_2)(x_1 - \bar{x}_1) + \dot{x}_1(1 + k_2 + cT_{w,i} + cx_2)}{cx_1} + \tau T_e \quad (5.58)$$

A block diagram illustration of equation (5.58) can be seen in figure 5.8. The model is mathematically proofed stable, however there are no guarantees that the real system is stable. There are multiple reasons why the model and the real system may not behave exactly the same way. These include model simplification, parameter errors, actuator saturation and discretisation problems (e.g. the feedback law is calculated using a continuous system which is applied on a discrete system). To further examine the stability of the discrete system with actuator limits, a number of phase plots are simulated on the closed loop system. These are shown in figure 5.9. The simulations are done with four

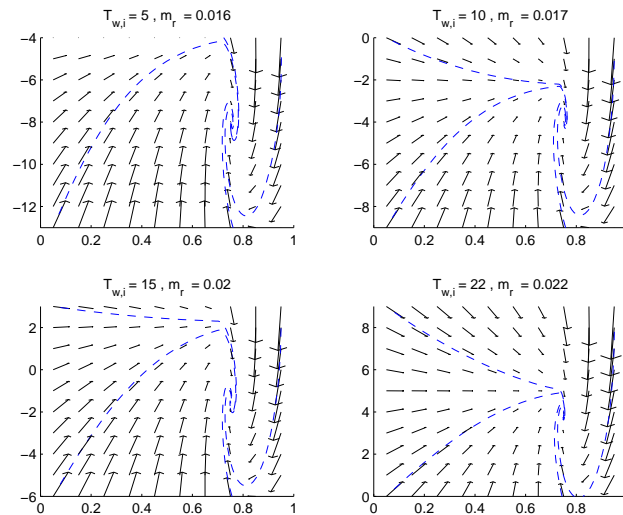


Figure 5.9: Phase plot of the system using the backstepping controller. A number of trajectories are shown with dashed lines.

different values of the water temperature (5, 10, 15 and 20 °C) and matching refrigerant flow. The same evaporator filling reference ($x_{1,ref} = 0.75$) is used for all the simulations. The simulation are started with a wide range for initial evaporator filling levels and evap-

5.3. BACKSTEPPING

oration temperature levels. All the trajectories converge to a single working point with a filling of approximately 0.75.

5.3.2 Backstepping Test

The backstepping controller is tested by performing an experiment. During the experiment the water inlet temperature is kept constant. The filling reference is set to 0.75. At approximately 350 s a step from 3800 W to 3000 W is applied to the cooling capacity. Figure 6.4 shows the measured filling and the measured superheat. The compressor speed and cooling capacity can be seen in figure 5.11.

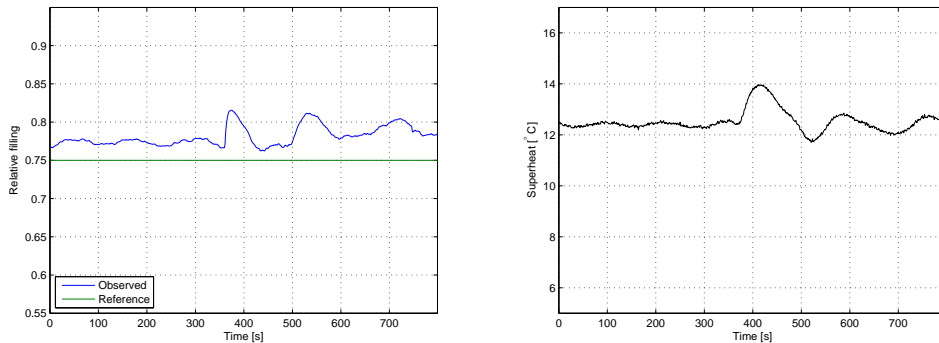


Figure 5.10: Calculated evaporator filling and measured superheat.

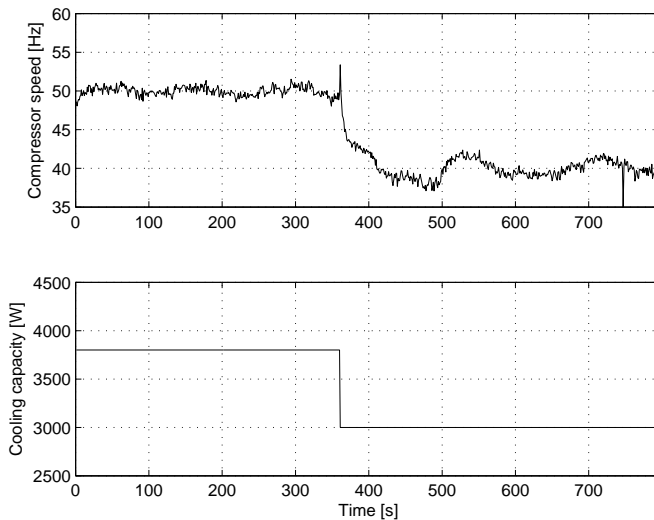


Figure 5.11: Compressor speed and cooling capacity.

5.3.3 Backstepping Summary

A evaporator filling controller has been developed using system models and the nonlinear backstepping method. The controller stability was analysed using Lyapunov stability theory combined with phase plots and found to be stable. Experimental data shows that the closed loop system is stable and able to track the reference during a step in cooling capacity with acceptable offset error.

Chapter 6

Supervisor

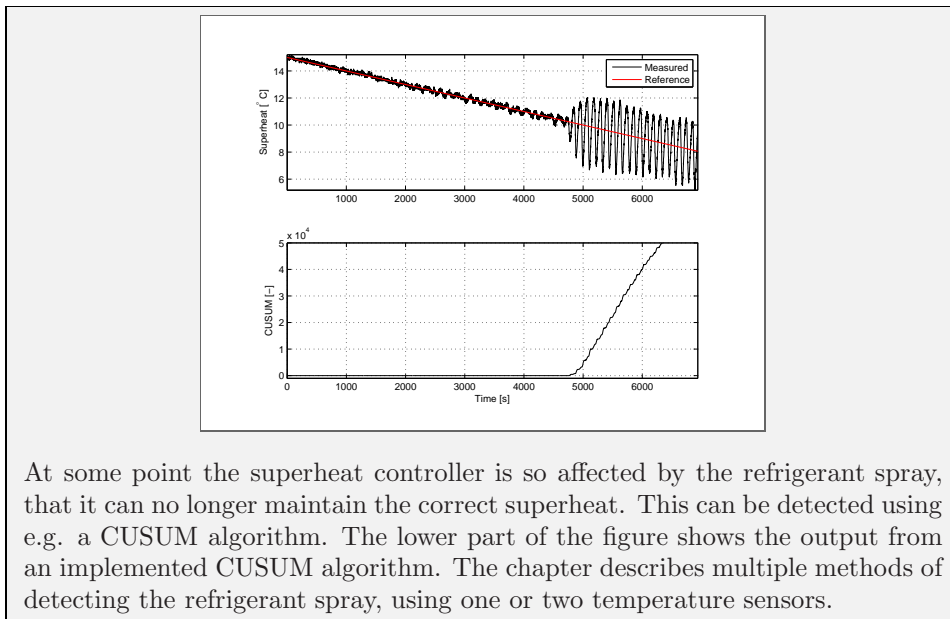
The previous chapters have described different superheat controllers capable of maintaining a given superheat level. The supervisor problem is how to find the optimal superheat temperature and how to handle situations where it is impossible to maintain the optimal superheat. The optimal superheat temperature may vary from system to system. It is therefore beneficial if the supervisor autonomously can estimate the optimal temperature e.g. once at the first system startup. Naturally, refrigeration systems are designed to match the highest possible sustained cooling requirement, it is therefore not always possible for the system to operate with optimal superheat under reduced cooling requirements. The threshold depends on the lower operating limit of the compressor.

In situation where the cooling requirement results in a far from optimal superheat temperature, it might be more efficient to switch the system on and off to match the capacity. The supervisor would have to calculate when it is more efficient to operate in the switching mode than to run continuously at a sub-optimal superheat. The superheat controllers are designed to converge to the superheat reference temperature within a short period after startup, which suggest using the switch method whenever the system is forced to use sub-optimal working points.

The focus of this chapter is on finding the optimal superheat. A number of possible methods are described. These include detecting the refrigerant spray using two temperature sensors. Detection using two sensors is the most elegant and robust, however methods using only one sensor are also described. The most promising method is by comparing the superheat reference with the measured superheat.

Resume:

The optimal superheat can be autonomous detected using knowledge about the system behaviour when the refrigerant starts to hit the temperature sensors. The next figure shows a measurement where the superheat reference is continuously decreased.



6.1 Superheat Setpoint

As described earlier the optimal superheat reference is approximately 2 degrees before the refrigerant spray starts to hit the first temperature sensor. Not all refrigeration systems have the same sensor placement or design of the evaporator. It is therefore reasonable to assume that the 2 degrees value is not a fixed value for all systems, but as soon as the spray is detected the refrigeration system is running in an (sub)-optimal configuration. If the optimal superheat temperature must be found for a given system it might be necessary to run a COP-test on the given system or class of systems. Experiments on multiple system and guidelines on how to place the sensors may limit this problem. In this thesis the optimal superheat is considered to be 2 degrees above the superheat where refrigerant spray is detected. Figure 6.1 illustrates the temperature sensor placement on the test system. There are multiple methods to detect overflow of the evaporator, i.e.

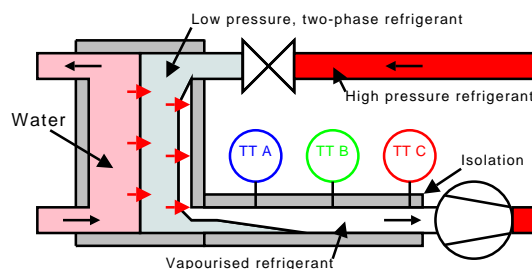


Figure 6.1: Measuring evaporator overflow.

the refrigerant spray. These methods includes:

- Evaluating the difference between temperature sensor TT A and TT B (or TT C).

- The difference between superheat calculated based on TT A and the modelled superheat. When the spray hits the sensors the calculated and estimated superheat values does not match. This could be detected using residuals.
- Observe the controlled superheat. The controller will be unable to maintain a constant superheat when the spray hits the sensors. This could be detected e.g. by looking at changes in superheat variance.

These different overflow detecting methods results in multiple ways to calculate optimal set point value for the superheat controller designed earlier in this thesis. These includes:

- Detect the temperature at which the overflow occurs using two temperature sensors. A few degrees must be subtracted.
 - Elegant,
 - Requires an extra sensor
- Detect the temperature at which the overflow occurs using one temperature sensor and a model of the superheat. A few degrees must be subtracted.
 - Requires no extra sensors.
 - Requires a valid model
- Detect the temperature at which the overflow occurs using one temperature sensor and knowledge of the normal superheat variance. A few degrees must be subtracted.
 - Requires no extra sensor and no model.

6.1.1 Two temperature sensors

The spray can be detected by comparing the superheat calculated using two different temperature sensors. The first superheat temperature is calculated as the difference between the evaporation temperature and temperature of sensor TT A. The second superheat temperature is calculated using temperature of sensor TT B. Figure 6.2 shows a measurement where the superheat reference is continuously lowered using a decaying ramp signal for the compressor speed. The upper part of the graph shows the measured superheat. The superheat controllers use TT A as the superheat feedback signal. When the spray hits sensor TT A the controller will see this as the superheat being too low and and try to increase it. The high gain will result in oscillations of the measured superheat. Sensor TT B, which is not affected by the refrigerant spray, will measure an increased superheat. The lower part of the graph shows the difference between the two superheat levels. A simple way to detect the refrigerant spray is to use a threshold. E.g. when the difference is more than 1 degree it must be caused by refrigerant spray hitting the first sensor. The advantage of using two sensor is that it is very simple and robust. It also does not require any model knowledge, making it easy to implement on a wide range of systems. The only negative property of using two sensors is the addition of the second sensor. Refrigerant spray detection using only one sensor is described in the next two sections.

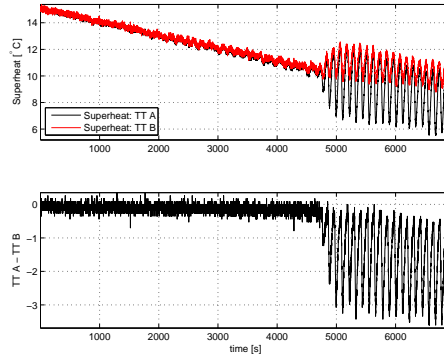


Figure 6.2: Superheat from TT A and TT B, difference between them.

6.1.2 Detection with model

The spray can be detected by comparing the model superheat output with the measured superheat. Figure 6.3 shows the principle of a residual generator. Residual generators are normally used to detect faults within a system. When e.g. an actuator, sensor or system component fails the system will no longer behave as described by the system model. The difference between the model output and the system output is used to generate the residuals. In more advanced systems residual decoupling can be used for isolating failures in the system. In this thesis the residual generator is not used to detect component faults, but to detect when the model does no longer describe the system correctly. The spray effect is not modelled, so when it hits the sensors the superheat model is no longer valid. This can be detected as a inconsistency between model and system output. The

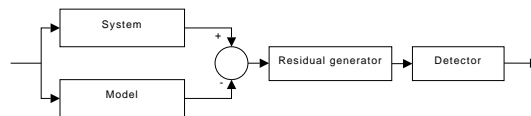


Figure 6.3: Residual generator.

model consist of the evaporator model described in equation (3.12) on page 29 and the superheat model described in equation (3.13) on page 29. The left part of figure 6.4 shows the measured superheat and the superheat from the model. The data is the same as in the two sensor section. It can be seen that the model does not include effects from the refrigerant spray. The right part of figure 6.4 shows the difference between the model and system output. To make a detector it is possible to use a CUSUM algorithm with a defined threshold. The CUSUM algorithm can be seen in equation (6.1) [Blanke et al., 2003]

$$S(k) = \sum_{i=1}^k s(z) \quad (6.1)$$

$$s(z) = \ln \frac{P\theta_1(z)}{P\theta_0(z)} \quad (6.2)$$

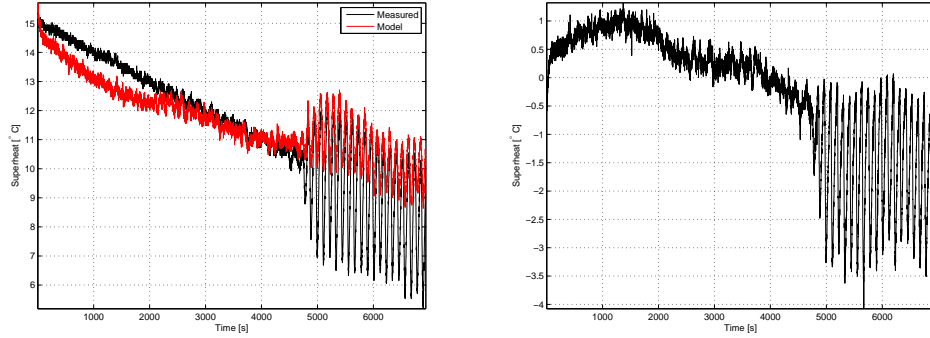


Figure 6.4: Measured and model superheat and the difference.

where:

$s(z)$ is the log-likelihood ratio of an observation z .

The log-likelihood is a measure of the probability that an observation z belong to a probability density function described by $P\theta_1$ rather than one described by $P\theta_0$. It is assumed that the probability density functions are normal distributed. The probability density functions can then be described by equation (6.3) and (6.4).

$$P\theta_1(z) = \frac{1}{\sigma_1\sqrt{2\pi}} \exp\left(-\frac{(z - \mu_1)^2}{2\sigma_1^2}\right) \quad (6.3)$$

$$P\theta_0(z) = \frac{1}{\sigma_0\sqrt{2\pi}} \exp\left(-\frac{(z - \mu_0)^2}{2\sigma_0^2}\right) \quad (6.4)$$

The CUSUM algorithm assumes a constant mean (u_o) and variance (σ_0) when $k < k_{error}$. Where k_{error} is the time at which an error occurs. It also assumes a constant mean (u_1) and variance (σ_1) when $k \geq k_{error}$. Using the data in figure 6.4 the following values can be found when $k_{error} = 4500$.

$$u_o = 0.4 \quad (6.5)$$

$$\sigma_0 = 0.1103 \quad (6.6)$$

The values after $k \approx 4500$ are approximately

$$u_1 = -1.6323 \quad (6.7)$$

$$\sigma_1 = 0.7485; \quad (6.8)$$

Implementing these values in the CUSUM algorithm, equation (6.1), yields the result seen in figure 6.5. The upper part of the figure is the data used in the CUSUM algorithm and the lower part is the output from the algorithm. It is clear that the simple CUSUM algorithm works, however the superheat model is quite parameter sensitive. If the parameters changes just 10% there will be a significant offset between the measured superheat and the modelled. This offset will be detected by the CUSUM algorithm and thereby falsely be detected as refrigerant spray. The data also shows that the model, even within its valid area, can have an offset from the measured value. This has the same effect as mistuned parameters. One way to remove the offset between the model and the

6.1. SUPERHEAT SETPOINT

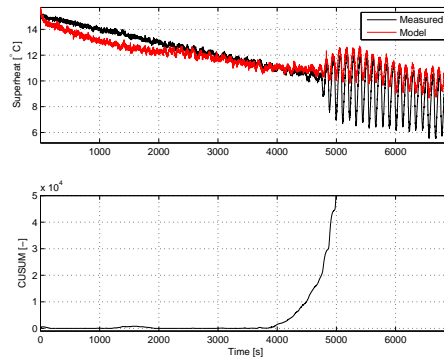


Figure 6.5: Input to and output from the CUSUM algorithm.

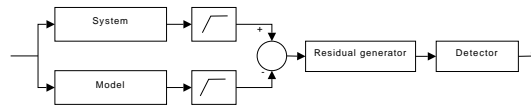


Figure 6.6: Residual generator, LP filtered input.

system output could be by high pass filtering the outputs. The idea is illustrated in figure 6.6. The previously described CUSUM algorithm implementation used a change in mean to detect the spray. Having high passed filtered the data the mean offset is removed. It is therefore necessary to detect the spray only as a change in variance. Figure 6.7 shows two different normal distributions $N(0, 0.1)$ and $N(0, 0.2)$. If a given measurement z is

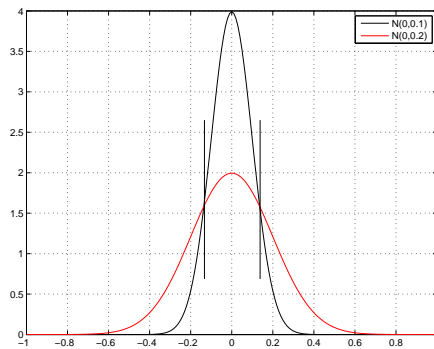


Figure 6.7: Two normal distributions $N(0, 0.1)$ and $N(0, 0.2)$.

between the two horizontal lines it is more likely that it belongs to distribution $N(0, 0.1)$ than $N(0, 0.2)$. If the measurement is outside the reverse is true. The upper part of figure 6.8 shows the high pass filtered data and the lower part shows the output from the CUSUM algorithm. It is clear that the detection algorithm works. It can however be seen that the model data is quite uniform. It should therefore be possible to detect the spray without using the model. This will be described in the next section.

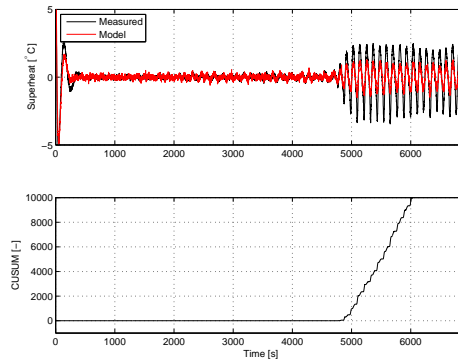


Figure 6.8: Input to and output from the CUSUM algorithm.

6.1.3 Detection without model

Based on the previously result is should be possible to detect the spray using only the measured superheat. Figure 6.9 illustrates the idea. The principle is that the variance

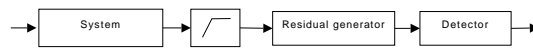


Figure 6.9: Residual generator, LP filtered input, no model.

of the superheat measurement increases when the spray starts to hit the temperature sensor. The variance CUSUM algorithm is the same as described previously. The upper part of figure 6.10 shows the high pass filtered data and the lower part shows the output from the CUSUM algorithm. The settling time for the filter is quite high due to the low frequency of the passband required to remove the offset. It is therefore necessary to set the first many samples of the CUSUM algorithm to zero. It is possible to avoid the use of

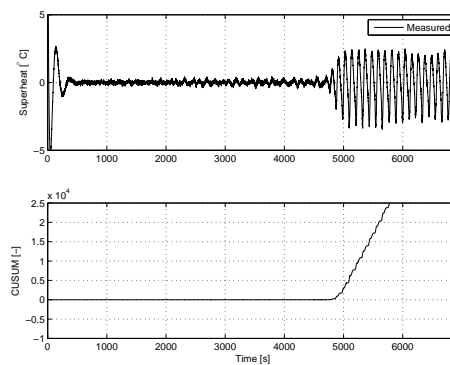


Figure 6.10: Input to and output from the CUSUM algorithm.

filters if the measured superheat is compared with the superheat reference. Figure 6.11 illustrates the idea. The upper part of figure 6.12 shows the data used by the CUSUM algorithm and the lower part shows the output.

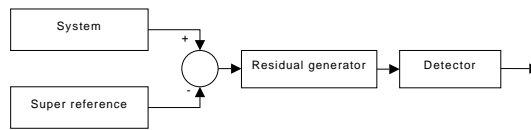


Figure 6.11: Residual generator, measurement and reference.

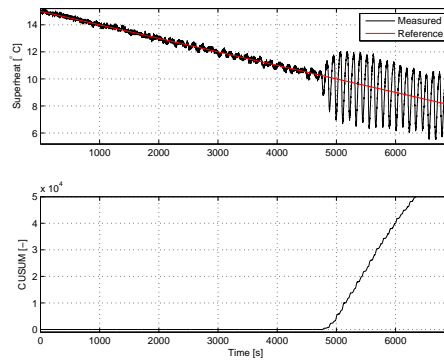


Figure 6.12: Input to and output from the CUSUM algorithm.

6.2 Summary

This chapter described multiple autonomous methods of finding the optimal superheat. The most promising method compared the superheat reference with the measured superheat. Refrigerant spray hitting the temperature sensor will render the controller unable to maintain a constant superheat level. This can be detected using a simple CUSUM algorithm.

Chapter 7

Conclusion

The overall purpose of this project was to develop and implement a set of controllers capable of controlling the available refrigeration systems. The motivation was an attempt to improve the energy efficiency compared to the controller implementations on present refrigeration systems.

To support the choice of focus, the main energy consumers were identified and the immediate optimisation possibilities discussed. The choice fell on the compressor, whose rotational speed can be continuously regulated through the use of a frequency drive. By choosing a constant condenser pressure, the compressor power minimisation problem turns out to be an evaporator pressure maximisation or superheat minimisation problem, with the constraint that liquid refrigerant should not reach the compressor.

Some unexplained behaviour at the transition to low superheats led to an experimental analysis of the superheat's influence on the compressor power consumption, not for a given setpoint, but relative to the actual cooling capacity (COP). The analysis suggest an optimal superheat temperature of around 12 °C for the available system configuration. At lower superheats, sprays of liquid refrigerant seems to exit the evaporator causing significant drops in the superheat measurement. This behaviour was later exploited in an algorithm developed to detect the phenomena and thus automatically find the optimal superheat reference.

Present refrigeration systems usually use a thermostatic expansion valve (TXV) to regulate the superheat. The TXV measures the evaporator outlet temperature and regulates the refrigerant flow to obtain a matching evaporator pressure. The compressor or other actuators influencing the evaporator may then be used offset how much flow is required to maintain a certain pressure, thus regulation the cooling capacity.

The available refrigeration system features an electronic expansion valve (EXV), which may be used to electronically mimic the function of a TXV but with more 'intelligence'. However the presence of a frequency drive for the compressor inspired a new control strategy, where the cooling capacity is directly controlled by the flow of refrigerant led through the evaporator, i.e. regulated by the EXV. The superheat is then controlled by regulating the compressor speed.

Changes to either refrigerant flow or superheat temperature acts as disturbances to the other. Given the time delays or constants present in the system, pure feedback control

might result in instability or very low performance.

To avoid the performance/stability problem both of these controllers were to include model-based control, hence models were made for the evaporator, the compressor and the EXV. The water tank was also modelled for tuning purposes. Most model parameters were estimated from experimental measurements.

Both the superheat and capacity controllers, i.e. compressor and EXV regulators, were based on model feedforward and PI feedback. The capacity controller was embedded in an outer loop which calculates a cooling capacity in a PI fashion from a temperature error, hence the system is capable of obtaining a reference temperature and keep it, if the load is within the systems operating range. If the load is too high the compressor will saturate due to the large amount of refrigerant which has to be removed. When the compressor saturates the superheat controller has no means of preventing the superheat from dropping below the optimal 12 °C or even flooding the compressor. To counter this potential hazard the capacity controller was designed to accept feedback from the superheat controller in terms of compressor overload: When the compressor is overloaded the capacity controller will throttle, i.e. the refrigerant flow is reduced, allowing the superheat controller to regain control of the superheat.

With superheat control as the main topic of the project, further two superheat controllers were implemented. Both based on nonlinear control theory, namely feedback linearization and backstepping.

The main subject of the thesis is to prove that it feasible to control the system using the new control strategy and to show that it offers better control of the superheat, which should yield a better system efficiency. Furthermore the improved control of the superheat should provide faster startup and thus a more efficient system during periods with low load.

The new control strategy succeeded in stabilising the system and in controlling the superheat level. It is possible to obtain an optimal superheat level over a wide range of working points. The system is furthermore able to startup and settle at the optimal superheat level within approximately 200 seconds. The new control strategy also provide full control over the cooling capacity through controlling the refrigerant flow with the expansion value.

The thesis proved that the refrigeration system is more efficient when running at the optimal superheat. A COP-measurement on a system controlled using a TXV operating under similar conditions is needed. It would then be possible to evaluate how much the new control strategy increases the efficiency.

Bibliography

- Åström, Karl Johan & Wittenmark, Björn (1995).
Adaptive control,
 second edition.
 ISBN 0201558661
 (Addison-Wesley, 1995).
- Auld, D.J. & Srinivas, K. (1995-2007).
Aerodynamics for Students
 (1995-2007).
[Http://www.aeromech.usyd.edu.au/aero/cvanalysis/node3.shtml#node43](http://www.aeromech.usyd.edu.au/aero/cvanalysis/node3.shtml#node43).
- Blanke, Mogens, Kinnaert, Michel, Lunze, Jan & Staroswiecki, Marcel (2003).
Diagnosis and Fault-tolerant Control.
 ISBN 3540010564
 (Springer, 2003).
- DuPont (2004).
Thermodynamic Properties of Suva® 134a,
 h-47752-2 edition
 (DuPont, 2004).
- Grald, E.W & MacArthur, J.W (1992).
A Moving-Boundary Formulation for Modeling Time-Dependant Two-Phase Flows
 (Int. Journal Heat and Fluid Flow, 1992).
- Guntoft, Søren & Laurtisen, Aage Birckkjær (2003).
Køleteknik,
 second edition.
 ISBN 8757121168
 (Nyt Teknisk Forlag, 2003).
- He, Xiang-Dong, Asada, Harry H., Liu, Sheng & Itoh, Hiroyuki (July 1998).
Multivariable Control of Vapor Compression Systems
 (HVAC&R Research, July 1998).
- Khalil, Hassan K. (2002).
Nonlinear Systems,
 third edition.
 ISBN 0131227408
 (Pearson Education International Inc., 2002).
- Larsen, Lars Finn Sloth (2005).
Model Based Control of Refrigeration Systems, Ph.D Thesis.
 ISBN 87-90664-29-9
 (Aalborg University / Central R & D Danfoss A/S, 2005).
- Petersen, Anders & Lund, Peder Andersen (2004).
Modelling and Control of Refrigeration Systems, Master Thesis
 (Aalborg University Institute of Electronic systems, 2004).
- Rasmussen, Henrik (2008).
Nonlinear Superheat Control of a Refrigeration Plant using Backstepping,
 pre-paper edition
 (Department of Electronic Systems, Aalborg University, 2008).
- Skovrup, Morten Juel (2001).
Thermodynamic and Thermophysical Properties of Refrigerants.
 ISBN 0849312914
 (Department of energy engineering - Technical university of Denmark, 2001).

BIBLIOGRAPHY

Appendix A

The Test Rig

Since the test rig has been described in details multiply times by previously groups and Ph.D projects [Larsen, 2005] [Petersen & Lund, 2004] only the most important components will briefly be described here. Figure A.1 shows a diagram of the system. The diagram shows all the major components such as the compressor, evaporator, condenser and expansions valves etc. The diagram also shows a number of transducers and control signals marked with an encircled four letter ID. All the transducers and control signal are interfaced with a Matlab Simulink model using National Instruments sampling boards. Datasheets on most of the components can be found on the attached CD.

A.0.1 Compressor

The compressor is a maneurop reciprocating compressors with type number MTZ32 made by Danfoss. The compressor is driven by a frequency drive making is possible to adjust the speed of the compressor between 35 and 60 revolutions per minute. The frequency drive is also made by Danfoss and the model number is VLT 5000. It is linear voltage controlled with a signal in the range between 0 and 10 volts. Also connected to the compressor is a transducer that measure the power usage.

A.0.2 Condenser

The condenser is a ACE model made by ECO. The refrigerant is cooled by forcing air through the condenser by a 500 mm fan. The fan is driven by a VLT AKD 500x frequency drive made by Danfoss. The frequency drive is controlled with an signal between 0 and 10 volts which yields a frequency between 0 and 50 Hz.

A.0.3 Expansion Valves

The systems includes two expansion valves. Only one expansion valve is used during operation, the other is disabled using manually controlled valves. The first is a Thermo-static expansion value (TXV) of type TEN 2 made by Danfoss. This expansion valves use a measure of superheat to adjust the flow of refrigerant. The other expansion value is an electronic expansion value (EXV) with model number MCV HVAC from Danfoss. This expansion value is controlled linear by a 0-10 volt signal. To measure the refrigerant flow through the active expansion valve a refrigerant flow meter is placed before the expansion

value. The flow meter is a Massflo Mass 6000 signal processing unit combined with a Massflo Mass 2100 flowmeter made by Siemens. A solenoid valve is mounted between the expansion valve and the flow meter. This valve is used to completely stop the flow of refrigerant.

A.0.4 Evaporator

The evaporator is a M2520L2G2X made by GEA with a cooling capacity of 4 kW. The refrigerant cools a water and antifreeze solution which are forced through the evaporator by use of a Grundfos UPE pump. To heat the solution a water heater from Metro with type number 620 is used. The water heater is equipped with a 6 kW heating element. The power can be controlled with a 0 to 10 volt input signal. The power is also measured with a power meter. The meter is called "JT04" on the diagram. However due to limitation in the measuring device, the power reading is not accurate. It saturates at approx 3400 watt and have problems reading values below 1500 watt.

A.0.5 Transducers

The system is equipped with a number of temperature transducers. These are of the type AKT 11 made by Danfoss. There are also a number of pressure transducers mounted on the system, these are of the type AKS 33 made by Danfoss. All the transducers interface the simulink model with a 0 to 10 voltage signal.

A.0.6 Matlab Interface

At the beginning of this project there existed a Matlab Simulink interface to the system. In table A.0.6 the input and output relation are described without including any components between the simulink model and the final component. E.g. the compressor speed is set using a value between 0-10 which result in a compressor speed between 35 and 60 Hz.

Component	Input	Output
Compressor	0-10	35 - 60 [Hz]
Fan	0-10	0 - 50 [Hz]
Exp. value	0-10	closed - open
Solenoid	Boolean	ON / OFF
Temp. transducer	Temperature	Temperature [$^{\circ}C$]
Pres. transducer	Pressure	Pressure [<i>Bar</i>]
Flow. transducer	Flow	Flow [<i>kg/s</i>]

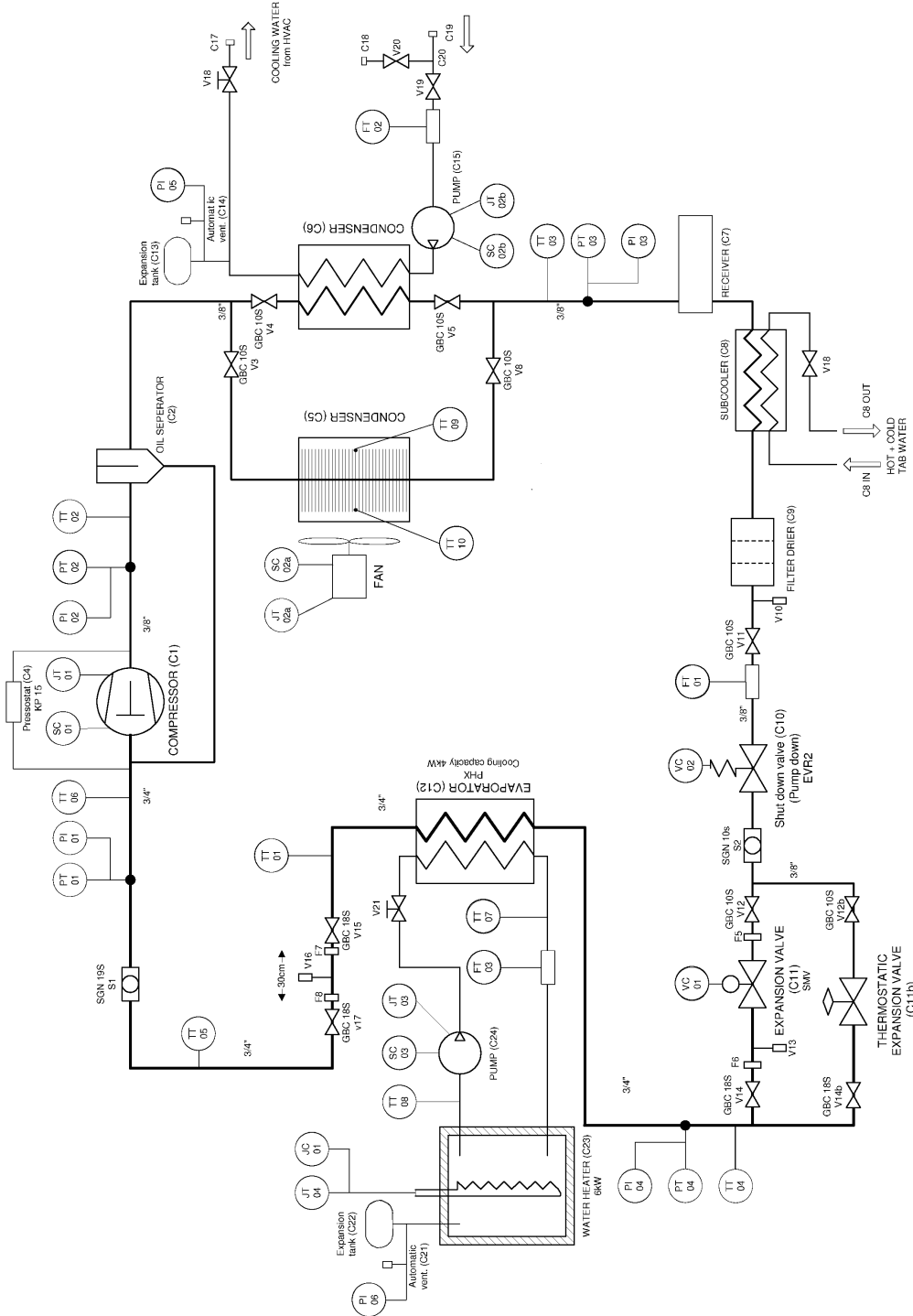


Figure A.1: Diagram of the test rig showing the key components.

Appendix B

Expansion Valve

In the following the unknown constant, K , of equation (3.28) will be estimated. The first dataset is recorded with the pressure difference held at different constant levels while steps are applied at the expansion valve control signal. The next two datasets are with increasing flow and respectively constant compressor RPM and constant evaporator pressure. The value of K is estimated from the first dataset and the measured and calculated mass flow is compared for all three sets. For simplicity the density is set to unity, which is assumed valid as the upstream refrigerant should be condensed and hence have an almost constant density, downstream the refrigerant is an unknown mix of gas and liquid hence is difficult to say anything about the combined density.

B.1 Presentation

Figure B.1 shows a number of plots from the first dataset. The middle frame reveals that the calculated value of K is not generally constant. The bottom frame shows measured and calculated flow for $K = 0.0152$. In this experiment the measured and calculated flows do not match until the valve has been opened a certain amount, then there is consistence between measured and calculated flow until the pressure is lowered the second time. In the last part of the set not even the dynamics seems consistent and the experiment was aborted.

Figure B.2 shows similar plots for the second dataset. At time $t \approx 1100$ the solenoid shuts due to low superheat in the evaporator. An interesting effect is that after the solenoid opens again the expansion valve controller can maintain the same mass flow with the valve less open although the pressure drop over the valve is unchanged. The bottom frame of the figure shows how the difference between the measured and the calculated flow is increasing until the solenoid shuts whereas it is much lower after the solenoid has reopened.

Figure B.3 is the plots of the last dataset. It shows no surprises as the measured and calculated flows are close to each other at all times.

B.2 Analysis

The previous figures show that the model is able to reflect measurements quite well, but under certain conditions there seems to be very little consistence between the two. In the problematic areas the measured flow is consistently lower than the calculated, which could be a result of either an obstacle temporarily stuck in the valve or drops in refrigerant density due to insufficient cooling in the condenser.

B.3 Conclusion

The expansion valve constant K has been estimated to a value of 0.0152 with the refrigerant density neglected and set to unity. The calculated flow is consistent with the measured flow under wide conditions, but occasionally the consistency is lost, presumably as a consequence of obstacles temporarily stuck in the valve or insufficient cooling in the condenser. The test rig has a dedicated subcooler (using tap-water), which might be used to ensure that the refrigerant is completely condensed before it enters the expansion valve.

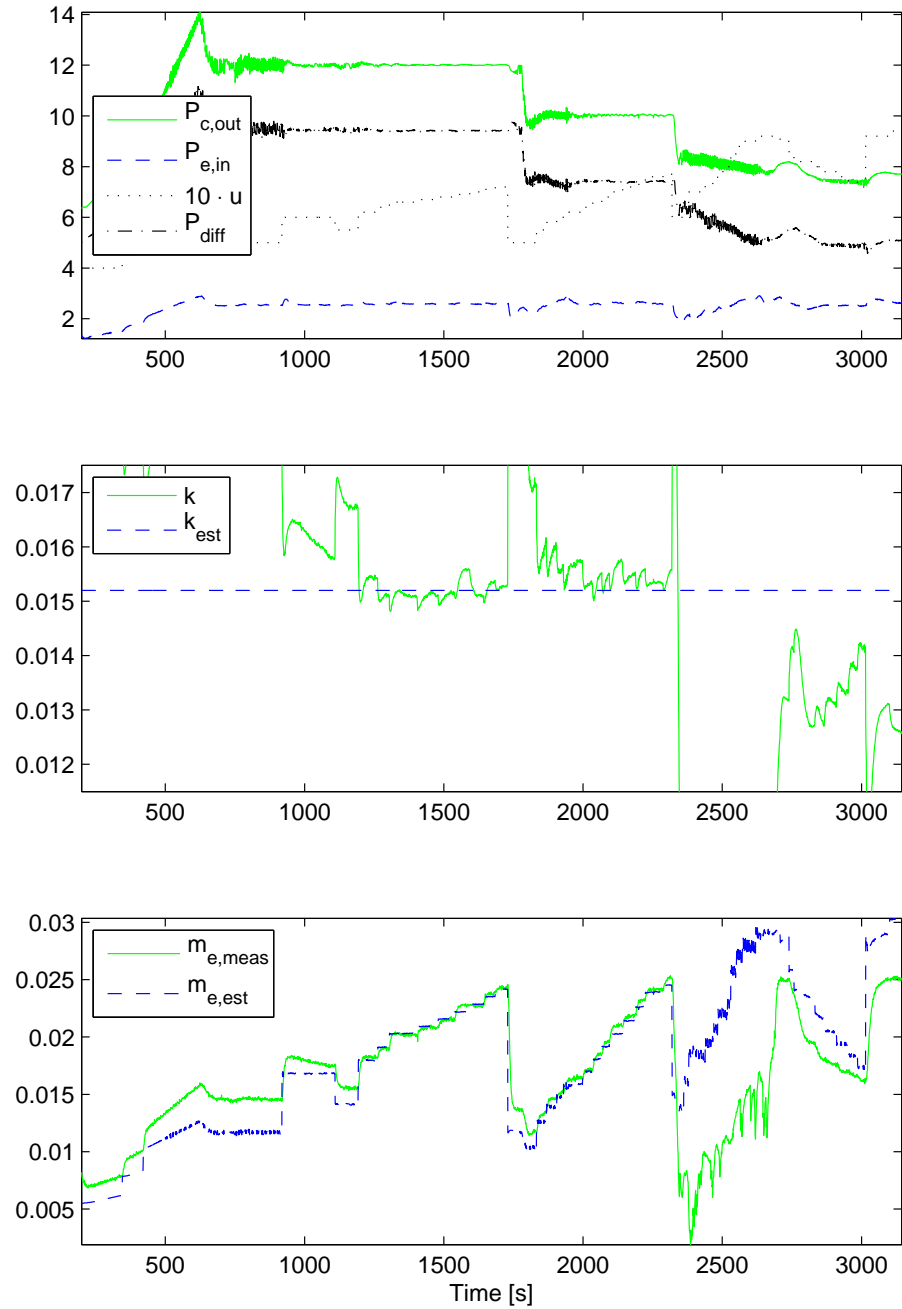


Figure B.1: Expansion valve constant estimation.

B.3. CONCLUSION

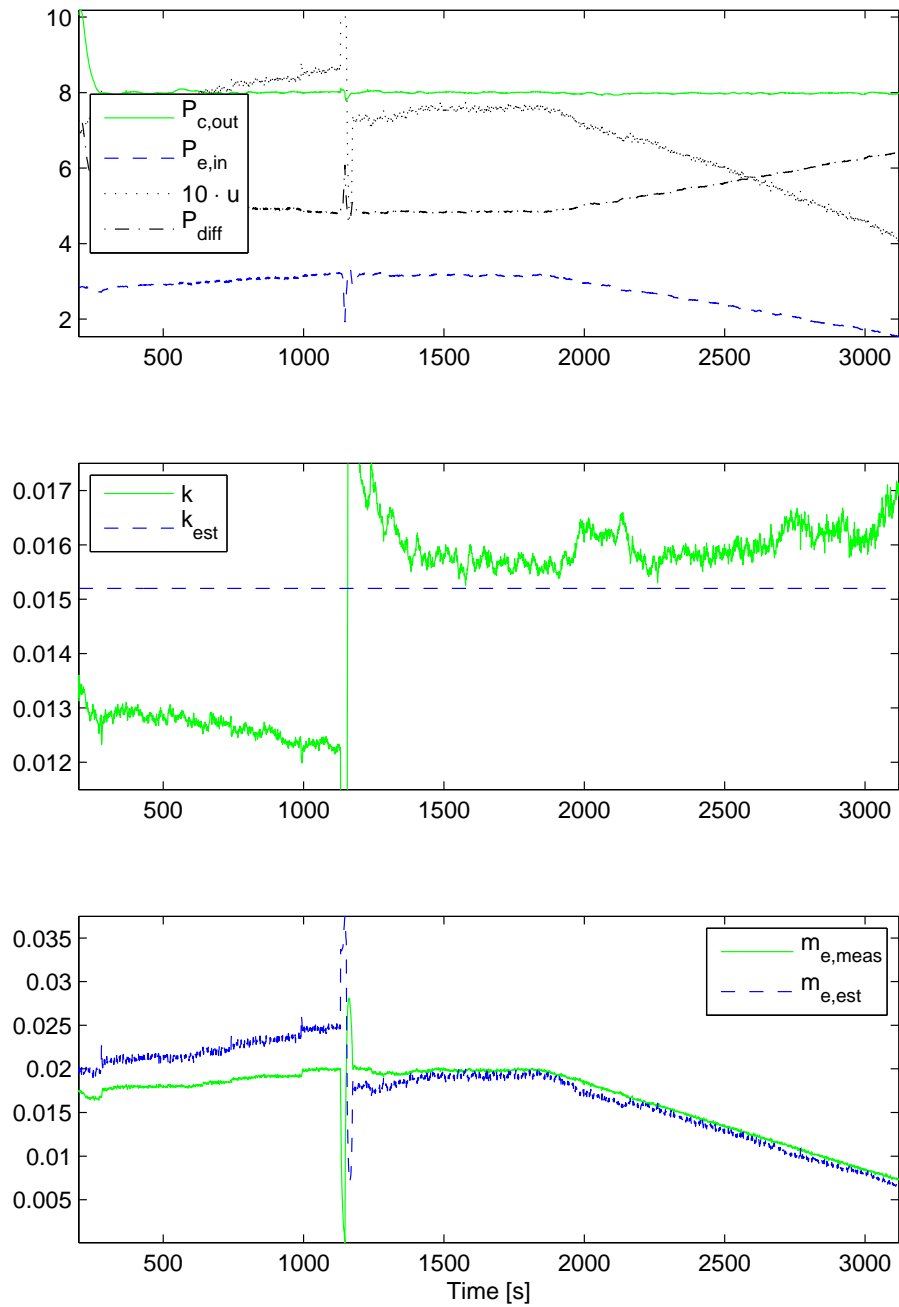


Figure B.2: Expansion valve constant verification.

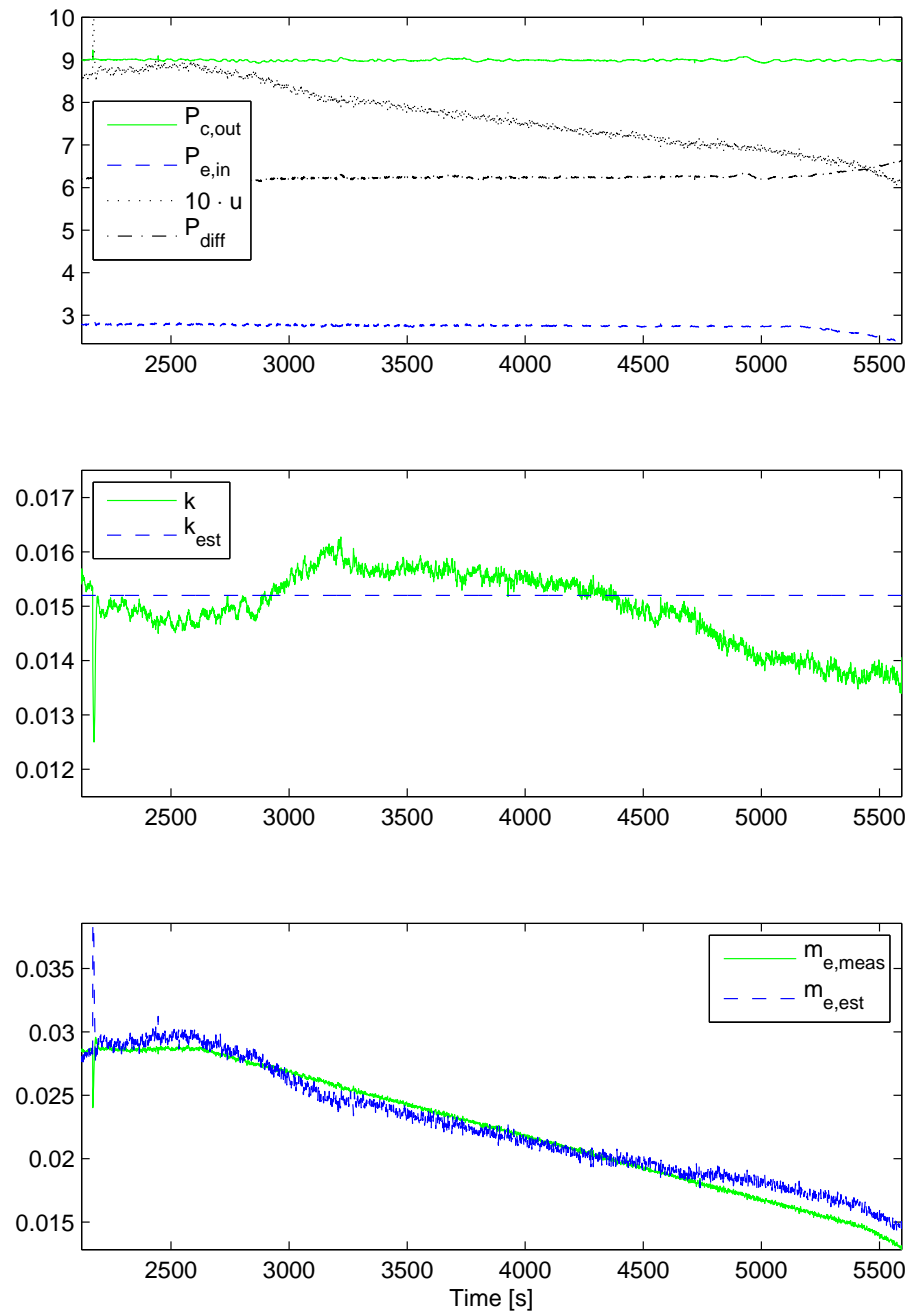


Figure B.3: Expansion valve constant verification.

B.3. CONCLUSION

Appendix C

COP Experiment

This appendix describes how the COP experiment was performed and analyse the recorded data. At the end of the appendix the results are commented.

C.1 Purpose

The purpose of the experiment is to measure the ratio between energy usage by the compressor and the resulting cooling capacity at different levels of superheat. The ratio is referred to as "Coefficient Of Performance" (COP).

C.2 Method

The experiment is performed using the controller design idea described in chapter 4 on page 49. Figure C.1 shows the implementation with setpoint values. A constant power

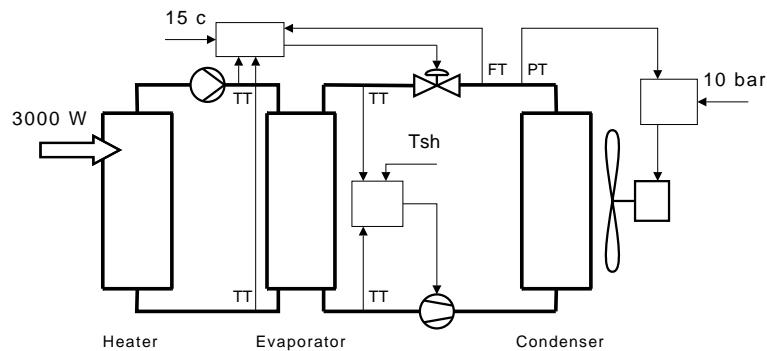


Figure C.1: Refrigeration system with controllers.

of 3000 W is applied to the heater. The setpoint for the refrigerant flow controller is 15 degrees. After a settling time the outflow water from the evaporator will reach steady state and the refrigerant flow will reach a steady state yielding a refrigerant flow matching 3000 W. The required cooling capacity is thus fixed near 3000 W. The

setpoint for the condenser controller is fixed at 10 bar. The superheat temperature can now be controlled with the setpoint to the superheat controller.

C.3 Calculating COP

Due to the slow dynamics of the refrigeration system the COP-value must be calculated over a long period of time to give an accurate result. An time period of 1 hour and 20 minutes are chosen for each superheat level. The power usage of the compressor is available from the frequency drive powering the compressor. Equation (C.1) describes how the cooling capacity is calculated.

$$Q_{cool} = \dot{m}_w \cdot (T_{w.in} - T_{w.out}) \cdot C_w \quad (C.1)$$

where:

- Q_{cool} is the cooling capacity [W]
- \dot{m}_w is the mass flow of the water / antifreeze solution [kg/s]
- $T_{w.in}$ is the temperature of the water/antifreeze solution into the evaporator [$^{\circ}C$]
- $T_{w.out}$ is the temperature of the water/antifreeze solution from the evaporator [$^{\circ}C$]
- C_w is the heat capacity of the water/antifreeze solution [J/kg $^{\circ}C$]

The cooling capacity is calculated by multiplying the temperature difference between the water running into the evaporator and the water running out of the evaporator with the heat capacity and the water flow. The heat capacity of the water / antifreeze solution is not know precisely but is around 3800 J/kg $^{\circ}C$. The exact value is not important because the COP-measurement will only be used to compare the efficiency of the system at different superheat levels. The setpoint for the superheat was changed in steps. During the experiment the following setpoints were used: 17, 15, 14, 13.5, 13, 12.5, 12, 11.5, 11, 10, 9 and 8 degrees.

C.4 Results

Figure C.2 show the measured superheat values. The COP-value for a given superheat level is calculated in the time interval between a black vertical line and a red vertical line. It is clear that the superheat controller is able to control the superheat levels. However is has the best performance at high superheat temperatures. Table C.1 shows the setpoint superheat, the measured superheat mean, the measured superheat variance and the resulting COP-value. The mean and variance describes how well the superheat controller kept the superheat at the setpoint.

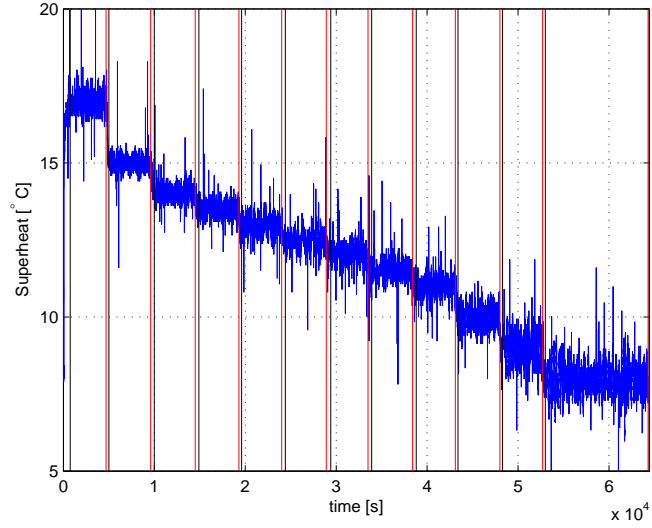


Figure C.2: Measured superheat.

Setpoint	Measured T_{sh} mean	Measured T_{sh} var	COP
17	17.00	0.074	2.23
15	15.01	0.044	2.23
14	14.00	0.042	2.29
13.5	13.50	0.051	2.29
13	12.99	0.069	2.33
12.5	12.48	0.082	2.34
12	12.00	0.088	2.33
11.5	11.50	0.070	2.33
11	11.01	0.094	2.31
10	10.00	0.129	2.28
9	9.00	0.236	2.26
8	8.00	0.223	2.25

Table C.1: Results from the COP experiment.

Appendix D

Derivation of f_{te}

The purpose of the f_{te} function is to calculate the steady state value of the evaporation temperature what will result in a given superheat. The input to the function are the refrigerant flow, temperature of the water and the desired superheat. The inflow and outflow refrigerant enthalpy are also passed to the function. The evaporation temperature can be calculated using equation (3.18) and (3.19) on page 30. These two equations are repeated here:

$$T_{sh} = (T_{w,i} - T_e) \left(1 - e^{-\frac{\sigma(L_e - t_e)}{C_r \dot{m}_r}} \right) \quad (D.1)$$

$$l_e = \frac{\dot{m}_r (h_o - h_i)}{(T_{w,i} - t_e) \alpha} \quad (D.2)$$

Inserting (D.2) into (D.1) and solving for t_e using Maple yields

$$T_{e,calc} = \frac{k_2 - T_w \cdot k_3}{k_0 - k_3} \quad (D.3)$$

$$f_{te}(T_{sh}, t_w, \dot{m}_r, h_o, h_i) \equiv T_{e,calc} \quad (D.4)$$

where

$$k_0 = \sigma \cdot (h_o - h_i) \quad (D.5)$$

$$k_1 = \frac{k_0 \cdot \exp\left(\frac{\dot{m}_r \cdot k_0 - \sigma \cdot L_e \cdot \alpha \cdot T_{sh}}{\dot{m}_r \cdot c \cdot \alpha \cdot T_{sh}}\right)}{c \cdot \alpha \cdot T_{sh}} \quad (D.6)$$

$$k_2 = \sigma \cdot T_{sh} \cdot (h_i - h_o) + T_w \cdot k_0 \quad (D.7)$$

$$k_3 = c \cdot \alpha \cdot T_{sh} \cdot \text{lambertw}(k_1) \quad (D.8)$$

To test the algorithm the evaporation temperature is calculated for a range of different water inlet temperatures and refrigerant flows. Equation (D.1) and (D.2) is then used to calculate the resulting superheat. Figure D.1 shows the superheat. It is clear from the figure that the equation calculated with Maple and implemented in Matlab is correct. Any faults would have shown up as superheat temperatures other than 12 °C

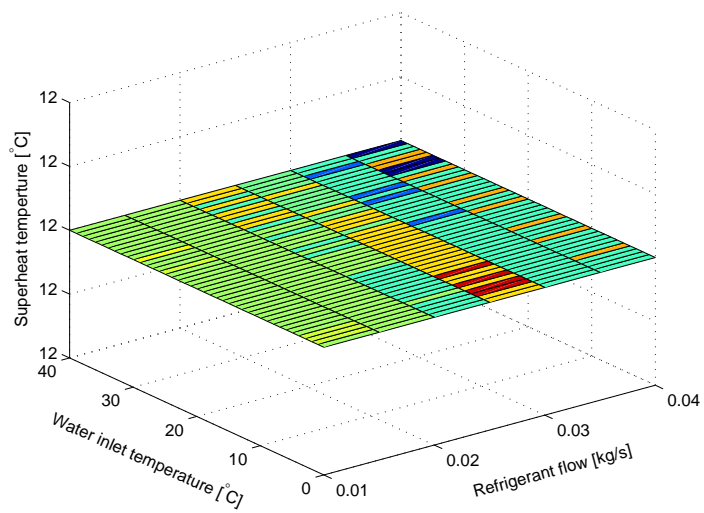


Figure D.1: Calculated superheat.

Appendix E

Working Point Consideration

Observations made during experiments with the system have shown unmodelled behaviour confined to a small subsets of the feasible working points. Figure E.1 shown an example of this property. The upper graph is the cooling capacity. A ramp signal is used as the reference. The middle graph is the measured superheat. In the time between 2500 and 3500 s the system seems to experience limitcycle-like behaviour. The bottom graph

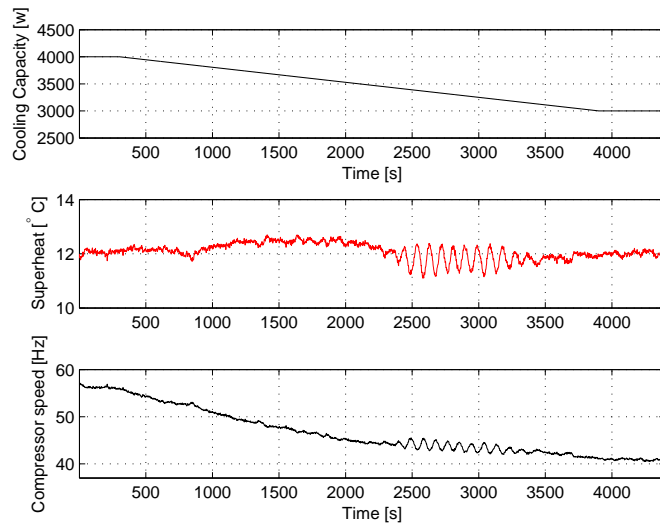


Figure E.1: Calculated superheat.

shows the control signal to the compressor. At first glance it could look like a 'normal' unstable system, due to too high controller gains. However this behaviour is only present in a limited set of working points where the gain in the system should not change and the system is also 'stable' both before 2500 s and after 3500 s. From working with the system it appears that the system changes such that the required compressor speed to maintain a constant superheat is changed. This idea is supported by figure E.2, which shows the compressor speed calculated using feedforward and the actual compressor

speed i.e. feedforward plus feedback. As it can be seen the actual signal changes level. As possible explanation of the limitcycle-like behaviour could be that the system acts as a hybrid system where the parameters changes back and forth between two states. And when the system is outside this subset of the working points the system is always in either state. During the experiments it has become apparent that there is a correlation

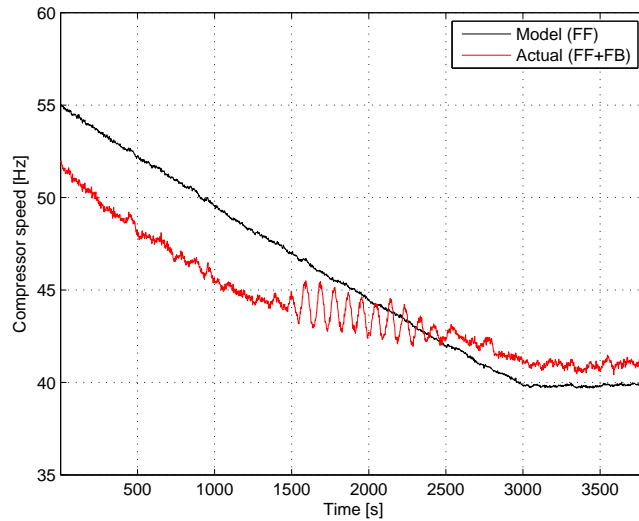


Figure E.2: Compressor control signal.

between this behaviour and the refrigerant gas volume outflow of the evaporator [m^3/s]. Figure E.3 shows the calculated refrigerant volume flow of 6 different measurements that all experience this behaviour. Common for all the measurements is that it happens at volume flows of approximately $1.7 \cdot 10^{-3} m^3/s$. The behaviour has not occurred at any other volume flows. This indicates that there must be some flow dynamics that affect the system at that refrigerant gas volume flow.

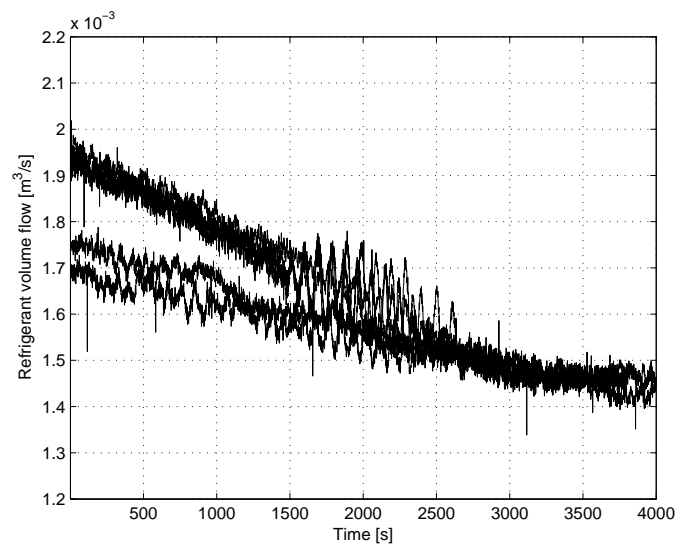


Figure E.3: Volume flow of the refrigerant gas.
